



***Neurodevelopment under the prism of
environmental challenges
Prenatal glucocorticoids and neurogenesis***

DISSERTATION
ZUM ERWERB DES DOCTOR OF PHILOSOPHY (PH.D.)
AN DER MEDIZINISCHEN FAKULTÄT DER
LUDWIG-MAXIMILIANS-UNIVERSITÄT MÜNCHEN

vorgelegt von
Anthodesmi Krontira

Aus
Patras, Greece

Jahr
2022

Mit Genehmigung der Medizinischen Fakultät der
Ludwig-Maximilians-Universität zu München

First evaluator (1. TAC member): *Prof. Dr. Dr. Elisabeth Binder*

Second evaluator (2. TAC member): *Prof. Dr. Magdalena Götz*

Third evaluator: *Prof. Dr. Florian Heinen*

Fourth evaluator: *Priv. Doz. Dr. Mirjam Landgraf*

Dean: **Prof. Dr. Thomas Gudermann**

Datum der Verteidigung:

18th of November 2022

Abstract

Prenatal development affects adult health. Exposures to a variety of prenatal environmental factors have important effects on fetal development and, in turn, are extensively associated with neurobehavioral, structural and functional phenotypes after birth. Developmental processes are in part promoted by orchestrated levels of glucocorticoids, which are steroid hormones involved in fetal organ maturation. Glucocorticoids also mediate the hormonal stress response of the organism as part of the hypothalamic-pituitary-adrenal axis. During pregnancy levels of glucocorticoids outside of the normal range, either due to maternal pathology including stress-related psychiatric disorders or to antenatal synthetic glucocorticoid treatments, have been associated with altered brain structural and neurobehavioral phenotypes after birth. Interestingly, developmental time-windows seem to interplay with the exposure to influence the direction of postnatal phenotypes. Exposures later in gestation are mainly associated with adverse outcomes while exposures earlier in gestation are additionally associated with potentially beneficial outcomes. While many studies have investigated the effects of glucocorticoids on late developmental time-windows, so far little evidence is available on their effects on early human cortical development and especially during the neurogenic period, which is when neurons are produced. Thus, the potential cellular and molecular underpinnings of the timing dependent divergent effects of glucocorticoids on postnatal phenotypes are not known.

To investigate these processes in a complex model of early human neurodevelopment that is reactive to environmental stimuli, I used induced Pluripotent Stem Cells-derived 3-dimensional cerebral organoids and combined them with *in vivo* mouse neurodevelopment. I found that application of glucocorticoids during neurogenesis increases neurogenic processes that are enriched in species with a gyrified brain, like humans, while are rare in species with a smooth brain, like rodents. These processes contribute to the increased neuronal production and cortical expansion seen in gyrencephalic species. More specifically, at the molecular level this effect is mediated by the glucocorticoid receptor, a transcription factor, which in turn activates *ZBTB16* by altering its methylation landscape in specific DNA regulatory elements. Subsequently *ZBTB16*, a transcription factor itself, increases the expression of *PAX6*, a key driver of neurogenesis, by activating its promoter. This results in increased numbers of progenitor cells expressing *PAX6* and *EOMES* (a marker of more mature progenitors) in the basal regions of the germinal zones in both organoids and mice. *PAX6*- and *EOMES*- positive progenitors are enriched in gyrified species while they are rare in species with smooth brains. The increased numbers of these highly proliferative and neurogenic progenitors lead to an extended neurogenic period and ultimately to increased production of deep layer neurons (*BCL11B*-

positive). Finally, the altered cellular architecture due to glucocorticoids and *ZBTB16* potentially mediates beneficial postnatal outcomes as indicated by causal associations with higher educational attainment and increased postnatal cortical thickness.

This work highlights the importance of early neurodevelopment and specifically of the neurogenic period as a sensitive time-window for glucocorticoid effects. In addition, the molecular and cellular mechanisms as well as the pathways identified could have profound implications for our understanding of glucocorticoid effects during early brain development that potentially mediate postnatal outcomes.

*«Δεν υπάρχουν ιδέες, υπάρχουν μονάχα άνθρωποι που κουβαλούν τις ιδέες,
κι αυτές παίρνουν το μπόι του ανθρώπου που τις κουβαλάει».*

Νίκος Καζαντζάκης

*“There are no ideas, there are only people who carry these ideas,
and they take the height of the people who carry them”.*

Nikos Kazantzakis

Contents

Abstract	v
Contents	ix
List of Abbreviations	xi
Statistical Significance	xii
1 Introduction	1
1.1 Pregnancy as a sensitive period for postnatal outcomes	2
1.2 Physiological rise of glucocorticoids during pregnancy	3
1.3 Glucocorticoids as mediators of environmental exposures	4
1.4 The complex biology of environmental effects embedding	10
1.5 Prenatal environment and neurobehavioral outcomes	12
1.6 Prenatal environment and brain structural outcomes	14
1.7 Cerebral cortical development in rodents and humans	15
1.8 Prenatal environment and neurogenesis	19
1.9 Modeling the human developing cerebral cortex	20
2 Rationale and Objectives	23
3 Materials and Methods	25
3.1 Induced Pluripotent stem cells	25
3.2 Cerebral organoids	25
3.3 Plasmids preparation	26
3.4 <i>In utero</i> electroporations of mice	26
3.5 Electroporations of human cerebral organoids	27
3.6 Glucocorticoid treatment	27
3.7 Immunofluorescence	28
3.8 Image analysis and Quantifications	28
3.9 Protein isolation and Western blot	29
3.10 RNA isolation and quantitative PCR	31
3.11 Luciferase reporter assays	31
3.12 CRISPR-Cas9 editions of hiPSCs	31
3.13 Flow Cytometry	33
3.14 Targeted Bisulfite Sequencing	33
3.15 Statistics	34
3.16 Bulk RNA sequencing	34
3.17 <i>ZBTB16</i> Expression UMAP Plots	35
3.18 STARR-qPCR	35
3.19 Mendelian randomization and PheWAS study	36
3.20 GO enrichment of <i>DiffBrainNet</i> results	37

4 Results	39
4.1 Glucocorticoids impact the cellular architecture of the developing cortex	39
4.2 The GR is responsible for the increase of basal progenitors	43
4.3 Glucocorticoids effects on the transcriptional landscape	44
4.4 <i>ZBTB16</i> is responsive to glucocorticoids in multiple tissues	45
4.5 <i>ZBTB16</i> : a glucocorticoid-responsive developmental transcription factor	47
4.6 Embedding of glucocorticoid effects with methylation	50
4.7 <i>ZBTB16</i> mimics the effects of glucocorticoids	51
4.8 <i>ZBTB16</i> is necessary for the effects of glucocorticoids	53
4.9 <i>ZBTB16</i> increases gyrencephalic-enriched basal progenitors in mice	55
4.10 <i>ZBTB16</i> activates a forebrain active promoter of <i>PAX6</i>	60
4.11 Gene by environment interactions and postnatal phenotypes	61
5 Discussion	68
5.1 GR is responsible for the glucocorticoid excess effects	69
5.2 Treatment paradigm and clinical relevance	70
5.3 Glucocorticoids impact gyrified species-enriched neurogenic processes	71
5.4 <i>ZBTB16</i> mediates the effects of glucocorticoids on neurogenesis	73
5.5 Glucocorticoids and beneficial postnatal outcomes	75
5.6 Limitations	77
5.7 Future directions	78
6 Conclusions	79
7 Bibliography	81
8 Appendix	99
8.1 Supplementary Figures	99
8.2 Supplementary Tables	107
List of Figures	131
List of Tables	133
Acknowledgements	135
Declaration of Contributions	137
Affidavit	a
Confirmation of Congruency	c

List of Abbreviations

2D	<u>T</u> wo <u>D</u> imensional	HPA	<u>H</u> ypothalamic- <u>P</u> ituitary- <u>A</u> drenal
3D	<u>T</u> hree <u>D</u> imensional	IF	<u>I</u> mmunofluorescence
Ab	<u>A</u> ntib <u>o</u> dy	IP	<u>I</u> ntermediate <u>P</u> rogenitor
ACTH	<u>A</u> drenoc <u>o</u> rticotrophic	iPSC	<u>I</u> nduced <u>P</u> luripotent <u>S</u> tem <u>C</u> ell
ANOVA	<u>A</u> nalysis <u>O</u> f <u>V</u> ariance	IZ	<u>I</u> ntermediate <u>Z</u> one
aRG	<u>A</u> pical <u>R</u> adial <u>G</u> lia	logFC	<u>l</u> og <u>f</u> old <u>c</u> hange
AVP	<u>A</u> rginin <u>V</u> asopressin	MAST	<u>M</u> odel-based <u>A</u> nalysis of <u>S</u> ingle-cell <u>T</u> ranscriptomics
BP	<u>B</u> asal <u>P</u> rogenitor	MDD	<u>M</u> ajor <u>D</u> epressive <u>D</u> isorder
bp	<u>B</u> ase <u>P</u> air	MR	<u>M</u> ineralocorticoid <u>R</u> eceptor
bRG	<u>B</u> asal <u>R</u> adial <u>G</u> lia	MRa	<u>M</u> endelian <u>R</u> andomization
CNS	<u>C</u> entral <u>N</u> ervous <u>S</u> ystem	mRNA	<u>m</u> essenger <u>R</u> NA
CP	<u>C</u> ortical (like) <u>P</u> late	MZ	<u>M</u> arginal <u>Z</u> one
CRH	<u>C</u> orticotropin- <u>R</u> eleasing- <u>H</u> ormone	oRG	<u>O</u> uter <u>R</u> adial <u>G</u> lia
DE	<u>D</u> ifferentially <u>e</u> xpressed	PFC	<u>P</u> refrontal <u>C</u> ortex
Dex	<u>D</u> examethasone	PheWAS	<u>P</u> henome <u>W</u> ide <u>A</u> ssociation <u>S</u> tudy
DMSO	<u>D</u> imethyl <u>S</u> ulfoxide	STARR	<u>S</u> elf- <u>T</u> ranscribing <u>A</u> ctive <u>R</u> egulatory <u>R</u> egion
DOHaD	<u>D</u> evelopmental <u>O</u> rigin of <u>H</u> ealth <u>a</u> nd <u>D</u> isease hypothesis	SNP	<u>S</u> ingle <u>N</u> ucleotide <u>P</u> olymorphism
E	<u>E</u> mbryonic	SVZ	<u>S</u> ubventricular (like) <u>Z</u> one
EB	<u>E</u> mbryoid <u>B</u> ody	TBS	<u>T</u> argeted <u>B</u> isulfite <u>S</u> equencing
FC	<u>F</u> low <u>C</u> ytometry	TF	<u>T</u> ranscription <u>F</u> actor
FDR	<u>F</u> alse <u>D</u> iscovery <u>R</u> ate	UMAP	<u>U</u> niform <u>M</u> anifold <u>A</u> pproximation and <u>P</u> rojection
GO	<u>G</u> ene <u>O</u> ntology	VZ	<u>V</u> entricular (like) <u>Z</u> one
GR	<u>G</u> lucocorticoid <u>R</u> eceptor	WHO	<u>W</u> orld <u>H</u> ealth <u>O</u> rganisation
gRNA	<u>G</u> uide <u>R</u> NA		
GW	<u>G</u> estational <u>W</u> eek		
GxE	<u>G</u> ene by <u>E</u> nvironment		
hCOs	<u>h</u> uman <u>C</u> erebral <u>O</u> rganoids		

Statistical Significance

Notation key for statistical significance throughout the thesis:

Notation	Adjusted p-value
****	< 0.0001
***	< 0.001
**	< 0.01
*	< 0.05
<i>n.s.</i>	> 0.1 (not significant)
Notation	Nominal p-value
#	< 0.05

1 | Introduction

Prenatal development is a critical determinant of health outcomes after birth. The notion that the intrauterine environment has lasting impacts on health throughout life was first posed by dr. Barker, an English epidemiologist. He was among the first to implicate prenatal with adult health by showing that maternal death rates directly related to pregnancy and child birth in 1911–1914 predicted death rates of people living in the same areas in 1987 [1], and that systolic blood pressure was inversely correlated with birth weight, a proxy of the intrauterine environment, in 10-year-old children [2].

The fundamental studies of dr. Barker created the basis for extensive research and discussion on the importance of development for postnatal outcomes that are summarized by three hypotheses: “the Developmental Origin of Health and Disease hypothesis (DO-HaD)” [3], [4], “the fetal programming hypothesis” [5] and “the developmental programming hypothesis” [4]. All three theorize that exposures to environmental challenges during prenatal critical periods can have lasting impacts on the development of cells, tissues and circuits leading to sustained health effects throughout life.

The central nervous system (CNS) undergoes vast changes during development, making it very plastic and malleable to external stimuli. A variety of prenatal exposures including maternal psychopathologies, stress, malnutrition, endocrine problems, drugs, but also beneficially enriched environments have been linked to a multitude of postnatal outcomes at the metabolic, cardiovascular, neurobehavioral but also brain structural level [6]–[8]. Among the most studied early environmental factors able to influence postnatal neurobehavioral health is maternal psychopathology and specifically stress-related disorders [8]. In recent years there is a plethora of research on the effects of maternal psychopathology and stress on outcomes for the offspring, given the high prevalence of psychiatric disorders and syndromes during pregnancy.

In fact, during pregnancy, the prevalence rates of suffering from any mental disorder are approximately 19% [9] to 25% [10], a number double the one in non-pregnant women at least for the United States [11]. A plethora of reasons could account for this increase, including co-parenting relationships, financial and demographic circumstances, psychological factors and physiological changes due to hormonal regulation during pregnancy [11]. Importantly, maternal psychopathology is significantly associated with preterm birth and lower birth weight, both proxies of non-physiological development of the embryo, in more than 140,000 women [9], highlighting the importance of maternal health for the developing embryo.

Environmental exposures have also been implicated with increased prevalence rates of mental disorders in pregnant women. The COVID-19 pandemic, for example, significantly increased the rates of anxiety, depression, psychological distress and insomnia among pregnant women with the percentages reaching 31% and 37%, for depression and anxiety respectively, to 70% for psychological distress [12]. These effects of environmental challenges highlight the important role of the environment on brain disorders prevalence and reflect the complex biology of neurobehavioral and mental disorders, as biological manifestations of complex interactions of the environment with physiology.

1.1 Pregnancy as a sensitive period for postnatal outcomes

During pregnancy vast changes occur both to the mother and the fetus, making this period highly sensitive to environmental stimuli and critical for the development of the fetus. The pace of fetal brain maturation is much faster than in any other period of life. The majority of critical steps for a normally functioning nervous system happen prenatally, including the closing of the neural tube, neurogenesis, neuronal migration and parts of synaptogenesis [7] (see also “Cortical development length in humans and rodents”, *page 16*). This creates a sensitive window when the developing brain is highly susceptible to harmful effects from a number of environmental exposures including maternal psychopathology, nutrition, infections, toxins, drugs and others [6]. Aside from the adverse impacts, pregnancy also poses a sensitive window for possible beneficial effects, where the fetus adapts its prenatal development to face postnatal life. For example, nutritional deprivation during pregnancy is associated with the development of the “thrifty phenotype” hypothesis, which suggests that early life metabolic adaptations exist to help the offspring survive in low-food postnatal environments but at the same time could mediate maladaptive phenotypes when food postnatally is plentiful [11]. This is also a very good example of the “mismatch hypothesis”, which theorizes that vastly different prenatal and postnatal environments could lead to maladaptive responses [5], when, in principle, developmental programming should prepare the fetus for a specific environment and lead to better fitness postnatally. Apart from the fetus though, the mother also undergoes vast changes during pregnancy to support fetal growth. The maternal hormonal system undergoes the most dynamic changes compared to any other period of life, while there are reports for changes in neuronal structure and signaling during pregnancy [11].

Thus, gestation is an important time-window sensitive to environmental effects. A number of studies have shown that different exposures during pregnancy have lasting impacts on the developing fetus and mediate postnatal adverse and beneficial outcomes on structural phenotypes of the brain, behavior and neurodevelopmental trajectories [11], [13], [14].

1.2 Physiological rise of glucocorticoids during pregnancy

A system that undergoes vast changes during pregnancy is the hypothalamic-pituitary-adrenal (HPA) axis. The HPA axis produces steroid hormones that are important for the maturation and function of a plethora of organs. In addition, it is the main stress response system of the human body. During physiological function and in response to stress the hypothalamus releases corticotropin releasing hormone (CRH) and the posterior pituitary gland releases vasopressin (AVP). They, in turn, bind to receptors of the anterior pituitary gland and lead to the production of adrenocorticotrophic hormone (ACTH- cleaved from proopiomelanocortin). ACTH is released in the blood stream and stimulates the production of glucocorticoids, cortisol in humans and corticosterone in mice, from the adrenal cortex. Glucocorticoids bind to steroid receptors, glucocorticoid receptor (GR) and mineralocorticoid receptor (MR) expressed in the brain, which act as transcriptional activators or repressors leading to transcriptional responses. This leads to an ultrashort feedback loop, thus terminating the HPA axis activation and secretion of glucocorticoids [15] (Figure 1a).

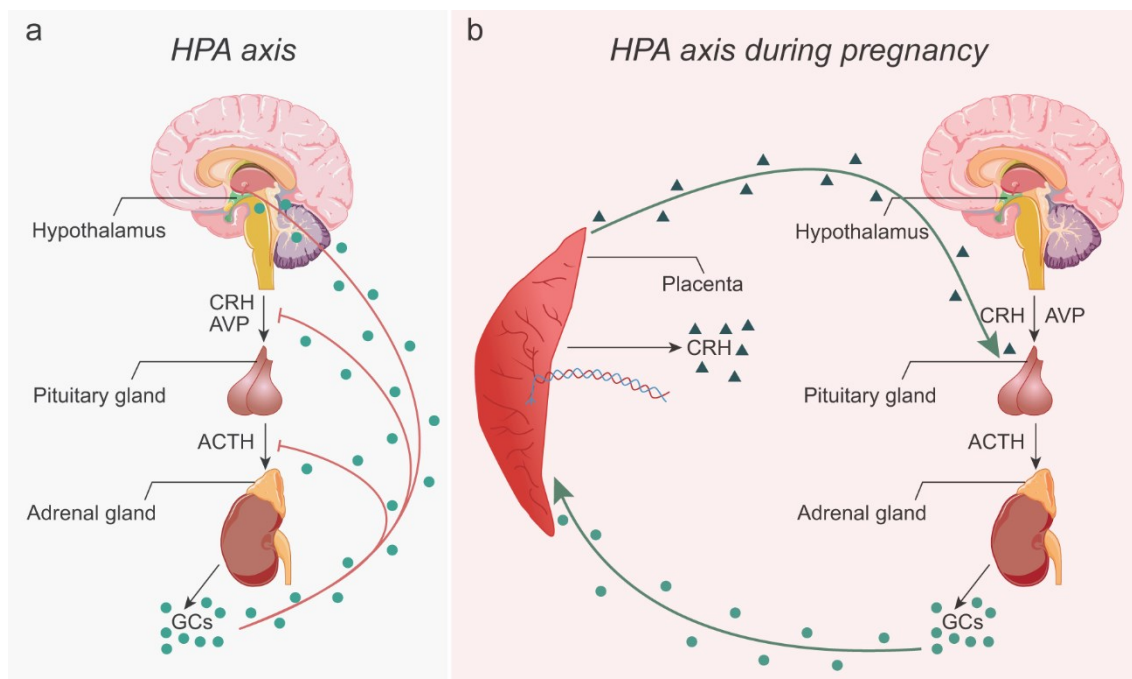


Figure 1| Hypothalamic- Pituitary- Adrenal axis in physiology and pregnancy. **a**, The hypothalamus releases CRH which stimulates the production of ACTH from the pituitary gland. ACTH activates the release of glucocorticoids, cortisol in humans and corticosterone in mice, from the adrenal glands. Glucocorticoids terminate the HPA axis activation by binding to steroid receptors which, in turn, lead to an ultra-short negative feedback loop. **b**, During pregnancy, the placenta also has the ability to release CRH. In contrast to the negative feedback loop at the level of the hypothalamus, glucocorticoids trigger a positive feedback loop at the level of the placenta. This stimulates the production of placental CRH which in turn stimulates the release of glucocorticoids thus leading to enhanced activity of the HPA axis during pregnancy. CRH, corticotropin releasing hormone; AVP, vasopressin; ACTH, adrenocorticotrophic hormone; GCs, glucocorticoids; HPA, hypothalamic-pituitary-adrenal axis. Parts of the figure have been modified based on images from SMART (Servier Medical Art, <http://smart.servier.com/>).

During pregnancy, the placenta also produces CRH in both the maternal and fetal compartments. The placental CRH is identical structurally and functionally to the one from

the hypothalamus and can exert the same effects on ACTH production and thus increases peripheral cortisol release from the adrenal glands of the mother. In contrast to the negative feedback loop that glucocorticoids stimulate in the hypothalamus, maternal and fetal glucocorticoids during pregnancy increase the production of CRH from the placenta. This creates a positive feedback loop and thus leads to higher levels of basal maternal and fetal HPA axis activation and in turn to higher production of glucocorticoids (Figure 1b) [11], [16].

In fact, from the end of the 1st trimester to the end of gestation placental CRH production increases 40-fold, the pituitary gland of the mother doubles in size and cortisol levels increase 3- to 5- fold [11], [17]. In parallel, the CRH-binding proteins (CRH-BP) and the GCs-binding proteins (corticosteroid-binding globulin- CBG) decrease [18], [19]. During the first two trimesters of pregnancy, these binding proteins are present in the maternal and fetal plasma at concentrations that greatly exceed the ones of CRH, in the case of CRH-BPs, or of GCs, in the case of CBGs. They function by binding their ligands thereby making them inactive. Close to the end of gestation, in the last three weeks, their concentrations drop resulting in free forms of CRH and GCs which can exert their functions [19]. It is considered that the decrease in the binding proteins along with the concomitant increase of their ligands, CRH and GCs, trigger the onset of parturition [18].

In addition to parturition, elevated levels of CRH and GCs during the end of gestation have been implicated with a plethora of other functions. They are associated with fulfilling energetic needs of the mother by stimulating hepatic gluconeogenesis and with suppressing inflammation [20]. They help with fetal lung maturation by stimulating the production of surfactant-associated proteins which help lower the surface tension and participate in innate lung immunity [21]. In addition, they have been shown to contribute to the development of the brain by affecting, among others, neuron to neuron and neuron to glia interactions [22] and synaptic properties [23].

These massive changes in the maternal and fetal HPA axes highlight the importance of glucocorticoids for the development of the fetus. In turn, these observations suggest that glucocorticoids outside of the physiological range could have profound implications on development but also on postnatal function.

1.3 Glucocorticoids as mediators of environmental exposures

1.3.1 Environment and maternal HPA axis

The fact that prenatal environmental exposures have a large impact on offspring neuro-behavioral and physiological outcomes after birth is largely accepted, but the mediation of these effects by maternal glucocorticoids is less clear [6]. In humans, the picture is

complex. If the HPA axis does really mediate the effects of maternal psychopathology, for example, we would expect to find increased levels of circulating glucocorticoids in response to maternal stress and mood symptoms. This is less true, with studies reporting non-existent or very small effects on maternal glucocorticoid levels due to stress [17]. As already mentioned, human pregnancy is accompanied with sharp increases of cortisol close to term, in response to CRH production from the placenta, leading to increased functioning of the maternal HPA axis even under physiological environments. Thus, the already high functioning maternal adrenal cortex could have reduced capacity to respond to environmental exposures, in turn dampening the effects of the environment on maternal HPA axis activity.

This introduces though the concept of divergent effects of the same exposures during different time-windows of development. Maternal HPA axis hyperactivity is a feature specific to later pregnancy, with the highest levels of placental CRH and cortisol found in the third trimester [11]. That could mean that the effects of the environment on maternal HPA axis and in turn mother to embryo glucocorticoid signaling could be different early on in human pregnancy, when placental CRH production is low.

1.3.2 Glucocorticoids as mediators of environmental outcomes

Animal studies support this idea. Placental CRH release is a unique feature of humans and some primates, thus we can assume that in rodents, for example, environmental exposures effects on HPA axis activity and glucocorticoids circulation would not be dampened at any time-point during gestation [24]. In fact, a plethora of animal studies have shown that maternal stress effects are mediated by glucocorticoid signaling from the mother to the fetus [16], [17], [25], [26]. Exogenous administration of ACTH or glucocorticoids has been shown to mimic prenatal stress effects at all levels [17], [26]. Barbazanges *et al.* [27], studied the effects of stress and maternal corticosterone on offspring HPA axis activity, using repeated restraint stress at the last week of pregnancy of adrenalectomized or not rats with or without corticosterone substitution. They found that blocking maternal corticosterone secretion suppressed the prolonged stress-induced corticosteroid response of the offspring, usually found as a response to prenatal stress. Interestingly, corticosterone substitution in adrenalectomized mothers reinstated the effects of the stressor on the offspring HPA axis activity, providing a clear indication that maternal glucocorticoids are, at least in part, an important mediator of prenatal environmental exposures effects to the embryo.

In fact, a phylogenetic meta-analysis of prenatal stress on offspring glucocorticoids across 14 vertebrate species, including mammalian, primates and non-primates, reptilian and avian species, found a positive effect of prenatal stress on glucocorticoids, indicating

that HPA axis reactivity to prenatal stress is evolutionary ancient and conserved [28]. Thus, increased glucocorticoid signaling during pregnancy seems to be at least one of main mediators of environmental exposures, like prenatal psychopathology and stress, effects during prenatal development.

1.3.3 Circular effects of glucocorticoids on offspring HPA axis

The levels of circulating glucocorticoids can also increase due to effects on the fetal HPA axis. Prenatal excess of glucocorticoids has been shown to directly impact the fetal HPA axis, leading to increased basal functioning and reactivity in the offspring [29], [30]. In turn, imbalances in physiological HPA axis activity have been extensively associated with neurobehavioral alterations, highlighting the importance of this system [31]. Prenatal glucocorticoids have been associated with increased basal plasma corticosterone levels of the offspring. This effect has been connected with two processes: first, a reduction in the density of *Nr3c1* and *Nr3c2* (genes encoding the GR and MR, respectively) in the hippocampus of the offspring [32]. These steroid receptors are implicated in the negative feedback loop that inhibits the hormonal stress response [30], thus their reduction leads to higher basal fetal HPA axis activation (Figure 2b). Second, studies have associated prenatal excess of glucocorticoids with increased placental CRH release [16]. Placental CRH, in turn, activates the maternal and fetal HPA axis, enhancing the positive feedback loop that results in higher glucocorticoid levels (Figure 1b). CRH itself has also been shown able to cross the blood-brain barrier and influence the function of the fetal brain and specifically of the hippocampus [30].

A plethora of studies have provided evidence for circular effects of glucocorticoids on fetal HPA axis activity. Low dose dexamethasone treatment during late pregnancy in sows resulted in increased levels of plasma ACTH and cortisol concentrations for the offspring [33] and effect true also in rats [34]. Moreover, in humans, prenatal synthetic glucocorticoids exposure increased the offspring's cortisol responses and HPA-axis function to a postnatal stressor in the first 2 days of life. The infants that received glucocorticoids earlier in pregnancy (mid-gestation) had significantly higher cortisol responses than infants with later gestational exposure [35], highlighting that different gestational time-windows may confer divergent effects on postnatal phenotypes. So prenatal glucocorticoid excess is not only associated with increased basal functioning of the offspring HPA axis but also with increased reactivity to postnatal stressors, highlighting a cycle whereby prenatal excess of glucocorticoids increase fetal HPA axis activity leading to even higher levels of them and resulting in high basal activity after birth. This in turn creates a bigger response to a secondary stressor, thus altering the physiological responses of the offspring hormonal stress axis.

1.3.4 Altered placental functioning increases glucocorticoids

Another mechanism via which the prenatal environment can increase glucocorticoid signaling is through the placenta. Physiologically, during pregnancy the placenta acts as a biological protective barrier for the embryo from the circulating maternal cortisol. The fetal part of the placenta, and the fetal brain in fact, express an enzyme important for the protection of the fetus from glucocorticoids, 11 β -hydroxy-steroid dehydrogenase type 2 (11 β -HSD2) [36]. 11 β -HSD2 catalyzes the transformation of active cortisol in humans and corticosterone in rodents to their inactive forms (cortisone and 11 β -dehydrocorticosterone respectively). This results in a significant decrease of the amounts of maternal to fetal glucocorticoid signaling, with as little as 3-10% of them reaching the fetus [6].

A cortisol tracer study in an *ex vivo* placental perfusion model found only 3% of the maternal cortisol reaching the fetal circulation. This number increased to 7.3% when the activity of 11 β -HSD2 was inhibited [37]. This highlights the importance of 11 β -HSD2 for the placenta barrier but it also shows that the placenta is not impermeable and that there must exist additional protective mechanisms. In fact, there are a number of other enzymes such as p-glycoprotein and three adenosine triphosphate binding cassette transporters that also protect the fetus from high maternal cortisol levels [36], [37].

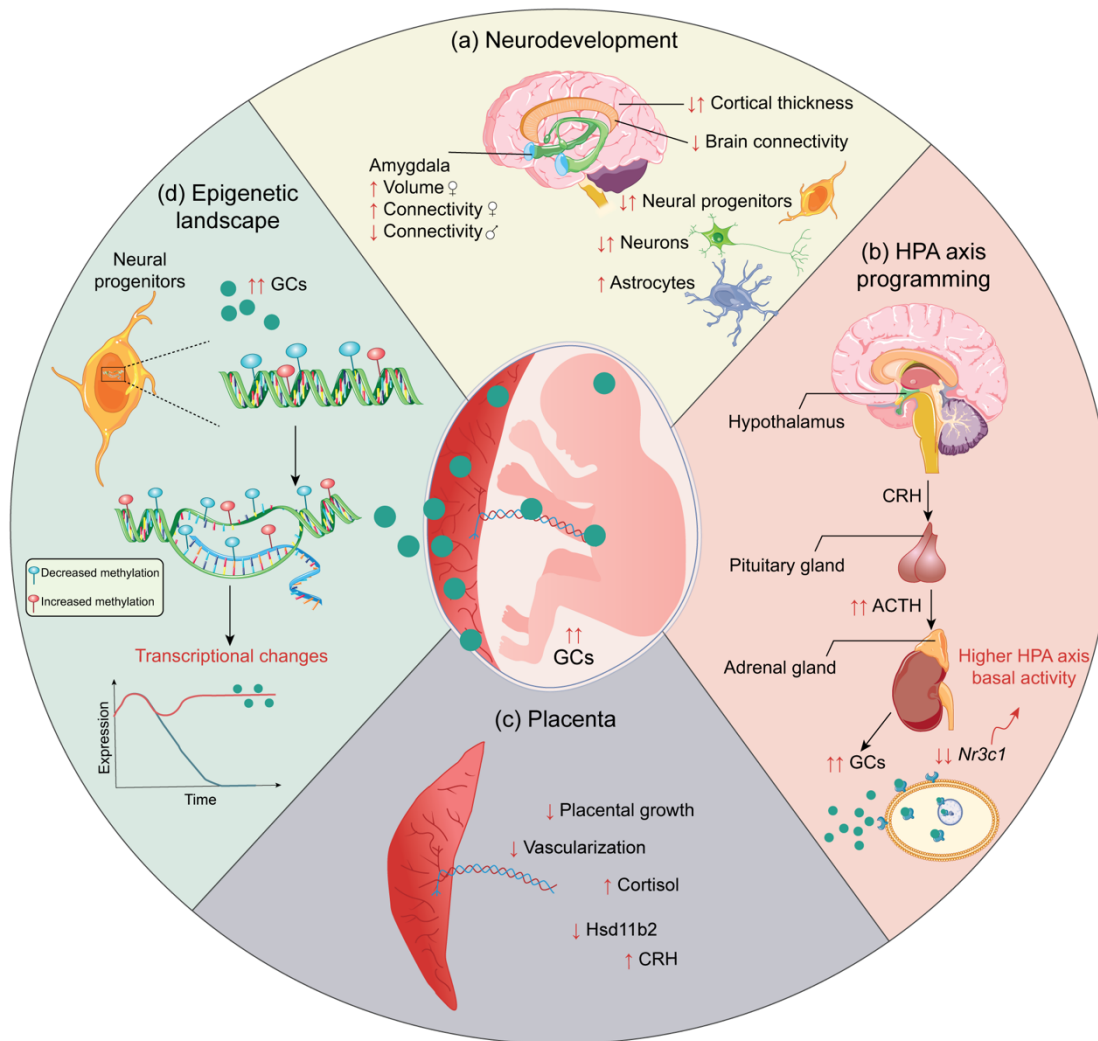


Figure 2| Glucocorticoid effects on multiple organ systems during development. **a**, Glucocorticoid excess impacts the developing brain at the cellular architecture and brain-region levels. **b**, Glucocorticoid excess results in high basal functioning and reactivity of the offspring HPA axis. **c**, Glucocorticoid excess impacts the ability of the placenta to act as a protective barrier. **d**, Embedding of glucocorticoids effects can be mediated via the epigenetic landscape. HPA, hypothalamic-pituitary-adrenal axis; CRH, corticotropin releasing hormone; AVP, vasopressin; ACTH, adrenocorticotrophic hormone; GCs, glucocorticoids; HSD11 β 2, 11 β -hydroxysteroid dehydrogenase type 2. Parts of the figure have been modified based on images from SMART (Servier Medical Art, <http://smart.servier.com/>). Figure modified from Krontira *et al.*, TINS, 2020 [26].

Interestingly, environmental stimuli seem to circumvent this protective barrier. Studies have found that high prenatal Trait anxiety is negatively correlated to *11 β -HSD2* placental mRNA expression and activity [38]. Along the same lines, it has been shown that prenatal stress, in the form of prenatal restraint stress, or other physiological stressors such as tail-cuff blood pressure test, in the last days of pregnancy in rodents resulted in reduced placental mRNA expression of *11 β -Hsd2* [39]. In addition to the actual effects of the prenatal environment on *11 β -HSD2*, elevated glucocorticoids have been shown to inhibit placenta vascularization, resulting in reduced placental growth and as a consequence incomplete protective barrier [40] (Figure 2c). Thus, high prenatal stress and

anxiety can lead to increased fetal exposure to glucocorticoids, result of reduced expression and activity of *11 β -HSD2* and of inhibited placental growth.

1.3.5 Antenatal corticosteroid treatment

Excess of glucocorticoids prenatally can also result from antenatal corticosteroid treatments. The physiological sharp increase of endogenous glucocorticoids during the 3rd trimester is the basis for the use of antenatal corticosteroid treatment in pregnancies at risk for preterm birth. Thus, synthetic glucocorticoids, like betamethasone and dexamethasone, are extensively used in western medicine to boost fetal organ maturation, given the importance of physiological glucocorticoids on organ development. Synthetic glucocorticoids are administered as early as the 22nd gestational week (GW) and up to 34th GW, when there is a risk for preterm delivery within seven days, to help with fetal lung maturation [41]. The guidelines propose the use of either two doses of 12mg betamethasone given intramuscularly 24 hours apart or four doses of 6mg dexamethasone, intramuscularly, every 12 hours.

In addition, they are prescribed to pregnancies that are at risk for congenital adrenal hyperplasia (CAH) [42]. CAH is an autosomal recessive disorder characterized by impaired cortisol synthesis, which affects 1 in 10,000 to 1 in 15,000 births, being one of the most common autosomal recessive disorders in humans. It is caused by mutations in genes encoding enzymes important for the production of steroid hormones by the adrenal cortex, including glucocorticoids and sex hormones, like androgens, estrogens and progestogens. In 95% of the cases it is due to deficiency of the enzyme 21-hydroxylase, which catalyzes the biosynthesis of aldosterone and cortisol and leads to prenatal androgens' excess. This, in turn, poses a risk for virilization of female fetuses [43]. The most common treatment is dexamethasone administration aiming to suppress fetal androgen production and thus reduce or ameliorate virilization symptoms. The guidelines propose the use of dexamethasone, starting before the 7th GW, so mid- first trimester, in mothers who previously had a child suffering from CAH, to prohibit the formation of the labioscrotal folds. The genetic test to define if the fetus indeed suffers from CAH is done at the beginning of the 2nd trimester. Only then the decision is made about the treatment which will continue throughout gestation only for female pregnancies homozygous for the mutations. That means that in two out of three cases the corticosteroid treatment, given for approximately five weeks already, was a precaution measure and not in fact needed [42]. The guidelines propose the use of 1.5mg per day [44].

The treatment plan for antenatal corticosteroids remains the same since it was first proposed in 1972, with multiple aspects of the plan, including drug choice, dose and treatment interval, never systematically evaluated [45]. Synthetic glucocorticoids are poor

substrates of the placental protective enzymes (see “Placental functioning under environmental exposures” section, *page 7*), thus they have the ability to cross the barrier freely, resulting in very high penetration in the fetal compartments [26]. The doses given to pregnant mothers are very large and designed to persist for an extended period of time, surpassing two weeks [45]. This is one additional mechanism of how excess of glucocorticoids can happen during gestation. Given the ability of synthetic glucocorticoids to elude the natural protective barriers, their use should be cautious.

Thus, glucocorticoid signaling to the fetus outside of the normal range can result both from maternal mood disorders and from antenatal corticosteroid use. A plethora of evidence exists on associations of glucocorticoids themselves or of environmental stimuli with postnatal phenotypes for the offspring at the behavioral and somatic levels. The molecular mechanisms that could mediate these effects are a large research field given the complexity of the biological mechanisms responsible for the interactions of the environment with somatic processes.

1.4 The complex biology of environmental effects embedding

1.4.1 Epigenetic embedding of environmental exposures effects

One of the mechanisms shown to embed the effects of glucocorticoids at the molecular level is epigenetics [46], [47] (Figure 2d). Epigenetics describe the mechanisms that control the expression of genomic information without including any changes on the actual DNA sequence and provide more mechanistic insights into environmental effects.

In the early 2000s a potential molecular mechanism of how the environment can impact the epigenetic landscape was proposed by studying the effects glucocorticoids on transcription of the liver-specific tyrosine aminotransferase (*Tat*) in rat’s liver cells during development. *Tat*’s expression rises physiologically close to term to fight against the hypoglycemic conditions. It was shown that glucocorticoids, either as dexamethasone treatment of a liver cell line *in vitro* or as the physiological surge of corticosterone in rat liver closing to term *in vivo*, resulted in a stable DNA demethylation of cytosines in the promoter region of the gene, followed by reversible chromatin remodeling. During development the demethylation happens before the expression of *Tat* and, as shown *in vitro*, it creates epigenetic memory that results in three to five times increased expression of it compared to naïve cells after a second hormonal stimulation [48].

This study is one of the first to describe a potential molecular mechanism of how glucocorticoids affect transcription and importantly to reveal the existence of stable epigenetic changes that can affect future transcriptional responses. For the nervous system, a study using a human hippocampal immortalized neuronal progenitor cell line and a complex

scheme of dexamethasone treatment either during proliferation and differentiation or only during differentiation with or without a recovery period of three weeks of no treatment at all, showed that although the transcriptional changes caused by dexamethasone are mostly alleviated by the recovery period, DNA methylation changes persist and affect genes that play roles in neurogenesis, organ development, transcription and neuronal differentiation. Confirming the observation of enhanced *Tat* responses to a second exposure, they also showed that the demethylation events created a “poised” state that resulted in stronger transcriptional responses to a future exposure. Interestingly, by creating a poly-epigenetic risk score using 24 CpG sites, result of cross-referring the CpG sites with dexamethasone-induced altered methylation in the hippocampal line and dexamethasone-associated changes in human blood samples, they found a significant association of dexamethasone effects with maternal anxiety, highlighting the importance of glucocorticoid signaling for prenatal stress effects via the epigenetic landscape [49]. These results provide important mechanistic insights on how environmental exposures including glucocorticoids may mediate their effects on neurodevelopmental and neurobehavioral alterations. Apart from epigenetic changes, one other aspect that contributes to the puzzle is genetic moderation.

1.4.2 Gene by prenatal environment interactions

Psychiatric and neurobehavioral outcomes arise from the complex interaction of the environment with genetics [50], an effect not different for prenatal and postnatal exposures [65,66].

Glucocorticoids have been shown to interact with different haplotypes in the *FKBP5* (FK506 binding protein 5) locus, an important gene of the glucocorticoid response, to shape its epigenetic state dynamically on a single CpG level. The effect of an acute dexamethasone exposure was tested in 228 CpGs in blood samples of healthy individuals at baseline and after the exposure with high accuracy targeted bisulfite sequencing (HAM-TBS) of the *FKBP5* locus. Methylation levels of the majority of CpGs, mostly located near a GR-binding site, were decreased following dexamethasone and returned to baseline after 23 hours. Interestingly, for more than half of the CpGs the dexamethasone-induced methylation changes were dependent, in an additive or interacting way, of the allele genotype with higher methylation changes for the risk allele carriers. This underlines the importance of the genotype for DNA methylation sensitivity to GR activation [52]. Notably, another study in human blood of *FKBP5* risk allele carriers has described a genotype-dependent increase of *FKBP5* transcription via a three-dimensional chromatin loop in individuals that had experienced early life child abuse [53]. Another study on the effects of various prenatal environmental factors and genotypes on DNA methylation

of newborns showed that SNPs (single nucleotide polymorphisms) close to a variably methylated region interacted with the prenatal environment to better describe the methylation changes (GxE explained 40,58% of the variance whereas genotype only explained 29.98%). The environmental factors that had the biggest impact were betamethasone treatment, maternal age and metabolism, and in fact the SNPs that contributed to these effects were enriched for psychiatric disorders such as autism and attention-deficit disorder [54].

These studies provide important mechanistic insight of how glucocorticoids and early life stressors interact with genetics to alter the epigenetic landscape, thus translating the effects of the environment on the molecular level. The interaction of the environment with the genetic and the epigenetic landscape is an important molecular mechanism for the intergenerational transmission of prenatal environmental exposures, leading to lasting effects on offspring neurobehavioral state and HPA axis function but also on the structure and function of the nervous system after birth.

1.5 Prenatal environment and neurobehavioral outcomes

The effects of the prenatal environment on offspring neurobehavioral outcomes have been long discussed in the literature. Birth weight, a proxy of the intrauterine environment, has been associated with increased risk for ADHD, impairments in executive function, reduced educational attainment and increased frequency and severity of depression and psychosis-like symptoms [6]. Birth weight is an interesting measure but it mirrors a variety of prenatal environments, neurodevelopmental trajectories and fetal genetics. Focusing on prenatal maternal stress has also revealed a plethora of adverse effects on offspring behavior including temperament alterations, cognitive impairments and motor functioning, all of which are associated with higher psychiatric risk [55]. In fact, maternal distress has been associated with increased risk for internalizing and externalizing symptoms, anxiety, depression and conduct problems of the offspring [7]. A prospective longitudinal study of the Avon Longitudinal Study of Parents and Children cohort showed that prenatal maternal anxiety and depression were significantly associated with higher emotional and behavioral symptoms and a two-fold increase in the risk of mental disorder in offspring, with no diminished effects sizes till adolescence [56]. Maternal stress is an important environmental exposure but its effects are also confounded by the maternal genetic landscape. Pure environmental exposures have also been associated with intergenerational outcomes. For example, epidemiological research on birth cohorts from the Dutch Hunger Winter of 1944, when food intake was dramatically reduced, showed that offspring of women who were pregnant at the time had a two-fold increased risk for schizophrenia and major affective disorders in adulthood [57], [58] (Figure 3).

In addition to complex environments, prenatal excess of glucocorticoids has also been associated with effects on behavior, cognitive functioning and psychiatric risk for the offspring after birth (Krontira *et al.*, TINS, 2020 [26] and [59]). Late gestation dexamethasone treatment in rats was associated with impaired copying with adverse environments later in life [60]. Importantly, antenatal corticosteroid treatment has been associated with increased risk for neurodevelopmental and psychiatric disorders after birth. A large retrospective cohort study of more than 529,000 singleton infants born at term studied the effects of synthetic glucocorticoid administration (treatment according to the guidelines -between the 22nd and 34th GWs) on neurodevelopmental outcomes at five years of age. The outcomes measured were audiometry, visual testing and physician's diagnosis of neurocognitive disorders. They found a statistically significant increase in the cumulative rate of any neurodevelopmental problem and specifically of neurocognitive disorders associated with synthetic glucocorticoids treatment [61]. Another very large retrospective cohort study of more than 670,000 singleton term births in Finland analysed the effects of antenatal corticosteroid treatment on risk for any mental and behavioral disorder the first ten years of life [62]. Treatment exposure was significantly associated with higher risk of any mental and behavioral disorder, as diagnosed using ICD-10 (International Statistical Classification of Diseases and Related Health Problems, Tenth Revision) (Figure 3).

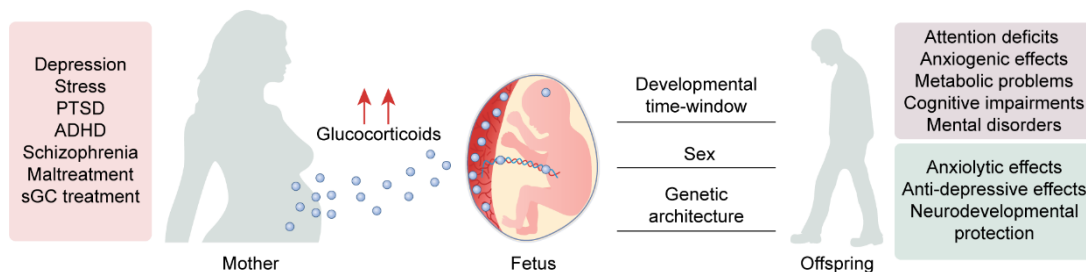


Figure 3| Neurobehavioral outcomes of prenatal environmental exposures. A plethora of prenatal environments, including stress-related psychiatric disorders and antenatal corticosteroid treatment, have been associated with mostly adverse postnatal outcomes for the offspring. The developmental time-window of the exposure, the sex of the fetus and its genetic architecture have been shown to mediate these effects. Prenatal exposures early on in the pregnancy have also been associated with neuroprotective outcomes, while exposures later in gestation are mainly associated with adverse postnatal outcomes. sGC, synthetic glucocorticoids. Figure modified from Krontira *et al.*, TINS, 2020 [26].

While the adverse neurobehavioral and psychiatric effects of the prenatal environment and of glucocorticoids specifically are very well characterized, divergent effects have been reported in the literature associated with the developmental time-window of exposure [63]. There is evidence to suggest that in early pregnancy the actions of glucocorticoids can be both positive and negative whereas in late pregnancy they tend to be on the adverse side [64]. In fact, the majority of the studies already discussed focus on stressors after the second trimester whereas the two biggest studies [61], [62] on the

effects of antenatal corticosteroid treatment probably include offspring of pregnancies treated after the 25th GW, as they state. Studies both in humans and in animal models of glucocorticoid administration early on in the pregnancy have painted a different picture for their effects, with potentially beneficial outcomes. A recent meta-analysis including more than 1,25 million children, researched the effects of antenatal corticosteroid treatment on neurodevelopmental disorders, including neurodevelopmental delay, metabolic and cardiorespiratory outcomes in children born at term or preterm [65]. They found that a single course of glucocorticoid treatment in children that were born extremely preterm, between 22 and 27 GWs [66], was associated with significant reduction in risk of neurodevelopmental impairments, whereas for children born at term it was associated with higher risk of any mental and behavioral disorders. In humans, neurogenesis peaks at approximately 20 GW and is largely completed by the 28th GW which indicates that for the aforementioned study at least a part of the pre-term born children were treated during the neurogenic period. In fact, animal studies corroborate such divergent effects. In mice, dexamethasone administration at E14.5 (embryonic day 14.5), during neurogenesis, resulted in anxiolytic and anti-depressive effects for the adult offspring [67].

These studies indicate the importance of developmental time-windows for the effects of the environmental exposures, pointing to possible protective effects when the exposure is early in the pregnancy, possibly during the neurogenic period (Figure 3). In turn, exposures during the period that is responsible for the production of the main cell type of the adult brain, the neurons, could mean that effects at the structural level, for example brain regions size and thickness, could be possible.

1.6 Prenatal environment and brain structural outcomes

The fact that glucocorticoids can impact brain structure has been described in the literature. Even in adulthood, stress and glucocorticoids can affect brain structure at the cellular level with reported effects on dendritic spine density in the cortex, the hippocampus and the amygdala [68]. Prenatal environmental exposures have also been associated with a variety of brain structural outcomes for the offspring after birth (Figure 2a). Maternal childhood maltreatment was associated with lower offspring intracranial volume, primarily due to global differences in cortical gray matter [69]. Maternal prenatal stress was associated with reduced cortical thickness mainly of the frontal and temporal regions and elevated depressive symptoms at 7 years of age for the offspring [70]. Glucocorticoids have also been associated with structural effects on the brain of the offspring. This is true both for physiological variations in glucocorticoid amounts among pregnant women and developmental time-windows and for non-physiological excess of glucocorticoids, either as a result of complex exposures or of antenatal corticosteroid treatment. Larger

right amygdala volume in children at 7 years of age was associated with higher physiological maternal cortisol levels at 15 GWs. One unit increase of cortisol was associated with 6.4% of increased amygdala volume in girls but not in boys, highlighting sex-specific differences [71]. Elevated maternal cortisol concentrations have also been associated with stronger amygdala connectivity to regions involved in sensory processing, resulting in higher internalizing symptoms in females but not in males [72]. These studies point to the importance of physiological variation of glucocorticoids during gestation on offspring brain structure and function, especially associated with sensory processing and specific to girls.

Non-physiological levels of glucocorticoids have also been associated with structural effects. Repeated antenatal glucocorticoid therapy in offspring born at term was associated with lower cortical surface area and folding, in a small sample size of 10 infants [73]. Glucocorticoids have also been associated with cortical thickness. In a lifespan sample of 21,251 participants, aged 4 to 97 years old, cortical thickness of 34 regions was inversely correlated with the expression of both the glucocorticoid- (*NR3C1*) and mineralocorticoid- (*NR3C2*) receptor genes [74], whereas neuroactive steroid levels were positively correlated with gray matter thickness in multiple regions of the cingulate, parietal and occipital cortices [75]. Higher maternal cortisol levels during the 3rd trimester were associated with greater child cortical thickness primarily in frontal regions [76], whereas in adult MDD patients a complex pattern of increased cortical thickness in some areas, like the cingulate and prefrontal cortex, and decreased cortical thickness in other areas, like the temporal and frontal gyrus, has been described [77].

Thus, divergent effects of disease, prenatal environment and glucocorticoids have been reported for brain structural measurements but what is consistent is that there are effects at a brain-region level. The observed effects on cortical thickness point to a possible impact of the prenatal environment on neurogenesis, since this is one of the main mechanisms that can result in substantial differences in amounts of neurons leading to thickness phenotypes.

1.7 Cerebral cortical development in rodents and humans

1.7.1 Cortical development length in humans and rodents

The development of the cerebral cortex of mammals is an intricate process that consists of sequential steps that depend on each other to define the fate of the cells produced and lead to the final six-layered architecture of the cortical column. While the fate decisions per se are very similar between the murine and the human cortex, significant differences exist on developmental timings. Human pregnancy lasts approximately 40

GWs, which equals to ~280 days, with the human brain developing over the course of gestation starting from approximately the 4th GW with the neurulation. In contrast, murine pregnancy lasts 19 to 20 days, with neurulation starting at approximately E3 [78].

The vast difference in duration of pregnancy results in large changes of developmental timings for the fate decisions processes (Figure 4). Neurogenesis is the process of the birth of neurons from neural progenitor cells. In humans it lasts approximately 131 days, from the ~10th to the ~28th GW, thus spanning the time from mid-first trimester to the beginning of the third trimester. In contrast, mice have a much shorter neurogenic period which lasts approximately 9 days, from E10 to E18-E19.5 [79], [80].

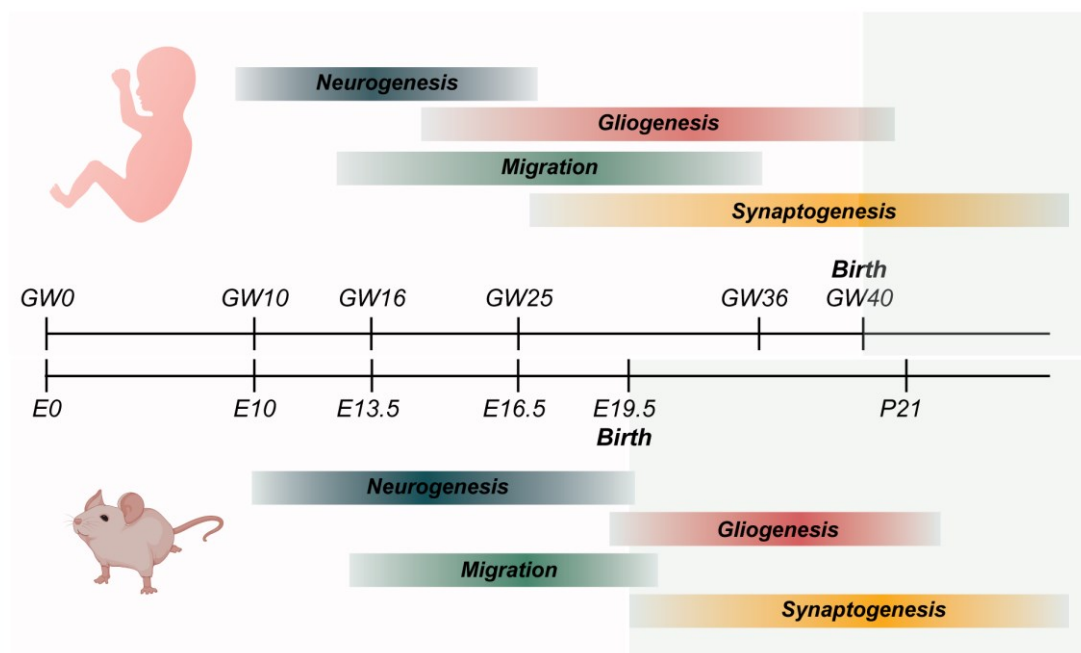


Figure 4| Developmental timeline of the fate decisions processes for the human and mouse cerebral cortex. Fate decision processes are very similar across mammals but human and mouse pregnancy have very different lengths. Human pregnancy lasts approximately 280 days and the mouse one 20. This leads to very different timelines for the fate decision processes. GW, gestational week; E, embryonic day. Figure inspired from [81] and [78]. The mouse icon is used with permission from Biorender.com.

In turn, neuronal migration in humans starts at approximately GW 18 and finishes at approximately GW 36, whereas in mice it starts at ~E14 [81]. The onset of gliogenesis, the process of glial cell production, follows neurogenesis. In mice these periods are almost completely temporally separated whereas in humans they happen in parallel for a long period of time [79]. Lastly, synaptogenesis, the process of creating functional synapses, in mice occurs almost in whole postnatally whereas in humans it starts in the third trimester and proceeds well into the postnatal life, even up to ~3.5 years of age [80].

Hence, humans exhibit a substantial increase of the neurogenic period in comparison to rodents. The increase in the length of the neurogenic period coupled with the change of

the primate basal progenitors to cells that can self-amplify in addition to generating neurons (a process discussed in the section below: “Temporal sequence of cortical neurogenesis”, *page 18*) is considered a hallmark of primate neurogenesis and determines the much bigger final number of neurons produced. In fact, humans have the most expanded neocortex in relation to body size from all other mammals, which contains 16 to 26 billion neurons, nearly 20% of the total neuronal number of the whole brain including the cerebellum [79].

1.7.2 Temporal sequence of cortical neurogenesis

The structure of the neocortex in six cytoarchitecturally distinct layers arises during the neurogenic period, which in all mammals, but the ferret, is concluded prenatally (Figure 5). The neocortex originates from a single layer of neuroepithelial cells that reside in the outmost apical part of the ventricular zone (VZ) and divide symmetrically to create the apical Radial Glia (aRG) [82]. aRGs are progenitor cells that populate the VZ. They have apico-basal polarity with the apical process contacting the ventricular surface and the basal process the basal lamina [82]. aRGs undergo symmetric proliferative divisions, thus producing two daughter cells of the same type, symmetric consumptive divisions, thus producing two basal progenitors (BPs- next maturity level progenitor type), asymmetric self-renewing divisions, thus producing one aRG and one BP and asymmetric consumptive divisions producing an intermediate progenitor (IP- a type of BP) and a neuron (a process called direct neurogenesis) [83]. aRGs divide in the VZ and their soma moves in an apico-basal fashion during the cell cycle phases, with it being closest to the apical side of the VZ for mitosis and closest to the basal side for S phase, a process that is called interkinetic nuclear migration [79], [83].

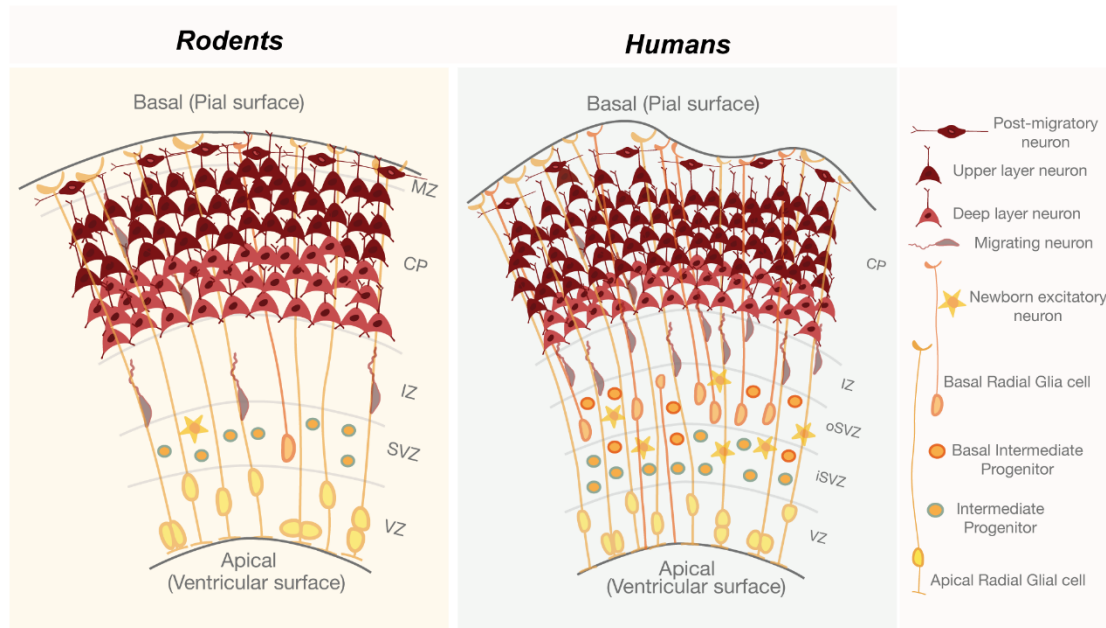


Figure 5] Neurogenesis in lissencephalic and gyrencephalic species. Gyrencephalic species, like humans, display an expansion of the SVZ which is populated by bRG cells that are very rare in lissencephalic species, like rodents. These cells have the ability to self-renew in addition to producing neurons, thus vastly increasing the neurogenic potential. VZ, ventricular zone; SVZ, subventricular zone; iSVZ, inner subventricular zone; oSVZ, outer subventricular zone; IZ, intermediate zone; CP, cortical plate; bRG, basal Radial Glia cell.

BPs populate the subventricular zone (SVZ), which is located basally in regards to the VZ and is the progenitor zone that exhibits the biggest expansion in gyrified species (species that have folded brains like primates, including humans, in comparison with smooth brain species like rodents, which are called lissencephalic species). The SVZ contains various types of BPs with different shapes and proliferative capacities. In lissencephalic species the most abundant type of BP is IPs, which exclusively express *Eomes* (also known as *Tbr2*), are non-polar and mostly divide once to generate two neurons. In addition to IPs, two more types of BPs are found. The basal RGs (bRGs, also known as outer RGs- oRGs) [84] which exhibit radial morphology with an apical and/or basal process and have high proliferative capacity, being able to perform all types of divisions that the aRGs can [85], [86] and basal IPs (bIPs) which are non-polar cells like the IPs but, in contrast to them, can also undergo all types of divisions as the aRGs and the bRGs [85], [87], [88]. These BPs are very rare in lissencephalic species but they are abundant in gyrencephalic ones, including humans [89], primates like chimpanzees, non-human primates like macaques [87] and in ferrets [90], [91]. The gyrencephalic-enriched BPs have a complex expression pattern of the RG marker *PAX6* and the IP marker *EOMES* [85]. The vast increase of these highly proliferative progenitors led to a secondary expansion of the SVZ in gyrencephalic species where it's subdivided in inner SVZ (iSVZ) and outer SVZ (oSVZ) [92].

The expansion of the germinal zones allows for a much bigger clonal size resulting from a single VZ-progenitor and thus leads to a higher number of neurons produced in gyrencephalic compared to lissencephalic cortices. In turn, the cortical projection neurons, which are produced locally from the progenitors already discussed, will migrate radially to their final place in the cortical plate (CP) using the processes of the progenitor cells as scaffold, while the interneurons migrate tangentially from their place of birth in the ganglionic eminences [93]. In the end, the excitatory and inhibitory neurons will result in the six-layered cytoarchitecture of the cortex known in adulthood.

1.8 Prenatal environment and neurogenesis

As already discussed endogenous and excess of glucocorticoids are important of brain development. Their effects, though, have rarely been studied on mammalian cortical neurogenic processes. Glucocorticoid effects on neurogenesis have been studied mainly in the context of postnatal hippocampal neurogenesis, where the majority of studies associate stress and elevated glucocorticoids with reduced proliferation and neuronal production [94]. Two studies from Anacker and colleagues using a human hippocampal progenitor cell line has shown dose-dependent divergent effects of glucocorticoids on proliferation which however always result in decreased neuronal differentiation. Low concentrations of cortisol (100nM) increased proliferation and decreased neurogenesis, in an MR-dependent manner, whereas high concentrations of cortisol (100 μ M) had the opposite effect on proliferation but still resulted in decreased neuronal differentiation, an effect dependent on the GR [95]. The authors associated these effects with enhancement of the Notch/HES signaling pathway and inhibition of the TGF β -SMAD2/3 and Hedgehog signaling pathways, as assayed by pathway enrichment analysis of gene expression data. In a subsequent study they pinpointed *SGK1* (serum and glucocorticoid-inducible kinase 1), a GR-responsive gene, as the mediator of the high cortisol induced reduction in proliferation [96]. The contrary effect was shown for neurogenesis on stress responsivity. In mice, increasing neurogenesis in the ventral dentate gyrus of the adult hippocampus conferred resilience to chronic stress by causing a decrease in the activity of stress-responsive cells, as assayed by *in vivo* Ca⁺ imaging of mature granule cells [97]. Thus, the literature suggests that at least for the hippocampus, neurogenesis is an important target of stress and glucocorticoids and that increasing it results in a protective effect from the neurobehavioral effects of stress.

The very few studies existing on glucocorticoids and cortical neurogenesis, which as discussed is concluded during the prenatal period, are centered around the use of 2-dimensional induced-pluripotent stem cells (iPSCs) derived models of progenitors and neurons. There the effect of glucocorticoids has consistently been shown to increase

progenitors' proliferation in a GR-dependent manner [67], [98]. One study of dexamethasone administration in mice at E14.5, which is in the neurogenic period of mice, found a significant increase of RG (Pax6+) and IP (Eomes+) cells, an effect that resulted in higher number of deep and upper layer neurons [67]. Interestingly they showed that dexamethasone administration during neurogenesis was associated with anxiolytic and antidepressant effects for the adult offspring, highlighting the neurogenic period as a potential developmental time-window that can mediate beneficial outcomes in response to environmental exposures, even ones that are known to mediate adverse outcomes when administered during other developmental windows.

1.9 Modeling the human developing cerebral cortex

Unravelling the mechanisms that underlie and modulate human cerebral cortical development has been a main focus of research. Given the scarcity and difficulty in finding and using human fetal post-mortem brain samples, scientists have turned to modeling. Animal models have been extensively used for many years. Rodents are widely used since their developmental processes share a lot of similarities with the human ones and genetic manipulations can be easily done in different developmental timings and with different ways [99]. Nevertheless, rodents are lissencephalic animals thus lacking the abundance of different BPs and the extensive expansion of the SVZ and of the CP, as already discussed. To fill these gaps, scientists work with other gyrencephalic species like macaques [87], ferrets [90], [91], [100], [101] and sheep [86]. Gyrencephalic species are valuable but, being bigger animals, they are difficult to maintain, expensive to use and at the basis they do not carry the human genetic code. This is an important point since we know that apart from human neoteny in neurogenic processes and the cytoarchitecture of the cortex, the genetic and epigenetic landscape differ with species-specific regulatory elements modulating gene expression patterns [102]. The past decade technological advances have allowed the creation of human 3-dimensional (3D) models of different regions of the brain, called organoids, from cultured embryonic stem cells or induced pluripotent stem cells (iPSCs) [103]–[112].

Brain organoids, or the more scientifically correct terms cerebral organoids (hCOs), cortical organoids, hippocampal organoids etc., are not models of the whole human brain. As the more specific names state they model regions of the brain. The most abundant protocols are focusing on cortical modeling [105], [109], [111], [113], while the efforts for modeling more than one regions are now focusing on assembling organoids of different regions in what is called assembloids [103], [104]. Organoids do not recapitulate all aspects of the human developing cortical cytoarchitecture but they do bear all cell types found in the human cerebral cortex, organized in layers resembling the human cortex

(Figure 6). In addition, originating from human stem cells, they have the genetic landscape of humans.

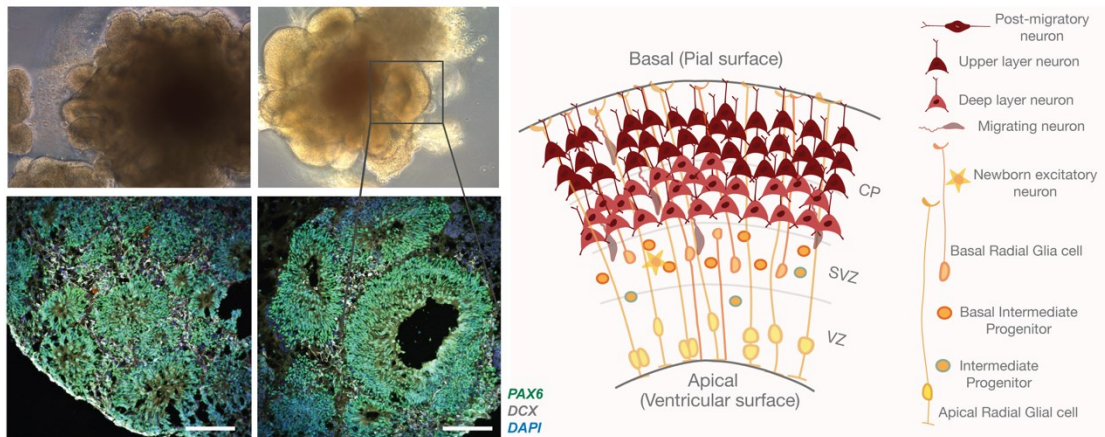


Figure 6| Human cerebral organoids from induced pluripotent stem cells. hCOs bear a number of ventricles which have different sizes and shapes but share a similar architecture, having all the cells found and enriched in the human developing cortex. hCOs, human cerebral organoids; PAX6, marker of radial glia cells; DCX, marker on newborn neurons; VZ, ventricular zone; SVZ, subventricular zone; CP, cortical plate.

When focusing on hCOs, so organoids made to model the cerebral cortex, there seem to exist two main schools of thought in making them. The first one focuses on un-patterned organoids, where the iPSCs are left to self-assemble into embryoid bodies (EBs), that include the three germ layers endoderm, mesoderm and ectoderm followed by a subsequent enrichment of the neuroepithelium guided by the intrinsic self-organizational cues and capacity provided by the cells and their environment [114], i.e. the medium they are grown into. Following that, they mature into 3D models that resemble the cellular architecture of the dorsal and ventral human developing cortex via media changes without the addition of signaling molecules [113]. The second one focuses on patterned cortical organoids of either dorsal or ventral identities [109], made by combining media changes with specific signaling molecules activating and repressing molecular pathways important for neurodevelopment and lineage specification. Both protocols have merits, with the first one being more unbiased and theoretically able to create organoids with different cortical regions (for example dorsal and ventral) in the same entity but running the risk of higher variability between organoids and the second one being more consistent and able to mature quicker but forcing the tissue to a specific fate not in the way that physiologically the process takes place.

The cerebral/cortical organoid ventricle shows the expected layering, with progenitor cells closer to the apical side, in the ventricular-like-zone (VZ), and neurons closer to the basal side in the cortical-like-plate (CP). The different progenitor types are also layered with the RG population in the VZ and the BPs located more basally in the subventricular-like-zone (SVZ). In addition, organoids bear all the BP types that are enriched in humans

but are rare in lissencephalic species (Figure 6), which are also located in the SVZ. Organoids show a rudimentary layering of the cortical plate with deep layer neurons closer to the apical side and upper layer neurons closer to the basal one. Single-cell sequencing studies have compared cell composition and differentiation lineages in organoids and fetal cortex and found that these share expression profiles [115]–[117] providing a level of validity for modeling the human developing cortex [107], [118]. Cerebral/ cortical organoids are thought to model the first and early second trimester stages of neurodevelopment, which as discussed is the developmental window that includes neurogenesis in humans. Nevertheless, scientists have cultured organoids for extensive periods of time showing that some neurons can make synapses and reach the maturity level of early postnatal periods [119].

On the other hand, organoids have many downsides too. The layers of the ventricle are compressed in a small space, they lack overlaying tissue and meninges, there is a level of variability between ventricles, they lack vascularization and body axes and, for most protocols, glial cells are scarce. These all are limitations of the model which should be considered when designing experiments with them so as for the correct controls to be included.

Nevertheless, 3D human models of the developing brain's different regions are valuable given their ability to contain the cell types of gyrified species in a meaningful 3D architecture and that they bear the human genetic landscape. Organoids are one additional model that, together with the animal ones, can be used to study the developing cortex in health and disease and in response to environmental stimuli.

2 | Rationale and Objectives

Prenatal exposures to environmental stimuli are extensively associated with health outcomes for the offspring after birth, both for physiology and behavior. Endogenous glucocorticoids are important for fetal organ maturation, including the brain. Excess of glucocorticoids can be a result of maternal psychopathology but also of antenatal corticosteroid treatments, used for lung maturity in at risk for premature birth pregnancies or administered throughout gestation for congenital adrenal hyperplasia. Thus, glucocorticoids are a prevalent prenatal environmental stimulus. The majority of studies investigating the roles of glucocorticoids have focused on exposures related to late pregnancy, often after the end of neurogenesis, and associate excess of glucocorticoids with adverse neurobehavioral outcomes. Interestingly, there seem to be divergent effects when glucocorticoid exposures take place early in development, during the neurogenic period, with potentially beneficial postnatal neurobehavioral outcomes. The effects of the environment and specifically glucocorticoids on mammalian embryonic cortical neurogenesis have rarely been studied. Importantly, a mechanistic and cellular detailed dissection in complex models of the human cortex is still lacking.

The work presented in this thesis aimed to dissect the effects of glucocorticoids on mammalian neurogenesis at the cellular and molecular levels and on associations to postnatal phenotypes. More specifically this work was centered around three aims:

- i. To analyse the effects of glucocorticoids on neurogenic processes and the cellular architecture of the developing cortex, using human 3-dimensional cerebral organoids and mouse model systems.
- ii. To define the molecular and signaling pathways mediating these effects.
- iii. To study how glucocorticoids interact with genomic and epigenomic regulatory mechanisms to determine postnatal long-term outcomes of the altered neurogenic processes.

Thus, this body of work was aimed at elucidating the neurogenic processes affected by prenatal administration of glucocorticoids with a focus on mammalian brain development and ultimately, at understanding how the prenatal environment can shape postnatal outcomes via effects on early neurodevelopment.

3 | Materials and Methods

All reagents used for all experiments are listed in Supplementary Table 13.

3.1 Induced Pluripotent stem cells

Line 1 human induced pluripotent stem cells (hiPSCs), derived from skin fibroblasts of a female donor [120], [121], were obtained from the RIKEN BRC cell bank. Line 2 hiPSCs were derived from NuFF3-RQ newborn foreskin feeder fibroblasts of a male donor [122]. MTA approvals were obtained. Matrigel-coated (1:100 diluted in DMEM-F12) 6-well cell culture plates were used for hiPSCs culturing in mTESR1 Basal Medium supplemented with 1x mTESR1 Supplement at 37°C with 5% CO₂. Passaging was done with Gentle Cell Dissociation Reagent. RevitaCell Supplement (1:100 diluted) was used the day of the dissociation to increase cell survival.

3.2 Cerebral organoids

Human cerebral organoids (hCOs) were created as previously shown by Lancaster *et al* [113] with some modifications. The first step was dissociating the hiPSCs in StemPro Accutase Cell Dissociation Reagent. Next, 9,000 single cells were plated into Ultra-low attachment 96-well plate round bottom wells in human embryonic stem cell medium (hESC, DMEM/F12-GlutaMAX with 20% Knockout Serum Replacement, 3% FBS, 1% Non-essential amino acids, 0.1 mM 2-mercaptoethanol) supplemented with 4 ng/ml human recombinant FGF and 50 µM Rock inhibitor Y27632 for 4 days to form embryoid bodies (EBs). They were cultured in hESC medium without bFGF and Rock inhibitor for an additional 2 days to form embryoid bodies (EBs). On day 6, neural induction started by changing the medium to neural induction medium (NIM, DMEM/F12 GlutaMAX supplemented with 1:100 N2 supplement, 1% Non-essential amino acids and 1 µg/ml Heparin) and the EBs were cultured for an additional 6 days. Approximately on day 12 (according to the EBs morphology), the EBs were embedded in Matrigel drops and transferred to 10-cm cell culture plates in neural differentiation medium without vitamin-A (NDM-A, DMEM/F12GlutaMAX and Neurobasal in ratio 1:1 supplemented with 1:100 N2 supplement 1:100 B27 without Vitamin A, 0.5% Non-essential amino acids, insulin 2.5 µg/ml, 1:100 Antibiotic-Antimycotic and 50 µM 2-mercaptoethanol) for 4 days to create hCOs. On day 16, hCOs were transferred onto an orbital shaker in NDM+A medium (same composition as NDM-A with the addition of B27 with Vitamin A in the place of B27 without Vitamin A) and were grown in these conditions at 37°C with 5% CO₂. NDM+A medium was changed twice per week.

3.3 Plasmids preparation

Multiple PCR inserts were simultaneously cloned by In-Fusion HD Cloning Plus into the linearized vector pCAG-DsRed2 (Addgene, #15777) to create the pCAG-ZBTB16-F2A-GFP plasmid. The human ZBTB16 ORF (NM_006006.5, 2034bp) sequence was amplified from a plasmid delivered from GenScript and the F2A-GFP from the Snap25-LSL-2A-GFP vector (Addgene, #61575). PCR primers were designed for the sequence of interest with extensions that are complementary to the ends of the linearized vector or the corresponding fragment (Supplementary Table 2). PCR was performed using the CloneAmp HiFi PCR Premix following manufacturer's instructions

After cloning the fragments for 3 h at 37°C, the new construct was transformed into StellarTM competent cells and grown for 16 h on agar plates containing 100µg/ml ampicillin. Single colonies were picked, plasmidic DNA was isolated with Qiagen plasmid kits and the genotype was checked with Sanger sequencing (Supplementary Table 2). The pCAG-F2A-GFP plasmid was created by cutting the ZBTB16 fragment out of the pCAG-ZBTB16-F2A-GFP plasmid using the BamHI and BglII restriction enzymes (Supplementary Table 2).

3.4 *In utero* electroporations of mice

All experiments and protocols were performed in accordance with the European Communities' Council Directive 2010/63/EU and were approved by the committee for the Care and Use of Laboratory animals of the Government of Upper Bavaria. All mice were obtained from the in-house breeding facility of the Max Planck Institute of Psychiatry and kept in group housed conditions in individually ventilated cages (IVC; 30cm x 16 cm x 16 cm; 501 cm²) serviced by a central airflow system (Tecniplast, IVC Green Line – GM500). Animals had ad libitum access to water and standard chow and were maintained under constant environmental conditions (12:12 hr light/dark cycle, 23 ± 2 °C and humidity of 55%).

Saline solution containing fentanyl (0.05 mg per kg body weight), midazolam (5 mg per kg body weight), and medetomidine (0.5 mg per kg body weight) was used to anesthetize the mothers by injected them intraperitoneally. The electroporation was done on E13.5 embryos as described in Nature Protocols by Saito *et al* [123]. In brief, Fast Green (2.5 mg/µL) was mixed with plasmids and injected at a concentration of 1 µg/µl. The DNA was electroporated into the cells by delivering 5 pulses applied at 40V for 50ms in 1sec intervals. The anesthesia was terminated by injecting buprenorphine (0.1 mg per kg body weight), atipamezole (2.5 mg per kg body weight), and flumazenil (0.5 mg per kg body weight). The brains were fixed at 3dpe and 6dpe (days post electroporation) in 4% PFA

(paraformaldehyde) for 16 h, cryo- preserved with 30% sucrose for at least 16 h and stored at -20°C in OCT. For immunofluorescence, 12 μm cryosections were prepared on SuperFrost™ slides.

3.5 Electroporations of human cerebral organoids

Line 1- hCOs were kept in antibiotic-free NDM+A medium for 3 h prior to electroporation. Day 43 hCOs were electroporated. The hCOs were collected and fixed 7 days post electroporation. During the procedure, an electroporation chamber was placed under a stereoscope. hCOs were placed in the chamber and using a glass microcapillary of 1–2 μL , Fast Green together with plasmid DNA was injected into different ventricles. Subsequently, 5 pulses of 80 V for 50 ms each with 500 ms intervals were applied to the hCOs. Following electroporation, hCOs were kept in antibiotics-free NDM+A media for an additional 24 h. Then, they were changed into the normal NDM+A media for 7 more days until fixation. hCOs were fixed using 4% PFA for 1 hour at 4°C , cryo- preserved with 30% sucrose for 16 h and stored at -20°C in OCT. For immunofluorescence, 16 μm cryosections were prepared on SuperFrost™ slides.

3.6 Glucocorticoid treatment

3.6.1 Human Cerebral Organoids

Day 43 hCOs of both lines were treated for 7 days with 100nM of dexamethasone (dex). To achieve the concentration used, dex was diluted in DMSO (dimethyl sulfoxide) in a concentration of 100 μM and subsequently diluted in NDM+A culture medium to a final concentration of 100nM. The DMSO control (vehicle- veh) underwent the same dilutions as described for dex. The medium was changed every two days. At the end of the treatment, hCOs were fixed using 4% PFA for 1 hour at 4°C , cryo- preserved with 30% sucrose for 16 h and stored at -20°C in OCT. For immunofluorescence, 16 μm cryosections were prepared on SuperFrost™ slides.

3.6.2 Fetal mice

I injected fetal mouse brains at E13.5 (embryonic day 13.5) with dex diluted in DMSO and analysed the effects at E16.5. To achieve $\sim 100\text{nM}$ of dex concentration I measured the volume of E13.5 mouse brains, by measuring the volume displaced when they are submerged in saline, to $\sim 25\mu\text{l}$. Thus, I injected 1 μl of 2.5 μM dex or veh into an E13.5 mouse brain ventricle to achieve a final concentration of $\sim 100\text{nM}$. For the effect of dex on *ZBTB16* transcription at least five different fetal mouse brains were analyzed per condition. After brain isolation both cortices were excised and RNA was isolated.

3.7 Immunofluorescence

The sections were post-fixed with 4% PFA for 10 min at RT. Sections were permeabilized with 0.3% Triton in PBS for 5 min. Subsequently, blocking was done with 0.1% TWEEN, 10% Fetal Bovine Serum and 3% BSA for 1 h at room temperature. Blocking solution was used to dilute the primary and secondary antibodies (Supplementary table 1) and nuclei were visualized using 0.5 µg/mL 4,6-diamidino-2-phenylindole (DAPI). Primary antibodies were incubated for 16 h at 4°C and subsequently secondary antibodies were incubated for 1 h at room temperature. Aqua Poly/Mount was used to mount the cover slips. For PAX6, EOMES, BCL11B, ZBTB16, SOX2, Ki-67, TBR1 and SATB2 antigen retrieval was performed prior to the post-fixation with PFA. For that, incubation with citric buffer (0.01 M, pH 6.0) for 1 min at 720 Watt and 10 min at 120 Watt was done, then the sections were left to cool down at RT for 20 min, water contents were restored with a 20 min incubation in half water half citric buffer solution and, finally, the sections were washed three times with PBS for 5 min.

3.8 Image analysis and Quantifications

Immunostained fluorescent stainings were visualized using a Leica laser-scanning microscope and analyzed with FIJI ((Fiji Is Just) ImageJ 2. 1. 0/1.53c; Java 1. 8. 0_172[64 bit]) [124]. For analysis of the hCOs, I included ventricles that fulfilled the following criteria: clear ventricular structure with elongated, radially-organized cells surrounding the ventricular zone (VZ- determined with DAPI staining), at least one cell electroporated in the VZ (for electroporation experiments) and expression of PAX6 and EOMES to define dorsal cortical ventricles. Cell counting was performed in one representative plane of a z stack using the cell counter tool in FIJI. For electroporations binning analysis was done.

3.8.1 Human cerebral organoids

Electroporations of hCOs: For each experiment, at least seven independent ventricles from at least five different Line 1-hCOs generated in three independent preparations grown in different times were analyzed. Analysis of the *ZBTB16* phenotype in the electroporation experiments was performed by always comparing hCOs electroporated with *ZBTB16*-F2A-GFP plasmid vs F2A-GFP control plasmid from the same batch of organoids. Throughout the area of the electroporation, bins were set as follows: the maximal distance between the most migrated GFP-positive cell and the apical surface of the ventricle was measured and divided into three equally-heighted bins. Bin A is mainly comprised of the VZ, bin B of the outer-most basal part of the VZ and the SVZ and bin C of

the CP. As normalization I used the number of GFP-positive cells in total or per bin as specified in each section.

Dexamethasone effects on hCOs: For each experiment, at least twelve independent ventricles from at least six different Line 1-hCOs and at least five independent ventricles from at least three different Line 2-hCOs, generated in two independent preparations per hiPSC line grown in different times were analyzed. Analysis of the dex phenotype was performed by always comparing hCOs grown in parallel in the same batch. For analysis of the dex effects in hCOs, VZ and SVZ were defined by the cell shape and proximity to the apical zone. The VZ area presented elongated, radially-organized cells positive for radial glia markers (PAX6, SOX2) but not for basal progenitors' markers (EOMES). The area on top, assigned as SVZ, was positive for basal progenitor markers. Areas were defined and measured in FIJI using the ROI Manager tool. As normalization I used the measured area's surface.

3.8.2 Fetal mice

In utero electroporations: For each experiment and condition, at least eight mouse cortical sections from five different embryos collected from two littermates were analyzed. For analysis of the *in utero* electroporations in mice, I did binning analysis. A cortical column that had the majority of electroporated cells was chosen and the bins were set as follows: the maximal distance between the most migrated GFP-positive cell in the cortical plate and the apical surface of the ventricle was measured and divided by five. The width of the bin was the width of the 40x lens image and it was the same for all sections and mice. As normalization I used the number of GFP-positive cells in total or per bin as specified in each section. For the non-cell autonomous phenotype analysis, total number of cells, not including the GFP cells, were counted and the data were normalized using a z-score process by normalizing each mouse data over the average, using the standard deviation, of the control mice data using the STANDARIZE function of Excel.

3.9 Protein isolation and Western blot

All steps of the protein isolation were done on ice. 40 μ l of 1x RIPA buffer supplemented with protease and phosphatase inhibitors were added to samples and a p-200 pipette was used to break down the hCOs. An insulin syringe was used to further disrupt the tissue. Samples were spun down at 13000 rpm at 4 °C for 15 min. The supernatant containing the protein was transferred to a new tube and stored at - 80 °C. For each experiment three biological replicates were included each bearing the homogenate of

three individual hCOs. The protein concentration was determined using the Bradford assay. Samples and 1x RIPA buffer were diluted 1:150. A standard curve (STD) was prepared using a 1 mg/ml BSA solution at different concentrations from 0-15µg/ml. Duplicates of all samples and the STD (100µl) were loaded to a transparent 96- well plate. 50µl of 1:1 diluted in PBS Protein-Assay solution (Bio-Rad, 5000006) were added. UV absorbance was measured with the Epoch Microplate Spectrophotometer (BioTek) at 595nm. 25µg of protein was diluted in 5µl Roti Load and the remaining volume with autoclaved milliQ water to reach 22µl, the protein solutions were vortexed and incubated at 95 °C for 5 minutes, stored on ice for 5 minutes and centrifuged at maximum speed at 4 °C for 5 minutes. 20µl of the samples and 6µl of a 180kDa protein ladder were loaded to the prepared 8 % gel. Electrophoresis was conducted in the BIO-RAD Electrophoresis Chamber (1658006FC) at 120V. 1x transfer buffer was prepared by adding 200 ml of 10x towbin buffer and 300 ml of 100 % methanol to 1.5l milliQ water. The PVDF membrane was activated by incubating it 15 seconds in 100% methanol, 2 minutes in milliQ water and then at least 5 minutes in 1x transfer buffer. The blot was assembled as follows: sponge, filter papers, PVDF membrane, gel, filter papers, sponge. Air bubbles were removed, and everything was put in a transfer chamber filled with 1x transfer buffer and a cool block. The blotting was performed for at least 16 h at 4 °C at 25V. After the transfer, the membrane was incubated first in 100 % methanol for 15 seconds and then dried for at least 15 minutes followed by Ponceau staining. The membrane was completely destained by incubating in 1x TBST for 10 min at 23 °C. Subsequently, the membrane was blocked for 1 hour at 23°C in 5 % milk powder in 1x TBST. Primary antibodies were diluted in 5 % milk powder. The membrane was incubated with the primary antibodies for at least 16 h at 4°C shaking. The next day, the membrane was washed three times with 1x TBST. Secondary antibodies were diluted in 5% milk powder solution and the membrane was incubated with the secondary antibodies for 1 hour at 23°C on a shaker. Subsequently, the membrane was washed three times for 5 minutes with 1 TBST. The dilutions for all antibodies used can be found in (Supplementary Table 1). The membranes were incubated in a 1:1 mixture of HRP Substrate Luminol Reagent and HRP Substrate Peroxide Solution for 5 minutes. Imaging was performed using the Bio-Rad ChemiDoc XRS+ System. For each membrane, a colorimetric image, and a series of chemiluminescence images with increasing exposure time in high sensitivity mode were acquired. The quantification was performed in the Bio-Rad Image Lab Software (Version 6.1). Relative protein expression levels were quantified and normalized with ACTIN as endogenous gene.

3.10 RNA isolation and quantitative PCR

The RNeasy Mini extraction kit was used according to the manufacturer's instructions for total RNA extraction. For each experiment three biological replicates were included each bearing the homogenate of three individual hCOs. The Maxima H Minus Reverse Transcriptase with oligo(dT)₁₆ primers and random hexamers in a 1:1 ratio was used for complementary DNA (cDNA) synthesis. Quantitative PCR (RT-qPCR) reactions were run in technical quadruplicates using PrimeTime qPCR Primer Assays (Supplementary Table 2) and PrimeTime® Gene Expression Master Mix on a LightCycler 480 Instrument II (Roche). Relative gene expression levels were quantified using the relative quantification method and normalized with POLR2A and YWHAZ as endogenous genes.

3.11 Luciferase reporter assays

Luciferase assays were designed to assess the activity of the three human *PAX6* promoters [125], P0, P1 and Pa, under ZBTB16 overexpression. The promoter sequences were cloned into the firefly luciferase (Luc2) reporter expression pRP vector by VectorBuilder. The human ZBTB16 expression plasmid was generated by VectorBuilder using the pRP backbone. 500ng of total plasmid DNA (75% of human ZBTB16 expression plasmid, 15% of reporter plasmid and 10% of the pCAG-F2A-GFP, as internal control of transfection efficiency) were transfected into 72000 HeLa cells in a well of a 24 well plate using Lipofectamine 2000 following manufacturer's instructions. All transfections were carried out in triplicates. HeLa cells were cultured in DMEM-F12 medium supplemented with 10% FBS and 1x Antibiotic-Antimycotic. The medium was refreshed the next day and 48 h after transfected cells were PBS washed and incubated for 15 min at RT in 1x passive lysis buffer. Plates were kept at least 1 hour at -80°C. Next, the lysate was scraped and centrifuged at full speed for 30 sec at 4°C. 20µl of the supernatant was subjected to the luciferase assay with the addition of 50 ul D-luciferine (Beetle Juice luciferase assay) by using a Tristar multimode reader (Berthold). The luminescence measurement was done for 5 sec with 2 sec delay. In addition, 50µl of the lysate were assessed for GFP fluorescence. The luciferase reading was normalized over the GFP results for each well. Data is shown as fold changes over the control plasmid.

3.12 CRISPR-Cas9 editions of hiPSCs

CRISPR-Cas9 editing was used to create genomic deletions of the ZBTB16 exon 2 and of approximately 400 bp of the regulatory element centered on the rs648044 variant controlling ZBTB16 expression. Genome editing was done by electroporation of gRNA pairs

(crRNA/tracrRNA duplexes, alt-CRISPR IDT) and recombinant S.P. HiFi Cas9 V3 nuclease. crRNAs were designed using the Benchling webtool (<https://benchling.com>) and analysed for self- or heterodimers using the IDT OligoAnalyzer™ tool (<https://eu.idtdna.com/pages/tools/oligoanalyzer>) (Supplementary Table 12). To delete the region of interest, 300,000 Line 2 iPSCs were transfected with 35pmol of each gRNA (crRNA/tracrRNA duplex 1:1 in 1x Arci annealing buffer), 40pmol of Cas9 and 100pmol of electroporation enhancer in 26.57µl of the P3 primary cell 4D_X Kit S (Lonza, V4XP-3032) using the 4D-Nucleofector X Unit with the CA-137 program. Edited cells were plated into one well of 24-well plate coated with Matrigel 1:100 and cultured in supplemented mTESR1 Basal Medium and, for the day of the edition, with RevitaCell (1:100) at 37°C with 5% CO₂. For control editions, cells were electroporated with Cas9 without the addition of gRNAs. The next day the medium was changed to supplemented mTESR1 and cells were propagated approximately for 2-3 days till they reached 80-90% confluency. Next, cells were passaged into a well of a 6-well plate coated with Matrigel using Gentle Cell Dissociation Reagent and propagated until confluent. Subsequently, 89.5% of the cells were expanded, 10% of them were taken for bulk genotyping analysis and 0.5% were plated in a well of a 6-well plate coated with Matrigel to generate single-cell-derived clonal cell lines. Bulk and single cell DNA extraction was done using 30µl of QuickExtract DNA Extraction Solution. Briefly, cells were dissociated, pelleted, resuspended in the extraction solution and incubated at 65 °C for 10 min and 98 °C for 5 min. PCR was done using primers in Supplementary Table 2, the Q5 high fidelity master mix and 40ng of cell extract in a total volume of 10 µl. The thermal cycling profile of the PCR was: 98 °C 30 s; 35 × (98° 10 s, 65 °C 15 s, 72 °C 60 s); 72 °C 2 min. Automated electrophoresis technique (DNA screen tape analysis, Agilent) and Sanger sequencing (Eurofins, primers in Supplementary Table 2) were used to confirm the presence of CRISPR-Cas9-mediated knockout mutants in the bulk population and the single clones. For the ZBTB16 exon 2 edition I selected a heterozygous KO cell line (termed ZBTB16^{+/-} and ZBTB16^{+/+} for the control edition) showing by western-blot analysis a ~46% reduction in protein expression (Supplementary Table 1). The rs648044 is a heterozygous SNP in the iPSC cell line used (rs648044^{G/A}). From the edited single clones, I selected a heterozygous KO cell line of the enhancer element harboring only the G genotype (termed rs648044^{G/-} and rs648044^{G/A} for the control edition). The effect of the KO on ZBTB16 expression was assessed by RT- qPCR in veh and dex conditions and using POLR2A and YWHAZ for normalization (Supplementary Table 2).

3.13 Flow Cytometry

Line 2, ZBTB16^{+/+} and ZBTB16^{+/-} hCOs were collected for Flow Cytometry (FC) analysis at day 50 after 7 days of treatment with veh and 100nM dex and/or 1 μ M of the GR antagonist RU-486. Three to four samples per batch were analysed and each sample contained two individual hCOs. hCOs were enzymatically dissociated with accutase supplemented with DNase I at 37°C for maximum 40 min. During incubation, every 10 min the hCOs were additionally manually dissociated with a P1000 pipette. Once dissociated, the hCOs were centrifuged for 5 min at 300g and the pellet was resuspended in PBS. Next, cells were centrifuged and the cell pellets were fixed with 70% EtOH at -20°C for one hour. Subsequently, After the addition of 5ml washing buffer (PBS + 1% FBS) fixed cells were centrifuged for 30 min, at 4°C and 500g. The cell pellet was resuspended in 200 μ l staining solution (wash buffer supplemented with anti-PAX6 and anti-EOMES, Supplementary Table 1) and incubated for 30 min on ice. After the primary antibody incubation, 1ml of washing buffer was added and the stained cells were centrifuged for 30 min, at 4°C, at 500g. The cell pellet was resuspended in 200 μ l secondary antibody staining solution (wash buffer supplemented with anti-rabbit 488, anti-sheep 594 and DAPI, Supplementary Table 1) and incubated for 30 min on ice. The stained cells were filtered through an 100 μ m cell strainer and diluted in additional 200 μ l wash buffer. FACS analysis was performed at a FACS Aria (BD) in BD FACS Flow TM medium, with a nozzle diameter of 100 μ m. For each run, 20,000 cells were analyzed.

Gating strategy: SSC-A/FSC-A gates were used to exclude cell debris and FSC-H/ FSC-W to collect single cells. Gating for fluorophores was done using samples stained with secondary antibody only. The flow rate was set below 200 events/s.

3.14 Targeted Bisulfite Sequencing

Targeted bisulfite sequencing was performed following the original protocol [126]. DNA was isolated from day 50 hCOs that were treated with 100nM dex or veh for 7 days with the NucleoSpin Genomic DNA kit. 200ng of DNA from each sample were bisulfite treated in triplicate with the EZ DNA Methylation Kit. Twenty nanograms of bisulfite-converted DNA and 49 amplification cycles were then used for each PCR amplification (Supplementary Table 4) with the Takara EpiTaq HS Polymerase. Bisulfite converted triplicates were pooled and one PCR amplification was run for each amplicon and each sample. Quantification of PCR amplicons was done with an automated electrophoresis technique (2200 DNA screen tape analysis, Agilent), so that the amplicons could be pooled in equimolar quantities for each sample. Double size selection (200-500bp) was done with AMPure XP beads to remove primer dimers and high molecular DNA fragments. TruSeq

DNA PCR-Free HT Library Prep Kit was used according to the manufacturer's instructions to generate libraries. Each library was quantified with the Qubit® 1.0 (ThermoFisher Scientific), normalized to 4 nM and pooled. The Agilent's 2100 Bioanalyzer (Agilent Technologies) was used to check the library concentration and fragment sizes. Kapa HIFI Library kit was used to quantify the libraries. The Illumina MiSeq Instrument (Illumina) with their MiSeq Reagent Kit v3 (2Å~ 300 cycles) with the addition of 15% of PhiX Control v3 library was used to paired-end sequence the libraries.

3.14.1 Sequencing and Analysis of Targeted Bisulfite Sequencing

Sequencing was performed on an Illumina MiSeq system (Illumina, San Diego, CA) generating 300bp long paired-end reads. Reads were processed as described by Roeh *et al.* [126]. In brief, read quality was verified using FastQC [127], and cutadapt v1.11 [128] was applied to trim reads. Subsequently, reads were aligned to a restricted reference consisting of the amplicon sites using Bismark v0.18.2 [129]. Paired-end reads were stitched together using an in-house perl script. Using the R package methylKit v.1.6.3 [130] increasing Phred score quality cutoff to 30, methylation levels were extracted. Further filtering was conducted in R. On a per sample bases we excluded artifacts, low-coverage amplicons (sequencing coverage < 1000, 0 samples excluded) and samples with bisulfite conversion efficiency lower 95% (0 samples excluded). To test for significance individual CpGs of the same enhancer element were tested with two-way ANOVA and corrected for multiple comparisons with the two-stage step-up method of Benjamini, Krieger and Yekutieli.

3.15 Statistics

The statistical analysis was performed in GraphPad Prism (Version 9. 1.0 (2021)). Datasets were tested for normality with a D'Agostino & Pearson K2 Test. Groups were then compared with a t-test with Welch's Correction, a Mann-Whitney test, a two-way ANOVA with multiple comparisons corrected with the two-stage step-up method of Benjamini, Krieger and Yekutieli, or Fischer's exact test according to the type of data and distribution. The reported p-values are the corrected values. The representation means: ****: $p \leq 0.0001$, ***: $p \leq 0.001$, **: $p \leq 0.01$, *: $p \leq 0.05$, #: un-corrected $p \leq 0.05$, ns: $p > 0.05$.

3.16 Bulk RNA sequencing

RNA was isolated from day 45 Line 2- hCOs, in triplicates with 2-3 organoids per replicate, either treated with 100nM dex for 7 days or veh (DMSO). Libraries were made with the NebNext Ultra II Library kit with the ribosomal RNA eliminated with the rRNA Depletion kit, following manufacturer's instructions. Sequencing was performed on an Illumina

HiSeq4000 sequencer generating 150 bp long single-end reads. Read quality was verified using *FastQC* version 11.4 [127]. For adapter trimming and quality filtering the software *cutadapt* version 1.9.1 [131] was used. For read alignment and gene quantification *salmon* version 0.43.1 [132] was applied setting the parameters `noLengthCorrection` and `perTranscriptPrior` to account for the tag sequencing approach. Differential gene expression was assessed using the R package *DESeq2* [133].

3.17 ZBTB16 Expression UMAP Plots

Uniform Manifold Approximation and Projection plots (UMAP) [134] were used to visualize *ZBTB16* gene expression in a previously published single-cell RNA seq dataset (Cruceanu *et al.*, *AJP*, 2021 [135]). Specifically, *ZBTB16* expression was plotted in the day 30 and day 90 data subsets from cell-line 1 of the aforementioned dataset using the *SCANPY* [136] python package. The software environment and data processing used to produce these figures was identical to Cruceanu, Dony, Krontira *et al.*, *AJP*, 2021 [135].

3.18 STARR-qPCR

3.18.1 rs648044 cloning into STARR reporter plasmid

201 bp long DNA inserts (gblock, IDT) containing 200 bp putative regulatory element centered on the rs648044 (reference and alternative allele) and flanked by 15bp sequence homologous to the STARR reporter construct (Supplementary Table 3) were inserted by in-Fusion HD Cloning Plus into the human STARR-seq vector digested with *Sall* and *AgeI* following the manufacturer's instructions. The inserts had additionally 2bp to reconstitute the *AgeI* and *Sall* restriction sites lost during cloning. Subsequently, the constructs were transformed into Stellar™ competent cells and grown for 16 h on agar plates containing 100µg/ml ampicillin. Single colonies were picked, plasmidic DNA was isolated with Qiagen plasmid kits and the genotype was checked with Sanger sequencing (Supplementary Table 2).

3.18.2 U2OS-GR18 cells transfection

U2OS cells stably transfected with rat GR α (GR18 cells) [137] were cultured in Dulbecco's Modified Eagle Medium- high glucose supplemented with 10% FBS and 1x Antibiotic-Antimycotic. The Amaxa Nucleofector II Kit V was used to transfect two million cells with 2µg of plasmid in triplicates using the X-001 program (Lonza Bioscience). After 16 h cells were treated with 100nM dex or veh for 4 h. RNA was isolated with the RNeasy Mini extraction kit (Qiagen, 74104) according to the manufacturer's instructions.

3.18.3 cDNA conversion and qPCR

cDNA was generated using two gene specific primers for plasmid GFP and RPL19 as endogenous control (Supplementary Table 2) and the Quantitect Reverse Transcriptase kit following manufacturer's instructions. Regulatory elements activity was assessed with qPCR using primers for RPL19 and GFP (Supplementary Table 2). The qPCR was analysed with the relative quantification method and GFP expression was normalized over the RPL19 expression. Data are shown both as expression values and as fold changes (dex/veh).

3.19 Mendelian randomization and PheWAS study

All processing and analysis were conducted using R software [138]. To assess the potentially causal effect of *ZBTB16* on a range of phenotypes, rs648044 was used as genetic proxy with log fold-changes of the effect allele (A), averaged over STARR-qPCR experiments, ($\beta = 1.475794$, $SE = 0.1015$) used as exposure effect and variance estimates.

Outcome phenotype selection: Outcome phenotypes were selected from the MRC IEU OpenGWAS platform focusing on phenotype batches originating from the UK Biobank study, the NHGRI-EBI GWAS Catalog, and a GWAS on brain imaging phenotypes based on UK Biobank data (Supplementary Table 5) [139]–[142]. From the initial phenotype list originating from these batches, 8979 phenotypes from GWAS of European populations were selected after filtering out duplicates and phenotypes not of interest to this study (e.g., “Patient Care Technician responsible for patient data” or “Day-of-week questionnaire completion requested”). Duplicates were filtered using a semi-automated procedure including deletion of phenotypes with identical names and smaller GWAS sample size as well as manual filtering of phenotypes with high similarity in trait names (quantified using the restricted Damerau-Levenshtein distance >0.8 implemented in the stringdist package) [143]. This procedure resulted in a final phenotype list of 7503 phenotypes.

Mendelian randomisation analysis (MRa): The TwoSampleMR package was used for MRa [144]. Outcome data for rs648044 were extracted from phenotype summary data, which were available for 7323 outcomes, and effect and reference alleles were harmonised with exposure data. Wald ratio MRa estimation was applied as method of choice for single-SNP MR for all remaining outcome phenotypes [145]. To account for the multiple comparisons, P-values from all 7323 comparisons were corrected using the Benjamini-Hochberg method [146]. In results visualizations, the Bonferroni-corrected multiple comparison threshold is also provided as reference [147]. Scripts and data for PheWAS analyses are openly available via <https://osf.io/4ud6q/> for full transparency.

3.19.1 Illustration of PheWAS associations

Significant phenome-wide associations with brain region phenotypes were illustrated by overlaying human brain atlas regions as proxies of the regions of interest onto the MNI template in MRICroGI (version [v2.1.58-0](https://www.nitrc.org/projects/mricrogi/), <https://www.nitrc.org/projects/mricrogi/>). Due to the different analysis streams and granularities of the significant brain phenotypes, different atlases were used to portray the results (Supplementary Table 11). For illustration purposes, regions taken from probabilistic atlases were thresholded at 10 %. As a proxy for the circular insula ant thickness the “Hammersmith atlas” was used [148]. Medial lemniscus, cingulate gyrus part of cingulum, cingulum hippocampus, uncinate fasciculus, posterior limb of internal capsule, inferior fronto-occipital fasciculus, uncinate fasciculus, anterior corona radiata and the corticospinal tract were portrayed using the JHU ICBM DTI 81 white matter labels [149], the acoustic radiation was visualized using the Juelich histological atlas [149], the inferior longitudinal fasciculus, and the thalamic radiation by the JHU White Matter Tractography [150] and the superior thalamic radiation by the XTRACT HCP Probabilistic tract atlas [151].

3.20 GO enrichment of *DiffBrainNet* results

Enrichment of the *Zbtb16* differential network in the PFC was performed using FUMA GENE2FUNC [152] analysis based on Gene Ontology (GO, [153], [154]). Default parameters were used in FUMA, with all genes expressed above threshold in all brain regions in DiffBrainNet (n=12,830 genes- <http://diffbrainnet.psych.mpg.de/app/diffbrainnet>) as the background list. P-values were corrected using the Benjamini-Hochberg (FDR) method [155] to account for multiple comparisons. An FDR cut off of 5% was used for statistical significance.

4 | Results

4.1 Glucocorticoids impact the cellular architecture of the developing cortex

4.1.1 Human cerebral organoids have an active glucocorticoid receptor machinery

To gain a better understanding of the cellular and molecular underpinnings of glucocorticoid effects on the gyrencephalic-species enriched neurogenic processes I used hCOs as a model of human neurogenesis. I treated hCOs with dexamethasone and analysed the effects on the cellular, molecular and transcriptional landscape. The first step was to understand if hCOs have an active glucocorticoid-response machinery, by defining the expression pattern of the steroid receptors, GR and MR.

GR is expressed in a fraction of cells throughout the ventricular structure, from apical to basal side, the cortical plate and in stromal cells outside of the ventricle, while MR is very lowly expressed in hCOs (Cruceanu, Dony, Krontira *et al.*, 2021 [156]). GR protein is neither selective to one cell type nor ubiquitously expressed in all cells of each cell type but it is present in a variety of cell types, including the progenitor cells of the VZ and the neurons of the CP in hCOs (Figure 7b).

To model prenatal excess of glucocorticoids I chose to use dexamethasone for two reasons. Firstly, during development it is thought that MR is bound by physiological glucocorticoids, i.e. cortisol, that, as already discussed, are important for organ's maturation [157]. On the contrary, excess of glucocorticoids, in the context of maternal stress or antenatal corticosteroid treatment, are thought to act via GR. Dexamethasone binds with high affinity, approximately 30 times higher than cortisol, to the GR while it has little MR affinity [158]. Secondly, dexamethasone is the main synthetic glucocorticoid used as treatment in the context of antenatal corticosteroid therapy in pregnant women. Thus, by using dexamethasone, I was able to study both the specific glucocorticoid used during antenatal corticosteroid therapy and, in addition, the steroid receptor thought to respond to prenatal environmental exposures that cause glucocorticoid excess outside of the physiological range.

In order to define if hCOs have an active GR machinery, thus the GR is able to act as transcription factor when in presence of glucocorticoids, day 60 hCOs were treated with 100nM of dexamethasone for 12 hours and the GR patterns of expression and transcriptional effects were analysed with IF and qPCR (Figure 7a).

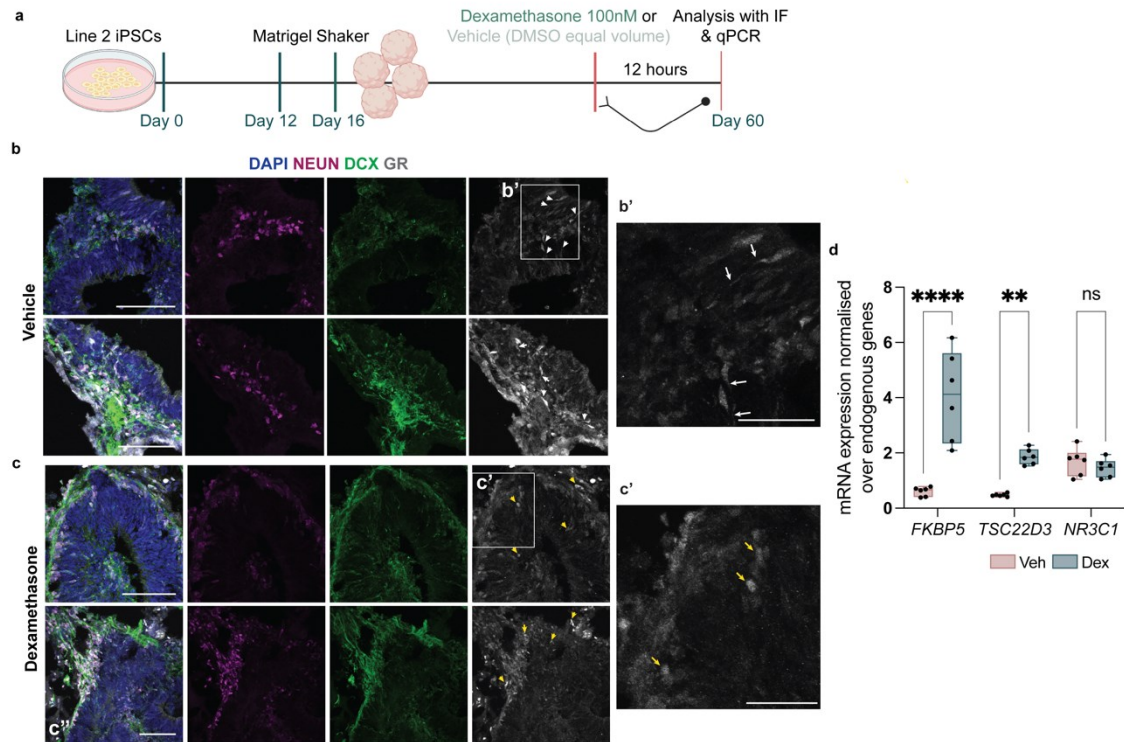


Figure 7 | Glucocorticoid receptor machinery in human cerebral organoids. **a**, Schematic of the treatment and analysis workflow in human cerebral organoids (hCOs). DMSO, dimethyl sulfoxide; IF, Immunofluorescence; qPCR, quantitative polymerase chain reaction. **b**, Representative images of GR expression in day 60 organoids in vehicle conditions. GR, glucocorticoid receptor; DAPI, 4',6-diamidino-2-phenylindole; NEUN, Neuronal nuclear antigen; DCX, Doublecortin; White arrows point to the cells with nuclear and cytoplasmic expression of GR; Scale bars, 100 μ m. **b'**, Zoom-in of cells exhibiting nuclear and cytoplasmic GR expression. **c**, Representative images of GR expression in day 60 organoids treated with dexamethasone. Yellow arrows point to cells with nuclear expression of GR; Scale bars, 100 μ m. **c'**, Zoom-in of cells exhibiting nuclear GR expression after dexamethasone stimulation. **d**, Normalised expression of known glucocorticoids-responsive genes in hCOs. FKBP5, FKBP Prolyl Isomerase 5; TSC22D3, TSC22 Domain Family Member 3; NR3C1, Nuclear Receptor Subfamily 3 Group C Member 1. P-values, as indicated by asterisks, were calculated using 2-way ANOVA with Benjamini, Krieger and Yekutieli multiple testing correction. Figures b' and c' are modified from Cruceanu, Dony, Krontira et al., *AJP*, 2021 [156].

GR was found both at the cytoplasmic and nuclear compartments under vehicle conditions (Figure 7b), but only at the nucleus after dexamethasone treatment (Figure 7c), pointing to an active molecular machinery able to fully activate GR. In fact, dexamethasone treatment leads to upregulation of the expression of known glucocorticoids-responsive genes, like *FKBP5* (FKBP Prolyl Isomerase 5) and *TSC22D3* (TSC22 Domain Family Member 3) whereas it does not affect the expression of GR (*NR3C1*, Nuclear Receptor Subfamily 3 Group C Member 1) (Figure 7d). This shows that hCOs have the ability to activate GR after glucocorticoids excess leading to changes of the transcriptional landscape of known glucocorticoids-responsive genes.

4.1.2 Glucocorticoids increase gyrencephalic species-enriched basal progenitors

Having seen that hCOs have an active glucocorticoids-response machinery I treated them at day 43 with 100nM of dexamethasone for seven days and started by analysing

the impact on the cellular landscape (Figure 8a). The concentration of dexamethasone was calculated as to approach the amounts passing from the pregnant mothers to the embryos as part of the antenatal corticosteroid treatment scheme (see Discussion for detailed explanation) and the length was chosen so as to be able to analyse effects both on progenitors but also on their progenies. Day 43 is a time-point in organoid's development that all the progenitor cell types are present, deep layer neurons' neurogenesis is at its peak and upper layer neurons' neurogenesis has started, thus it provides a time-point where dexamethasone effects can be monitored on multiple cell types of the developing cytoarchitecture.

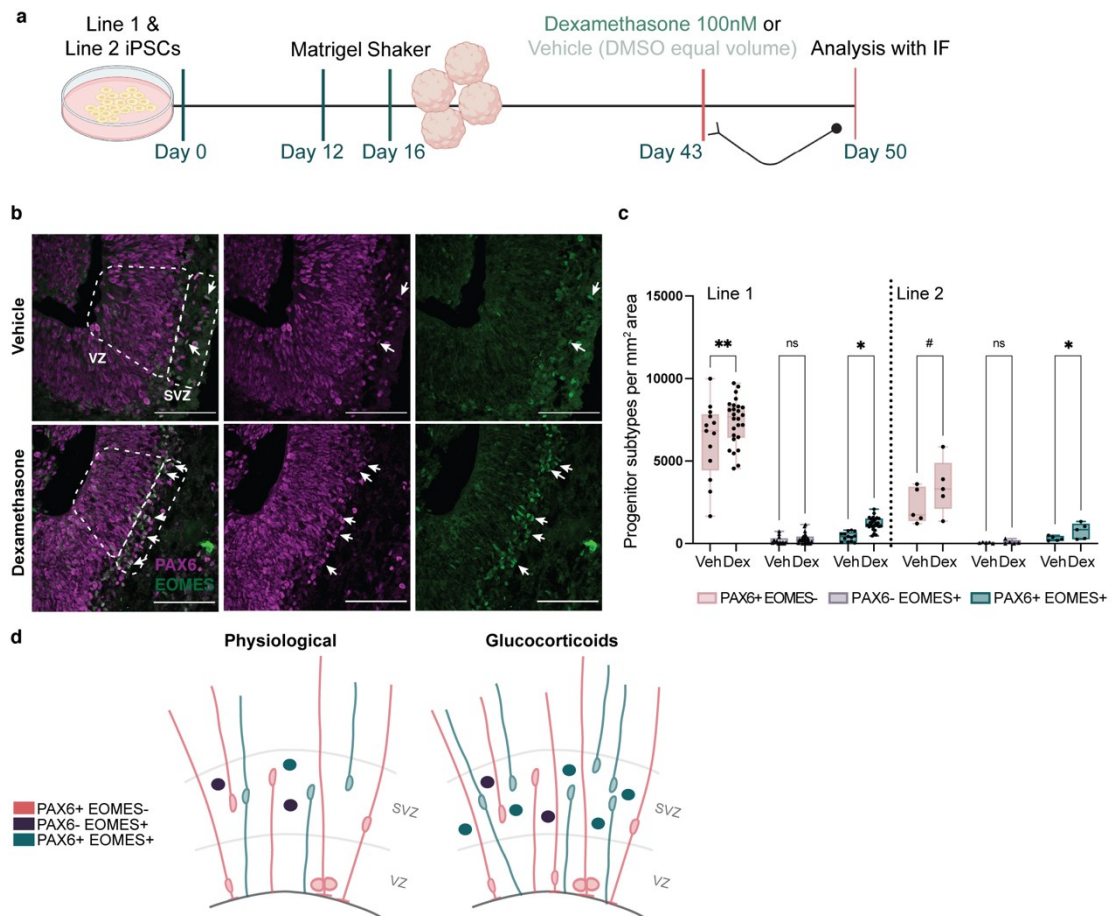


Figure 8| Glucocorticoids increase gyrencephalic species-specific basal progenitors. **a**, Schematic of the treatment and analysis workflow in human cerebral organoids (hCOs). DMSO, dimethyl sulfoxide; IF, Immunofluorescence. **b**, Representative images of day 50 hCOs at vehicle and dexamethasone conditions stained for PAX6 and EOMES. VZ, ventricular-like zone; SVZ, subventricular-like zone; PAX6, Paired box 6; EOMES, Eomesodermin; Arrows indicate cells that co-express PAX6 and EOMES; Scale bars, 100µm. **c**, Quantification of the progenitor subtypes in each treatment condition normalized by mm² of quantified total area in hCOs. Veh, vehicle; Dex, dexamethasone. **d**, Schematic of the glucocorticoids' effects on the developing neocortex. Box and whisker plots represent 25th to 75th percentile of the data with the centre line representing the median and whiskers representing minima and maxima. P-values, as indicated by asterisks, were calculated using 2-way ANOVA with Benjamini, Krieger and Yekutieli multiple testing correction.

To analyse the effects on different progenitor subtypes I stained for *PAX6* (Paired Box 6) and *EOMES* (Eomesodermin- also known as *TBR2*). *PAX6* and *EOMES* have an intricate expression pattern which is different between lissencephalic and gyrencephalic

species. In lissencephalic species, like rodents, *Pax6* is almost exclusively expressed by the aRGs that reside in the VZ and *Eomes* is expressed by IPs, the main progenitor BP type of rodents, in the SVZ. The expression pattern of these two TFs is mutually exclusive in lissencephalic species, where a molecular negative feedback loop ensures that these two proteins are rarely co-expressed. In contrast, in gyrencephalic species there is an overlap of the expression pattern of *PAX6* and *EOMES* in bRGs and bIPs of the inner- and outer- SVZ.

Treatment with dexamethasone consistently led to a significant increase of the double positive, PAX6+EOMES+, progenitors in hCOs derived from both iPSC lines (Figure 8b,c), in the SVZ (Supplementary Figure 1). Thus, glucocorticoids increase the BPs that are enriched in gyrified brains and are known to perform both proliferative and neurogenic divisions, thus contributing to the increased proliferative and neurogenic potential that drives cortical expansion (Figure 8d) [85].

In addition, dexamethasone led to an increase of the DCX (Doublecortin- marker of immature neurons) somata still found in the VZ (Figure 9a,b) and a parallel decrease of the DCX zone thickness in the CP of the hCOs (Figure 9c), pointing to later born neurons still migrating to their final place. This putative delay in neurogenesis could be explained by the increased numbers of the PAX6+EOMES+ BPs, which are known to perform proliferative and self-renewing divisions on top of the neurogenic ones.

The most important factors that determine the number of neurons produced are the types of progenitors, which also determines the clone size they can produce, and the overall length of the neurogenic period [79]. Thus, it could be speculated that glucocorticoids can contribute to two important aspects that determine the substantial expansion of the gyrified neocortex: they increase the number of gyrencephalic species-enriched BPs that have high proliferative and neurogenic potential and plausibly they extend the neurogenesis period. In fact, the molecular mediator of glucocorticoids-effects, *ZBTB16*, does lead to a vast increase of neuronal production as will be discussed in chapters 4.3 and 4.5.

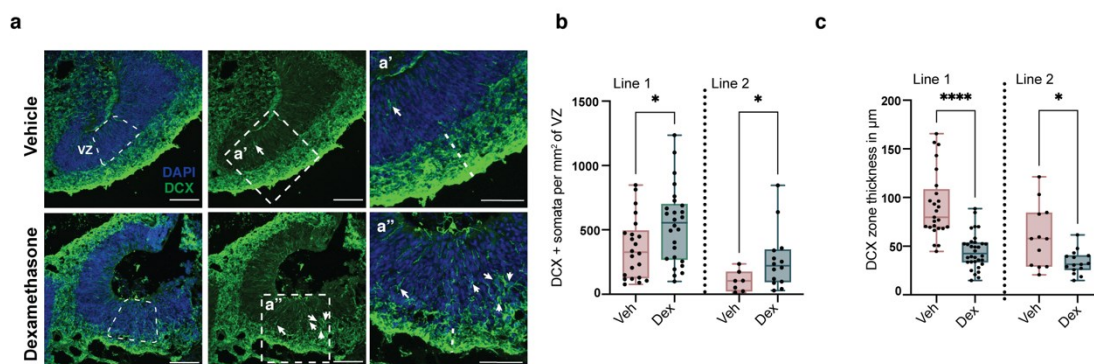


Figure 9| Glucocorticoids lead to delayed neurogenesis. a, Representative images of day 50 hCOs at vehicle and dexamethasone conditions stained for the immature neurons' marker DCX and the nuclear marker DAPI. VZ,

ventricular-like zone; Arrows indicate DCX positive somata in the VZ; DCX, doublecortin; DAPI, 4',6-diamidino-2-phenylindole; Scale bars, 100 μ m. **a'** and **a''**, Zoom-ins of the areas shown in vehicle and dex ventricles respectively. **b**, Quantification of DCX somata found in the VZ normalized per mm² of area. Veh, vehicle; Dex, dexamethasone. **c**, Quantification of DCX zone thickness in μ m. Box and whisker plots represent 25th to 75th percentile of the data with the centre line representing the median and whiskers representing minima and maxima. P values, as indicated by asterisks, were calculated using Mann–Whitney (two-tailed) comparison of treatment to control of each cell type.

4.2 The GR is responsible for the increase of basal progenitors

As already discussed dexamethasone preferentially binds to the GR. Nevertheless, at high concentrations it has been shown to also activate MR [159]. Even though MR is very lowly expressed in hCOs [156], I defined which of the two steroid hormones receptors mediates the effects of dexamethasone on BPs. To achieve that I treated hCOs with 100nM dexamethasone and/or 1 μ M of the GR inhibitor RU486 (also called mifepristone) [157] for seven days (Figure 10a) and analysed the effects on progenitor subtypes' numbers with Flow Cytometry (FC). FC analysis of hCOs treated with dexamethasone validated the specific effects of the glucocorticoid on increasing BPs that co-express PAX6 and EOMES (18% significant increase, Figure 10b,c). Inhibition of GR activation abolished this effect (1.1% non-significant change, Figure 10d,e), indicating that GR and not MR is responsible for mediating the effects of dexamethasone on BPs.

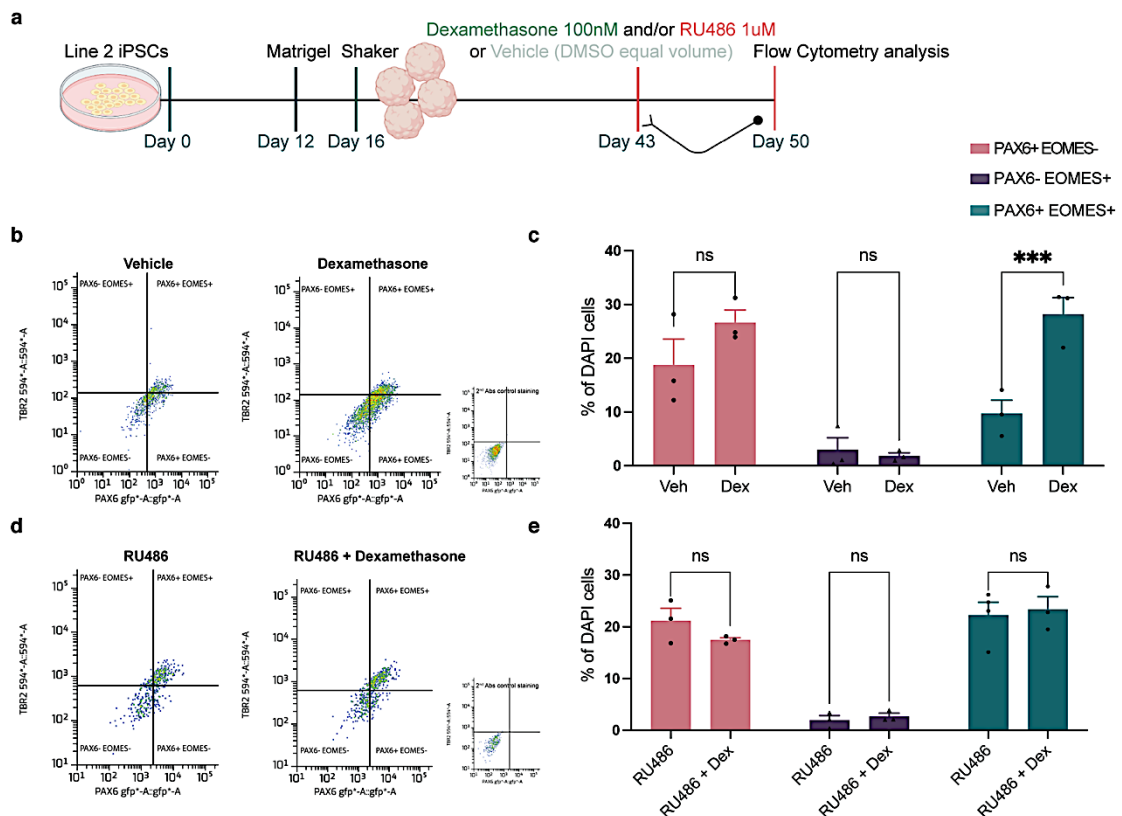


Figure 10| The GR and not the MR is responsible for the effects of dexamethasone on basal progenitors. **a**, Schematic of the treatment and analysis workflow in human cerebral organoids (hCOs). DMSO, dimethyl sulfoxide; RU486, mifepristone, is a selective GR inhibitor. **b**, Representative images of flow cytometry (FC) analysis of Control-2-derived hCOs per treatment condition. **c**, Quantification of the FC results. Percentages of DAPI cells in each progenitor subtype and treatment condition. Veh, Vehicle; Dex, dexamethasone. **d**, Representative images

of FC analysis of Control-2-derived hCOs per treatment condition. **e**, Quantification of the FC results. Percentages of DAPI cells in each progenitor subtype and treatment condition. Bar plots with error bars showing standard error of the mean (SEM). P values for **c** and **e** as indicated by asterisks, were calculated using 2-way ANOVA with Benjamini, Krieger and Yekutieli multiple testing correction.

4.3 Glucocorticoids effects on the transcriptional landscape

In order to identify genes and pathways possibly responsible for the cell-level findings on BPs, I analysed global transcriptional response mechanisms to glucocorticoids using a similar treatment paradigm as before in Line 2- hCOs and subjecting them to bulk RNA sequencing (Figure 11a). Differential expression (DE) analysis pointed to 50 DE genes (Supplemental Table 6) at an FDR (false discovery rate) cut-off of 10%. Given the effect of dexamethasone on progenitors, I aimed to fine-tune this gene list in order to focus on cell-type-specific responses from progenitors. To this end, I used a single-cell dataset, previously published from our lab (Cruceanu, Dony, Krontira *et al.*, AJP, 2021 [156]), which modeled GR activation and not lasting effects of glucocorticoids, by treating Line-2 day 30 hCOs with 100nM of dexamethasone for 12 hours. I cross-referenced the 50 bulk-DE genes with the cluster-specific-DE genes of the neural-progenitors and non-neural progenitors (Figure 11b, Supplemental Table 7).

I identified five genes that were DE in the bulk dataset, thus show large responses to glucocorticoids that persist through an extended period of seven days, and are selective to the neural progenitors' cluster when GR is activated (Figure 11c). Of these five genes, three were enzymes (*PNMT*- Phenylethanolamine N-Methyltransferase, *PLA2G2A*- Phospholipase A2 Group IIA, *QSOX1*- Quiescin Sulfhydryl Oxidase 1), one was a member of the tubulin family (*TUBA3A*- tubulin alpha 3A) and one was a TF (*ZBTB16*- Zinc Finger and BTB Domain Containing 16).

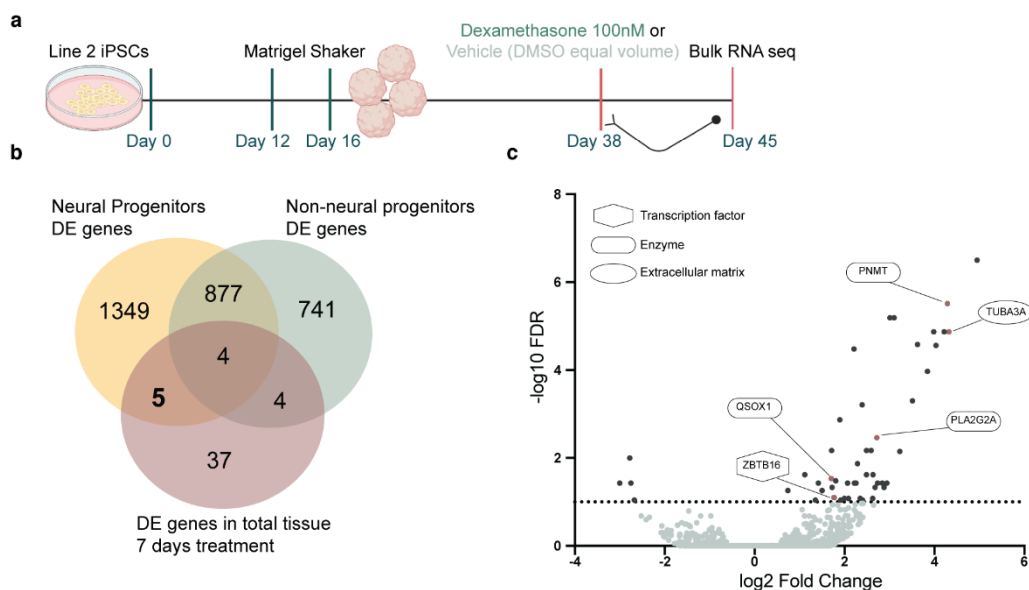


Figure 11| Transcriptomic effects of chronic treatment with dexamethasone on cerebral organoids. a, Schematic of the treatment and analysis workflow in human cerebral organoids (hCOs). DMSO, dimethyl sulfoxide; Seq,

sequencing. **b**, Venn diagram of DE genes from bulq RNA seq in 7-days day 45 treated hCOs and of DE genes in neural progenitors and non-neural progenitors from the single-cell data of Cruceanu et al., AJP, 2021 [156]. **c**, Volcano plot of the results of the bulq RNA seq. Grey dots, genes with non-significant expression changes at an FDR cutoff of 10%; Blue dots, genes with significant expression changes at an FDR cutoff of 10%; Red dots, five genes that have significant expression changes and are specific to neural progenitors; FDR, false discovery rate with Benjamini, Hochberg correction.

Given the essential role and specificity of TFs in determining developmental processes, I decided to focus on *ZBTB16*. *ZBTB16*, also known as *PLZF* (promyelocytic leukemia zinc finger protein), is a Krüppel-like zinc finger TF with nine zinc finger motifs in the C' terminus that comprise the DNA binding domain of the protein, a protein-protein interaction BTB/POZ domain at the N' terminus and lesser characterized middle RD2 domain. *ZBTB16* is known to regulate the balance of self-renewal and differentiation of stem cells in multiple organ systems [160], [161].

4.4 *ZBTB16* is responsive to glucocorticoids in multiple tissues

ZBTB16 is responsive to stress and glucocorticoids in multiple models and tissues. Repeated stress in mice has been shown to increase *Zbtb16* transcription in serotonin neurons [162], whereas dexamethasone was able to upregulate it in human peripheral blood [163]. In fact, *Zbtb16* is DE also in the prefrontal cortex (PFC) of adult mice that received 10mg/kg of dexamethasone intraperitoneally and were sacrificed four hours later (Figure 12a, Gerstner & Krontira *et al.*, Neurobiology of Stress, 2022- DiffBrainNet: <http://diffbrainnet.psych.mpg.de>) [164]. DiffBrainNet is an interactive resource of differential expression and network analyses in response to glucocorticoids in eight regions of the adult mouse brain. Using DiffBrainNet, one can identify molecular pathways important for basic functioning and response to glucocorticoids in a brain-region specific manner.

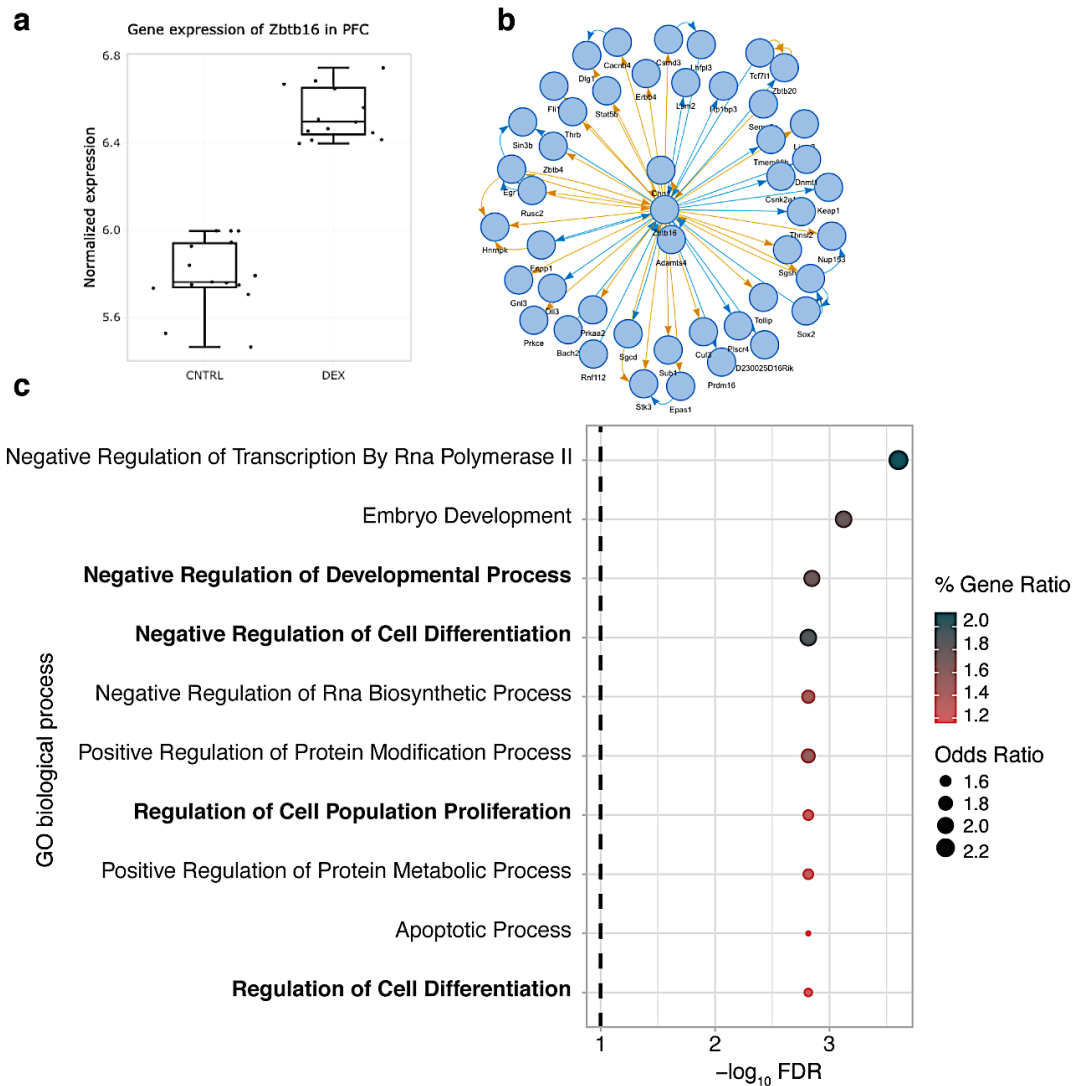


Figure 12| Differential network of *Zbtb16* in the adult mouse brain. (from Gerstner & Krontira *et al.*, BiorXiv, 2022 [165]). **a**, *Zbtb16* is differential expressed in the PFC of the adult mouse brain after 4 hours of 10mg/kg dexamethasone. PFC, prefrontal cortex. **b**, Differential gene neighborhood of *Zbtb16* in the mouse PFC. **c**, Top 10 biological processes enrichment analysis for the *Zbtb16* differential neighborhood. FDR, false discovery rate.

Using DiffBrainNet, I analysed the differential network of *Zbtb16* in the PFC (Figure 12b). The differential network only includes the connections that show altered strength in response to the stimulus, in this case dexamethasone, thus allowing for analysis of the specific processes correlated with the gene of interest after the exposure to the stimulus. The *Zbtb16* differential network is enriched for terms associated with cell proliferation and differentiation and embryo development (Figure 12c, Supplemental Table 8), suggesting that *ZBTB16* may mediate glucocorticoid effects on differentiation and proliferation processes, thus supporting my choice to move forward with this gene.

4.5 **ZBTB16: a glucocorticoid-responsive developmental transcription factor**

4.5.1 **ZBTB16 is dynamically expressed during neurodevelopment**

ZBTB16 has a very dynamic expression pattern during development with high expression early in gestation and then downregulation to very low levels. The time that *ZBTB16* is depleted is different among species. In mice, *Zbtb16* is expressed until E10.5 in the forebrain [166], but it is not expressed during the neurogenic period [167] (Supplementary figure 2a). In contrast in human fetal cortex it is expressed during neurogenesis (Supplementary figure 2b), highlighting a very important difference in the expression pattern of this TF between lissencephalic and gyrencephalic species. When focusing into its expression in different gyrencephalic species including humans, primates like chimpanzees and non-human primates like macaques, *ZBTB16* shows enriched expression in hCOs of humans and chimpanzees over the macaque ones (Supplementary figure 2c). In fact, zooming in one step more and looking at the timeline of its expression, it seems that *ZBTB16* is more highly expressed during human neurogenesis, over the other primates, when the important BPs marker, *EOMES* appears (Supplementary figure 2d). Lastly, focusing on cell types of human (Supplementary figure 2e) and chimpanzees (Supplementary figure 2f) hCOs, it seems that this TF is expressed in progenitors of both species but enriched in the RG population of human COs compared to chimpanzees' ones. Thus, in physiological development, during the neurogenic period *ZBTB16* is selectively expressed in gyrencephalic and not lissencephalic species, showing an enrichment in the human RGs and possibly during BPs specification. This points to a potentially interesting role of this TF in gyrified species-enriched neurogenic processes, especially when its levels are increased outside the normal range due to environmental challenges, like due to glucocorticoids.

To analyse the *ZBTB16* expression pattern in the model of the human developing cortex of this Ph.D thesis, I analysed its expression at the protein and RNA level from very early in the organoid development at day 20 until day 100, in hCOs derived from both iPSCs line, Lines 1 and 2. *ZBTB16* is very dynamically expressed with high expression early on, until approximately day 50, and decrease to low levels after that (Figure 13a,b). The steep decrease in *ZBTB16* expression coincides with the rise of mature neurons (MAP2-microtubule associated protein 2, Figure 13a). At the level of single-cell gene expression, *ZBTB16* is enriched in the RG cluster at day 30 (Figure 13c). In fact, 33.9% of the total cells of the RG cluster are *ZBTB16*+, versus 18.4% of cells in all remaining clusters, which accounts for 48.7% of all *ZBTB16*+ cells belonging to the RG cluster (Figure 13e).

At day 90, *ZBTB16* RNA is detected at very few cells across all cell types (Figure 13d). Only 11.1% of RG cells are *ZBTB16*⁺ versus 9.5% of cells in all remaining clusters expressing *ZBTB16*, which accounts for 24.8% of all *ZBTB16*⁺ cells belonging to the RG cluster (Figure 13e). Thus, *ZBTB16* is dynamically expressed in hCOs too and it is enriched in the RG cluster.

At the protein level, *ZBTB16* is found in the progenitor cells (SOX2⁺, SRY determining region Y- box 2) that are located in the VZ of the hCOs but not in mature neurons (MAP2⁺), highlighting the progenitor specific expression of this TF (Figure 13f).

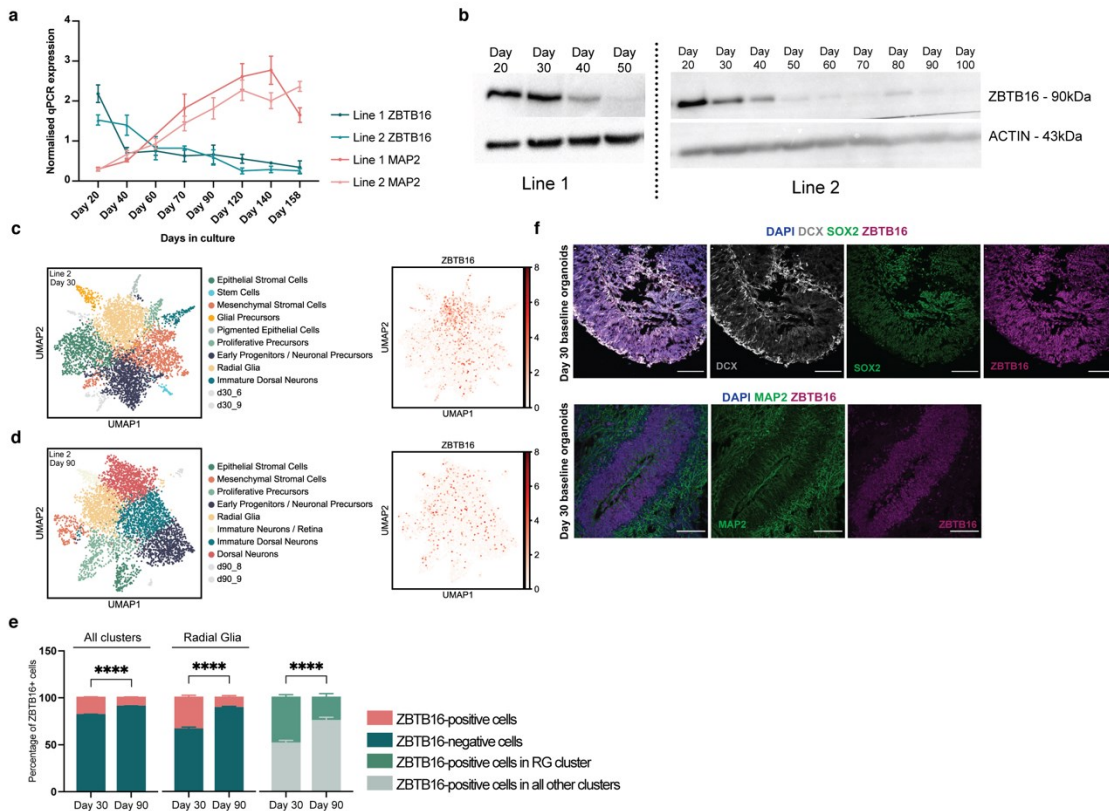


Figure 13 | ZBTB16 expression pattern in organoids and mouse cortex. **a**, qPCR expression of *ZBTB16* and *MAP2* in hCOs normalised over endogenous genes. qPCR, quantitative polymerase chain reaction; MAP2, mature neuronal marker. **b**, Western blot analysis of *ZBTB16* expression in hCOs from day 20 to day 100. hCOs, human cerebral organoids. **c**, UMAP plots of cell types and *ZBTB16* expression in day 30 hCOs from Cruceanu, Dony, Krontira *et al.*, AJP, 2021 [156]. **d**, UMAP plots of cell types and *ZBTB16* expression in day 90 hCOs from Cruceanu, Dony, Krontira *et al.*, AJP, 2021 [156]. **e**, Quantification of the percentage of cells that express *ZBTB16* in the single-cell dataset. **f**, Representative immunofluorescent images of *ZBTB16* protein expression in ventricles of hCOs. Scale bars, 100 μ m. Bar plots with error bars showing standard error of the mean (SEM). P-values, as indicated by asterisks, for **e**, were calculated with Fisher's exact test.

4.5.2 Glucocorticoids regulate *ZBTB16* expression levels in the developing cortex

In order to study if glucocorticoids lead to overexpression of *ZBTB16* also during development, as they do in adulthood, I treated hCOs with 100nM of dexamethasone for seven days (Figure 14a), mimicking the exact treatment paradigm that resulted in more BPs in the hCOs. Indeed, dexamethasone significantly increased *ZBTB16* expression both at

the RNA (Figure 14b) and at the protein level (Figure 14c,d) in organoids from both iPSC lines.

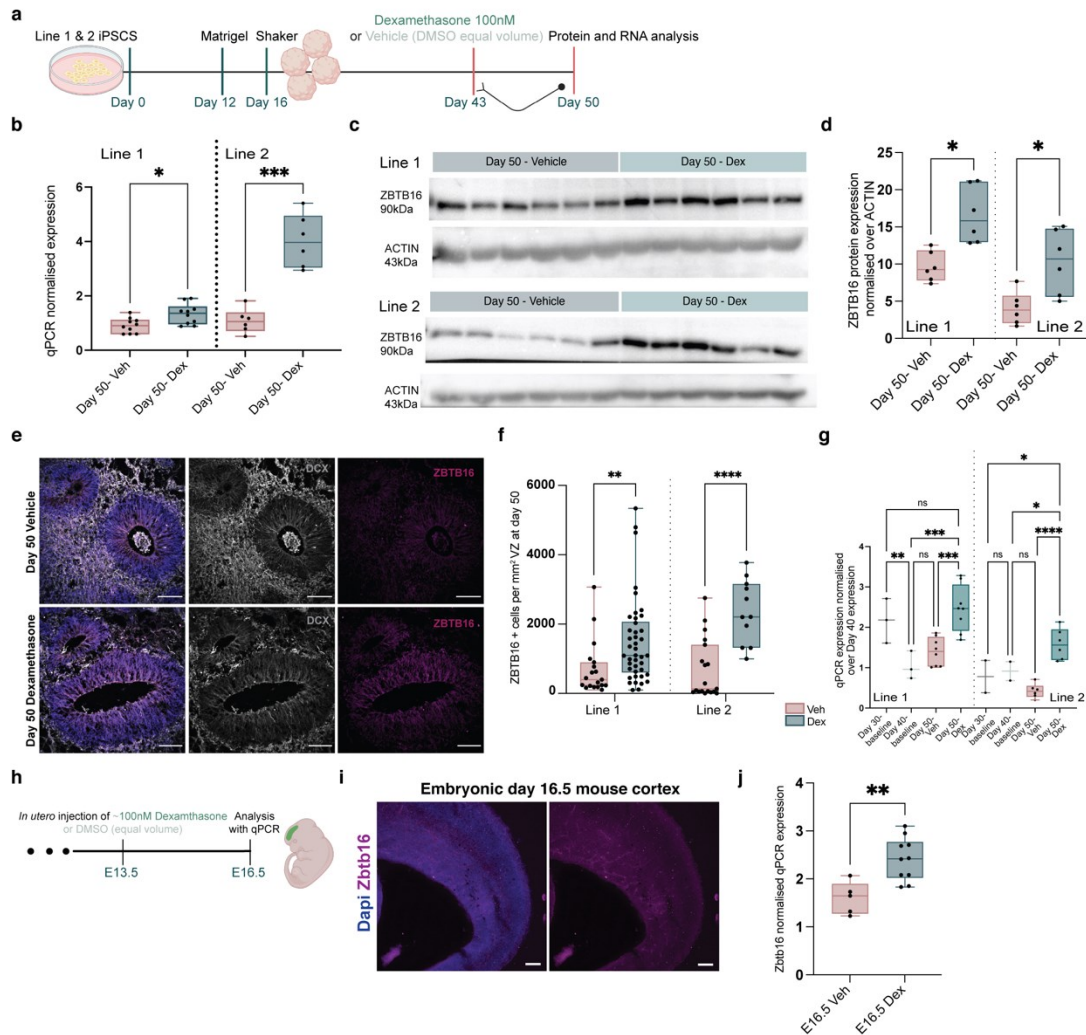


Figure 14| Glucocorticoids alter the expression pattern of ZBTB16 in organoids and fetal mouse cortex. **a**, Schematic of the treatment and analysis workflow in human cerebral organoids (hCOs). DMSO, dimethyl sulfoxide. **b**, Quantitative PCR results of the effect of 100nM 7 days dexamethasone treatment on ZBTB16 transcription in day 50 hCOs normalized over housekeeping genes. qPCR, quantitative polymerase chain reaction; Veh, vehicle; Dex, dexamethasone. **c**, Western blots of ZBTB16 and ACTIN proteins in hCOs treated with 100nM of dexamethasone at day 43 and analysed 7 days later at day 50. **d**, Quantification of the effect of 100nM 7 days dexamethasone treatment on ZBTB16 expression in day 50 hCOs normalized over ACTIN. **e**, Representative images of day 50 hCOs at vehicle and dex conditions stained for the immature neuronal marker DCX and ZBTB16. Dex, dexamethasone; Scale bars, 100µm. **f**, Quantification of ZBTB16 positive cells found in the VZ normalized per mm² of area. **g**, Quantitative PCR plot for ZBTB16 expression in hCOs normalized over housekeeping genes and expression at day 40. **h**, Schematic of the treatment and analysis workflow in fetal mouse brain. DMSO, dimethyl sulfoxide. **i**, Representative images of Zbtb16 expression in the mouse cortex mid-neurogenesis, at E16.5. Scale bars, 100µm. **j**, Quantitative PCR results of the effect of 100nM dexamethasone treatment on the expression of Zbtb16 in fetal mouse cortices by *in utero* injection in the ventricle of E13.5 fetal mice and analysed at E16.5. Data are normalized over housekeeping genes. Box and whisker plots represent 25th to 75th percentile of the data with the center line representing the median and whiskers representing minima and maxima. P values for **b**, **d**, **f**, **i** as indicated by asterisks, were calculated using Mann–Whitney (two-tailed) comparison of treatment and control; for **g**, were calculated using 2-way ANOVA with Benjamini, Krieger and Yekutieli multiple testing correction.

When focusing on the cell type specificity of the overexpression effect I found that dexamethasone increases ZBTB16 protein expression in the cells that populate the VZ, thus reinstalling its expression in cells that it is physiologically expressed until ~day 50 (Figure

14e,f). Interestingly, dexamethasone not only increases the expression of *ZBTB16* in the progenitor cells but it completely reverses its very tightly regulated developmental expression pattern by reversing its levels back to the ones of day 30 and earlier, so the early stages of neurogenesis, when it is physiologically highly expressed in hCOs (Figure 14g).

Similarly to the hCOs, *in utero* injection of approximately 100nM of dexamethasone in the ventricle of the developing mouse cortex at E13.5 (Figure 14h, see Methods for explanation) led to a significant increase of *Zbtb16* at E16.5 in the isolated cortices at the RNA level (Figure 14j), at a time-period when physiologically *Zbtb16* is not expressed in the mouse cortex (Figure 14i).

Thus, prenatal glucocorticoids increase *ZBTB16* expression irrespective of the species, both at the developing mouse cortex and at the model of the developing human cortex, the hCOs. Interestingly, that means that in mice glucocorticoids boost *Zbtb16* expression during the neurogenic period when it physiologically is never expressed and in hCOs they raise its expression during a developmental time-window of the neurogenic period when it is not expressed bringing its levels back to the ones of earlier neurogenesis time-points when physiologically it is expressed.

4.6 Embedding of glucocorticoid effects with methylation

To identify the molecular mechanism via which glucocorticoids alter the expression profile of *ZBTB16* I studied its methylation landscape in day 30 hCOs treated with 100nM dexamethasone for seven days with HAM-TBS (highly accurate method for targeted bisulfite sequencing) [126]. I used a panel of PCR primers (Supplementary Table 4) that cover intronic regulatory regions of *ZBTB16* where there are known GR-binding sites (Figure 15a).

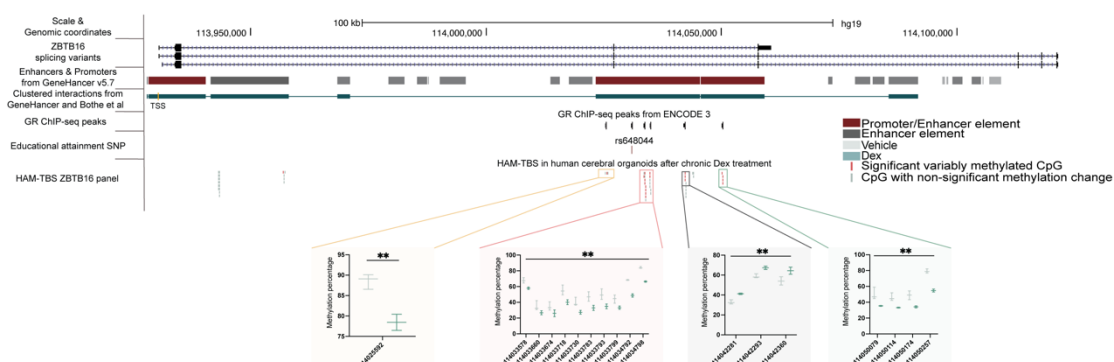


Figure 15| Glucocorticoids affect the methylation landscape of *ZBTB16*. a, Graphic representation of the *ZBTB16* locus, modified from the UCSC browser. GR, glucocorticoid receptor; ChIP, chromatin immunoprecipitation; Seq, sequencing; SNP, single nucleotide polymorphism. b, HAM-TBS results for CpGs with significantly altered methylation levels. HAM-TBS, highly accurate method for targeted bisulfite sequencing; Veh, vehicle; Dex, dexamethasone. P values for b, were calculated using 2-way ANOVA with Benjamini, Krieger and Yekutieli multiple testing correction. The correction was done for all the CpGs in each enhancer element.

Out of 55 CpGs covered, 36 were located around GR ChIP sequencing sites (GR-enhancers) and 19 in enhancer elements that do not have GR sites (non-GR-enhancers). From the 19 CpGs in non-GR-enhancers only 1 was significantly demethylated (Supplementary figure 3a, 4.5% less methylated, $p_{\text{adjusted}} < 0.01$). From the 36 CpGs in GR-enhancers, 18 showed significantly altered methylation levels after dex stimulation (Figure 15b and Supplementary figure 3b). Dexamethasone exposure significantly reduced the methylation level in 15 out of the 18 CpGs (from 8.46% to 24.54% less methylated, $p_{\text{adjusted}} < 0.01$) and increased it in 3 (from 8.38% to 10.29% more methylated, $p_{\text{adjusted}} < 0.01$) (Figure 15b). All significantly altered CpGs are located in enhancer regions that loop to the transcriptional start site of *ZBTB16* (“GeneHancer” track in Figure 15a and Bothe *et al.*, Life Science Alliance, 2021 [168]), indicating a change in the methylation signature of *ZBTB16* enhancer elements after GR activation that drives the response to GCs.

4.7 *ZBTB16* mimics the effects of glucocorticoids

Given that glucocorticoids increase BPs and that *ZBTB16* was pinpointed as a glucocorticoids-responsive developmental TF with a selective expression in progenitor cells of the primate neurogenic period, I next sought to analyse the effects of *ZBTB16* overexpression at the cellular architecture of the developing neocortex, thus mimicking the effects of glucocorticoids on its expression. To this end, I created a bicistronic vector that carries *ZBTB16* and GFP (green fluorescent protein) divided by an F2A sequence (see Methods for explanation), which results in independent expression of *ZBTB16* and GFP proteins from one vector (Supplementary Figure 4), thus allowing me to visualize whole cells with GFP irrespective of the localisation of *ZBTB16*.

To mimic the effect of dexamethasone on *ZBTB16* expression I electroporated hCOs at day 43, when *ZBTB16* expression is physiologically decreased (Figure 13b), and analysed them seven days later at day 50 (Figure 16a), following the exact time-points of the glucocorticoid stimulation treatment. In order to explore the effects of the overexpression in the different progenitors' subtypes of the apical and basal side of the ventricle, the electroporated area was divided in three bins of equal height and the effect of the TF's overexpression was analysed for the GFP+ cells. Bin A is mainly comprised of the VZ, bin B of the outer-most basal part of the VZ and the SVZ and bin C of the CP.

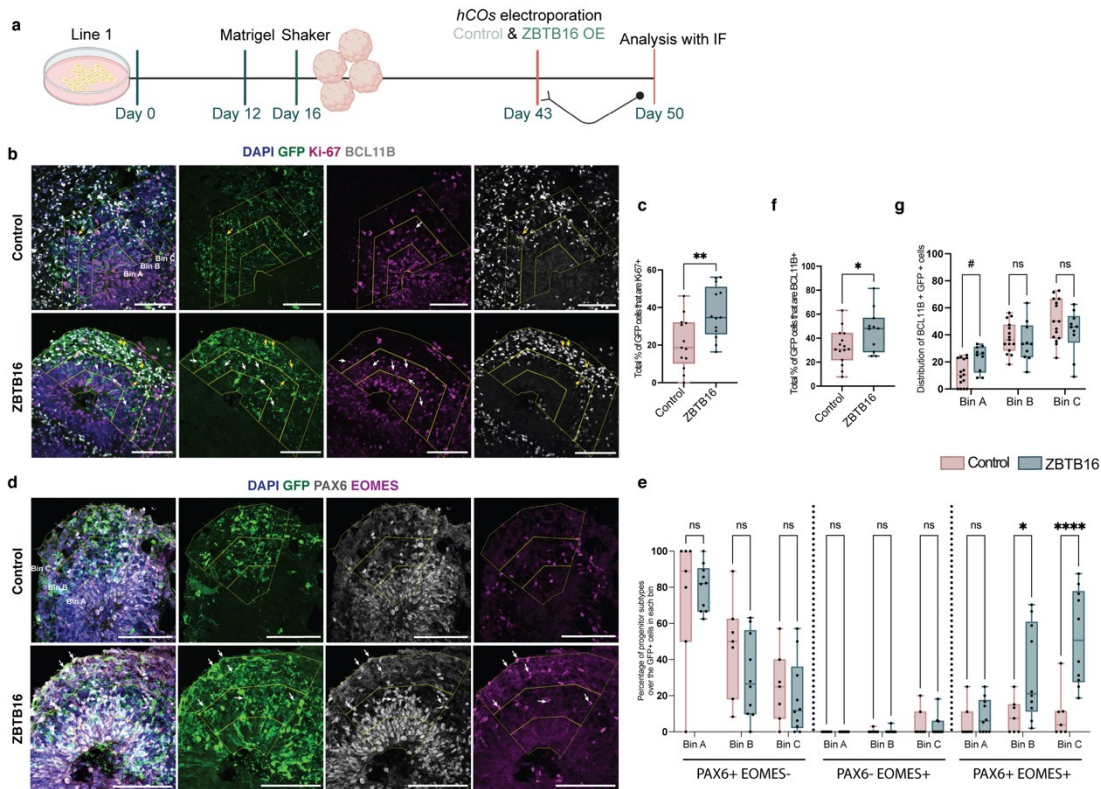


Figure 16| ZBTB16 mimics the effect of dexamethasone on basal progenitors. **a**, Schematic of the Line 1-derived hCOs electroporations and analysis workflow in human cerebral organoids (hCOs). OE, overexpression; IF, Immunofluorescence. **b**, Representative images of day 50 hCOs at control and ZBTB16 OE conditions stained for the proliferative marker Ki-67, the layer V neuronal marker BCL11B, GFP for plasmid and the nuclear marker DAPI. White arrows indicate GFP cells that express Ki-67; Yellow arrows indicate GFP cells that express BCL11B; Scale bars, 100 μ m. **c**, Quantification of the total amount of GFP cells that are Ki-67 positive normalized by total GFP cells. **d**, Representative images of day 50 hCOs at control and ZBTB16 OE conditions stained for PAX6, EOMES, GFP for plasmid and the nuclear marker DAPI. Arrows indicate GFP cells that co-express PAX6 and EOMES; Scale bars, 100 μ m. **e**, Quantification of the GFP cells belonging in the different progenitor subtypes in each bin and condition normalized by total GFP cells of each bin. **f**, Quantification of the total amount of GFP cells that are BCL11B positive normalized by total GFP cells. **g**, Quantification of the distribution of BCL11B+GFP+ cells across the three bins. Box and whisker plots represent 25th to 75th percentile of the data with the center line representing the median and whiskers representing minima and maxima. P values for **g** and **e** as indicated by asterisks, were calculated using 2-way ANOVA with Benjamini, Krieger and Yekutieli multiple testing correction; for **c** and **f** as indicated by asterisks, were calculated using t-test with Welch's correction of treatment and control. #, nominal p-value < 0.05.

ZBTB16 overexpression led to a significant increase of Ki-67+ cells (15.94% more Ki-67 cells after ZBTB16 overexpression-Figure 16b,c), indicating an increase in the proliferation potential. To dissect the phenotype of ZBTB16 overexpression in the different progenitor subtypes I used the same rationale as for the analysis of the dexamethasone phenotype and co-analysed the expression of PAX6 and EOMES (Figure 16d). Indeed, overexpression of ZBTB16 led to a significant increase of PAX6+EOMES+ cells in bins B and C (Figure 16e, 23.8% increase in bin B and 43.1% increase in bin C), which reflect the basal parts of the ventricle. Interestingly, there is a substantial increase of these gyrencephalic-enriched double positive progenitors (43.1%) in bin C which physiologically associates to the CP of the organoids, possibly pointing to an identity change of this bin to resemble an area bearing cells typically found in the inner- and outer- SVZ of

gyrencephalic species. Additionally, it's important to note that ZBTB16 overexpression has an effect similar to the one of dexamethasone on hCOs.

Given, the increased proliferative potential and the fact that with dexamethasone putatively extended neurogenesis was identified, I sought to analyse the effects of ZBTB16 on neuronal production. Overexpression of ZBTB16 led to increased numbers of layer V neurons expressing BCL11B (B-cell lymphoma/leukemia 11B, also known as CTIP2) (Figure 16b,f). However, these neurons are still migrating to their final place in the CP since their distribution was altered with more BCL11B+ cells still in the progenitors' zones (Figure 16g), pointing to later born neurons. This effect on neurogenesis is similar to the one seen with dexamethasone (Figures 8,9), overall suggesting that ZBTB16, like dexamethasone, increases the proliferative and neurogenic BPs and delays neurogenesis, which though happens and results in increased neuronal numbers.

4.8 ZBTB16 is necessary for the effects of glucocorticoids

Dexamethasone and *ZBTB16* upregulate PAX6+EOMES+ BPs in hCOs. Given the similarity of the phenotypes on gyrencephalic-enriched BPs, I sought to define how central *ZBTB16* is for the glucocorticoids' effects. To achieve that I used CRISPR-Cas9 to knock-out exon 2 of the *ZBTB16* locus in Line 2 iPSCs. Exon 2 encodes for more than 50% of the protein and includes the initiating ATG, the BTB/POZ domain and the first two zinc fingers of the binding domain [169] thus removing it leads to a truncated protein that is not able to act as a TF. I designed two guide RNAs (gRNAs) that encircle exon 2 (Supplementary figure 5a & Supplementary Table 12) and achieved a heterozygous knock-out by removing exon 2 from one of the two alleles of the locus (Supplementary figure 5b-d). A homozygous knock-out of exon 2 was not possible, likely due to lethality caused by the complete loss of *ZBTB16* in iPSCs. Indeed, from 93 single clones over three different CRISPR experiments 47 of them were heterozygous KO, so 51% efficiency for both gRNAs cutting at least one allele. Out of 93 clones none of them exhibited a deletion of exon 2 from both alleles either by both gRNAs or at least one gRNA cutting. In fact, I used a heterozygous knock-out single clone and tried to target the wild-type allele with the same set of gRNAs, which were proven to have high efficiency, and after having checked with Sanger sequencing that the wild type allele sequence was intact with no insertions or deletions. Again, out of 15 clones in none of them the deletion of exon 2 in the second allele succeeded. In these clones, the targeted allele was re-sequenced and no insertions or deletions were identified that could have led to stop codons. So for the following experiment I used an heterozygous knock-out clone, called from now-on *ZBTB16*^{+/-}, where in one allele exon 2 was deleted (Supplementary figure 5c,d) and the other allele was wild-type with no effects on its sequence, as was seen

with Sanger sequencing. As control cells I used Line 2 iPSCs that were put through the CRISPR experiment but without the use of gRNAs in order to account for potential non-specific cutting of the Cas9 protein, termed ZBTB16^{+/+}.

The first phenotype I observed was a markedly decrease of the size of EBs, spheroids in the first steps of the organoid protocol which are enriched with neural stem cells, with the ZBTB16^{+/-} cells (Supplementary Figure 5e,f), pointing to the importance of ZBTB16 for stem cells proliferation.

To analyze the importance of ZBTB16 for the glucocorticoids' effects on BPs I treated ZBTB16^{+/+} and ZBTB16^{+/-} derived hCOs with 100nM of dexamethasone at day 43 for seven days (Figure 17a), so matching the treatment paradigm and the developmental timepoints used for the dexamethasone experiment, and analysed progenitors' subtypes abundance with flow cytometry.

At day 50 ZBTB16 is physiologically very lowly expressed in hCOs, as already discussed. Dexamethasone treatment upregulated the expression of ZBTB16 in the hCOs from both genotypes, but for the ZBTB16^{+/-} derived hCOs the overexpression was significantly less than the one of ZBTB16^{+/+} hCOs (46% less increased- Figure 17b,c).

FC analysis showed that for the ZBTB16^{+/+} derived hCOs there was a significant increase of the PAX6+EOMES+ BPs (22.2% increase), similar to the levels found with the Line 2 organoids when they were analysed with FC after dexamethasone treatment (they showed a 18% increase, Figure 10) (Figure 17d,e), validating once again the effect of dexamethasone on increased gyrencephalic-enriched BPs. In contrast, in the ZBTB16^{+/-} hCOs there was no significant increase of the PAX6+EOMES+ BPs (6% non-significant increase- Figure 17f,g), indicating that ZBTB16 is required and is mediating the effects of glucocorticoids on the gyrified species-enriched double positive BPs.

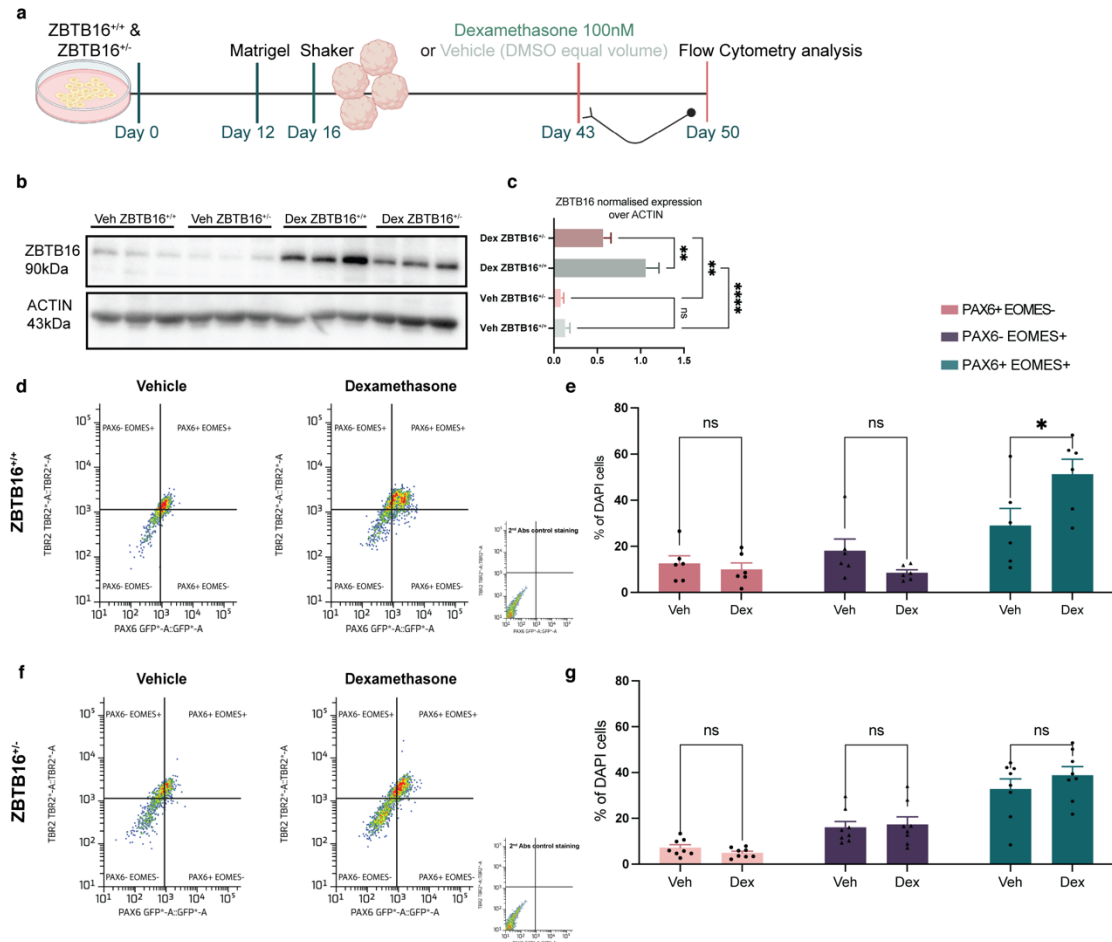


Figure 17 *ZBTB16* is necessary and sufficient for the effects of glucocorticoids on basal progenitors. **a**, Schematic of the treatment paradigm in *ZBTB16*^{+/+} and *ZBTB16*^{+/-} hCOs. **b**, Western blot of *ZBTB16*^{+/+} and *ZBTB16*^{+/-} hCOs at vehicle and dexamethasone conditions. **c**, Quantification of the levels of ZBTB16 expression normalized over ACTIN. **d**, Representative images of scatter plots from flow cytometry analysis of *ZBTB16*^{+/+} hCOs at vehicle and dexamethasone conditions. **e**, Quantification of the percentage of progenitors' subtypes over DAPI. **f**, Representative images of scatter plots from flow cytometry analysis of *ZBTB16*^{+/-} hCOs at vehicle and dexamethasone conditions. **g**, Quantification of the percentage of progenitors' subtypes over DAPI. hCOs, human cerebral organoids; Veh, vehicle; Dex, dexamethasone. Bar plots with error bars showing standard error of the mean (SEM). P-values for **e** and **g** as indicated by asterisks, were calculated using 2-way ANOVA with Benjamini, Krieger and Yekutieli multiple testing correction.

4.9 *ZBTB16* increases gyrencephalic-enriched basal progenitors in mice

ZBTB16 increases gyrencephalic species-enriched BPs in hCOs, which are a model of gyrencephalic species- neurogenic processes in which *ZBTB16* is physiologically expressed in the beginning of neurogenesis. I wanted to understand if overexpressing this TF during the neurogenic period of a lissencephalic species, where it is not physiologically present during neurogenesis, would result in a similar phenotype, thus indicate that this TF is regulating, at least some, aspects of gyrencephalic species neurogenic processes. To this end, I used *in utero* electroporations, with the same plasmids that were already discussed, to overexpress human *ZBTB16* in the mouse cortex at E13.5, when neurogenesis of deep layer neurons is at its peak and the birth of upper layer neurons

has started, and analysed the effects three days later at E16.5 (Figure 18a). To analyse effects meaningful for the mouse cortical architecture I divided the electroporated area in five bins of equal height, with bin A comprising mostly of the VZ, bin B of the SVZ, bin C of the IZ and bins D and E of the deep and upper layers of the CP.

The distribution of the GFP cells was altered when ZBTB16 was overexpressed, with more cells accumulating in bin B and less cells having reached the cortical plate in bin E (Figure 18b,c), indicating a possible identity change and/or delayed differentiation timing.

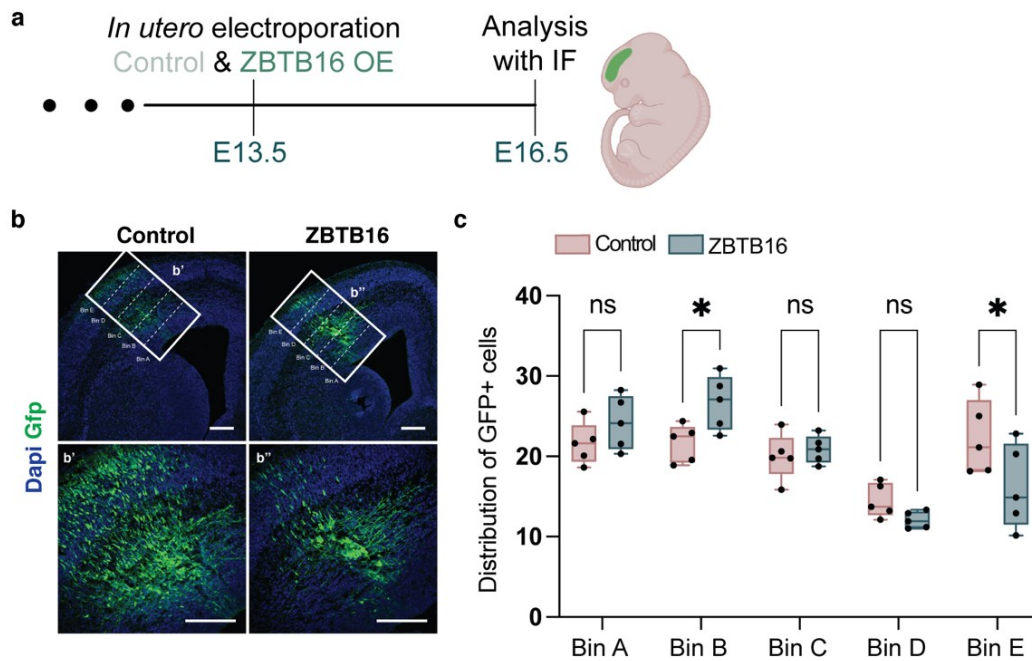


Figure 18| Distribution of GFP cells in the mouse cortex. **a**, Schematic of the in utero electroporations. **b**, Representative images of mouse brain cortices at E16.5 at control and ZBTB16 overexpression conditions. **c**, Quantification of the distribution of GFP cells in the mouse cortex. OE, overexpression; E, embryonic day; Scale bars, 100µm. Box and whisker plots represent 25th to 75th percentile of the data with the center line representing the median and whiskers representing minima and maxima. P values, as indicated by asterisks, were calculated using 2-way ANOVA with Benjamini, Krieger and Yekutieli multiple testing correction.

Next, I analysed the effects of the overexpression in the different progenitor subtypes. Indeed, ZBTB16 overexpression led to a significant increase of Pax6+Eomes+ progenitors in bin A (16.5% significant increase) and bin B (11.8% significant increase) (Figure 19). Interestingly in mice, not only were the Pax6-Eomes+ cells, which are the most abundant BP type of lissencephalic species, not increased but they were significantly decreased (Figure 19b- 10.6% decrease in bin A and 15.1% decrease in bin B), indicating that ZBTB16 overexpression in a lissencephalic species during the neurogenic period has the ability to increase a progenitor type that physiologically is very rare, even at the expense of the species-specific most abundant physiological BP type.

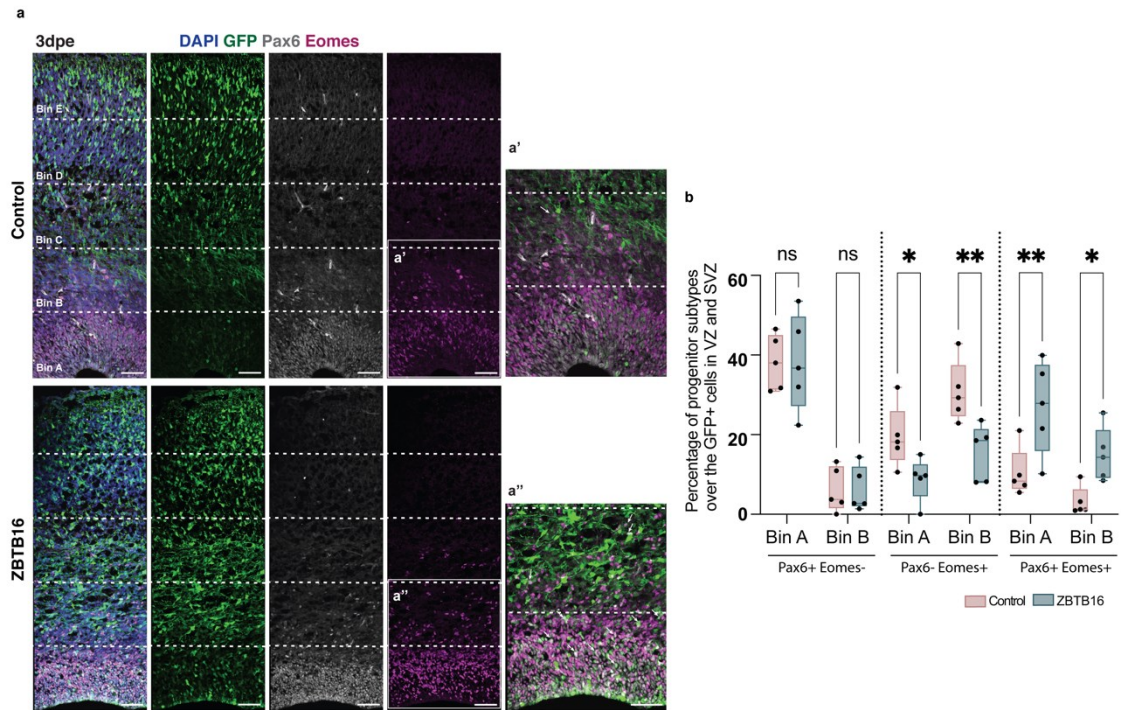


Figure 19 | *In utero* electroporations in mice. **a**, Representative images of the mouse cortices at control and ZBTB16 overexpression conditions. **b**, Quantification of the progenitor subtypes in bins A and B, normalized over the total number of GFP+ cells of each bin. 3dpe, 3 days post electroporation; VZ, ventricular zone; SVZ, subventricular zone. Scale bars, 50 μ m. Box and whisker plots represent 25th to 75th percentile of the data with the center line representing the median and whiskers representing minima and maxima. P-values, as indicated by asterisks, were calculated using 2-way ANOVA with Benjamini, Krieger and Yekutieli multiple testing correction.

Given that the double positive BPs have a high proliferative and neurogenic potential, I next analysed the potential impact they may have on neuronal output in mice. ZBTB16 overexpression led to a significant increase of deep layer neurons that are Bcl11b+ (Figure 20a,b, layer V- 33.36% significant increase) and Tbr1+ (Figure 20d,e, layer VI- T-box bran transcription factor 1- 4.3% significant increase) but not of upper layer neurons that are Satb2+ (Figure 20g,h, layer IV- SATB Homeobox 2- 3.3% non-significant decrease). Interestingly, even though there is a higher neuronal output, neurogenesis seems to be delayed since there is a mark change in the distribution of the neurons, even for upper layer neurons which in total are not more, with cells accumulating in the bins closer to the apical side and less cells having reached their final place in the CP (Figure 20c,f,i).

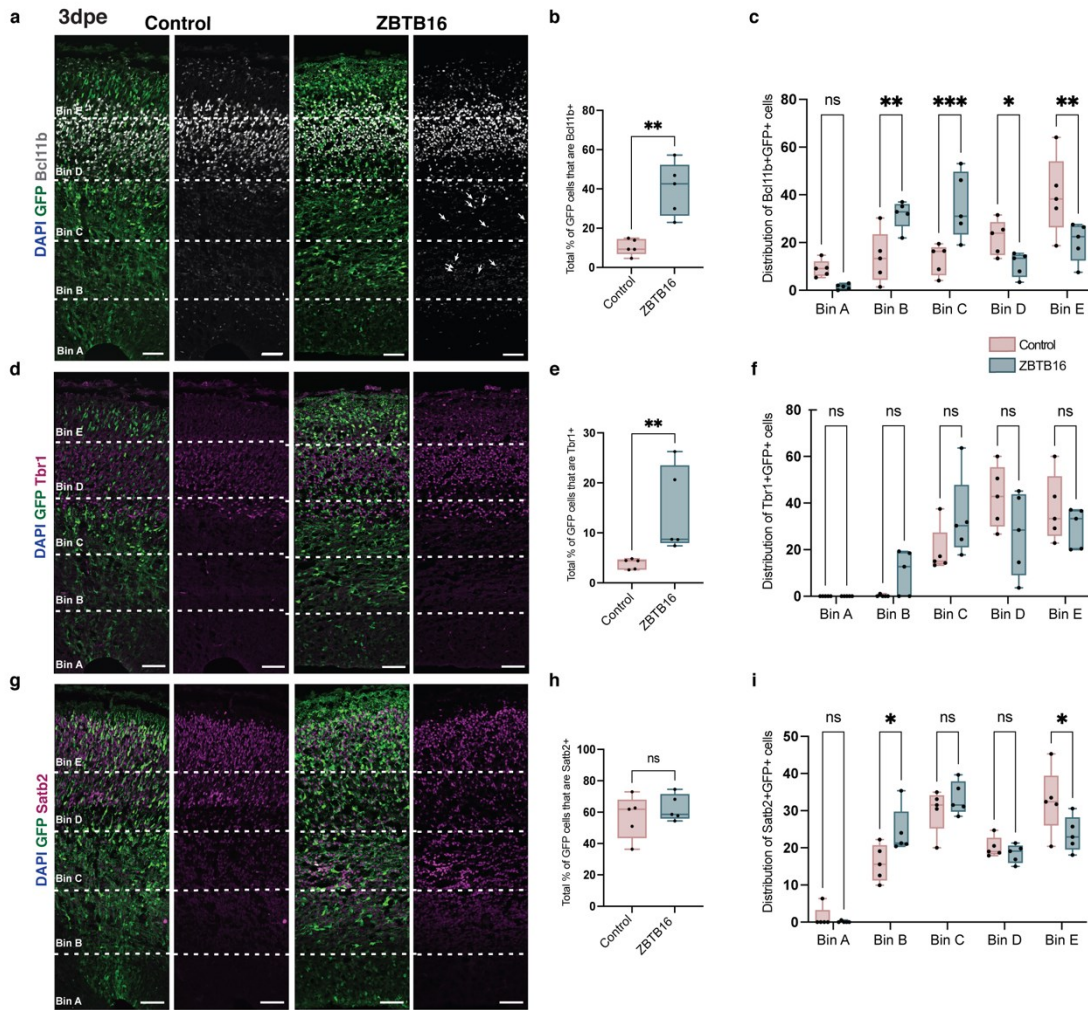


Figure 20 | Effects of ZBTB16 overexpression on the neuronal output in mice. **a**, Representative images of E13.5-E16.5 electroporated mouse brains stained for layer V neurons with Bcl11b. 3dpe, 3 days post electroporation. **b**, Total percentage of the GFP cells that are Bcl11b positive. **c**, Distribution of the Bcl11b+GFP+ cells in the different areas of the fetal mouse cortex. **d**, Representative images of E13.5-E16.5 electroporated mouse brains stained for layer VI neurons with Tbr1. **e**, Total percentage of the GFP cells that are Tbr1 positive. **f**, Distribution of the Tbr1+GFP+ cells in the different areas of the fetal mouse cortex. **g**, Representative images of E13.5-E16.5 electroporated mouse brains stained for layer IV neurons with Satb2. **h**, Total percentage of the GFP cells that are Satb2 positive. **i**, Distribution of the Satb2+GFP+ cells in the different areas of the fetal mouse cortex. Scale bars, 50 μ m. Box and whisker plots represent 25th to 75th percentile of the data with the center line representing the median and whiskers representing minima and maxima. P-values, as indicated by asterisks, were calculated using 2-way ANOVA with Benjamini, Krieger and Yekutieli multiple testing correction.

Thus, ZBTB16 overexpression in a lissencephalic brain leads to increased numbers of gyrencephalic species-enriched BPs, which are very rare under physiological conditions. In rodents, these cells also exhibit high neurogenic potential increasing the total output of deep layer neurons. Interestingly not only the neurons are increased but also their distribution is different, with more cells accumulating to the more immature zones. This could be explained by two hypotheses: first, neurogenesis is delayed and the neurons are still migrating to their final place or second, there is an additional migration defect which could mean that these cells are stuck and cannot reach their final destination in the CP. To distinguish which of the two hypothesis is true, a longer period after the *in*

utero electroporation needs to be analysed. To this end, I electroporated at E13.5 and analysed 6 days later at E19.5 (Figure 21a), which was also the date of birth for these mice.

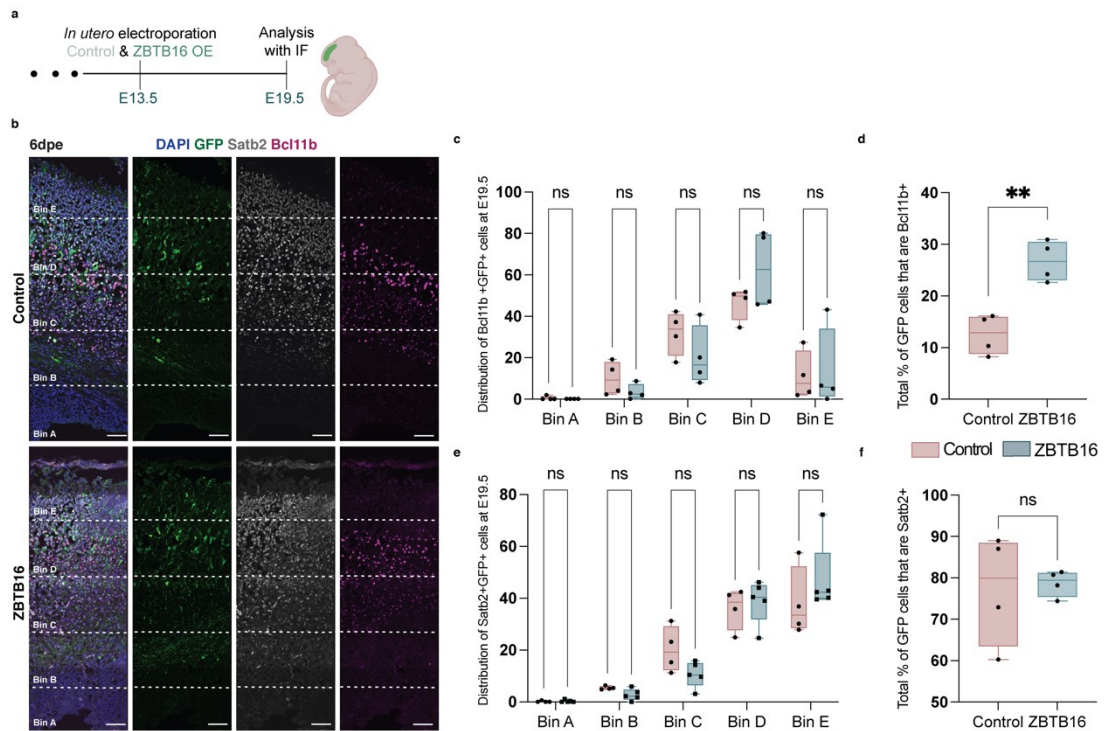


Figure 21| *In utero* electroporations of ZBTB16 overexpression from E13.5 to E19.5. a, Schematic of the *in utero* electroporation at E13.5 and analysed 6 days later at E19.5. E, embryonic day. **b**, Representative images of E13.5-E19.5 electroporated mouse brains stained for layer V neurons with Bcl11b and for layer IV neurons with Satb2. 6dpe, 6 days post electroporation. **c**, Distribution of the Bcl11b+GFP+ cells in the different areas of the fetal mouse cortex. **d**, Total percentage of GFP cells that are Bcl11b positive. **e**, Distribution of the Satb2+GFP+ cells in the different areas of the fetal mouse cortex. **f**, Total percentage of GFP cells that are Satb2 positive. Scale bars, 50µm. Box and whisker plots represent 25th to 75th percentile of the data with the center line representing the median and whiskers representing minima and maxima. P values, as indicated by asterisks, for **c,e** were calculated using 2-way ANOVA with Benjamini, Krieger and Yekutieli multiple testing correction and for **d,f** were calculated using Mann–Whitney (two-tailed) comparison of treatment and control.

Indeed, when analysing the distribution of the layer V Bcl11b+ and layer IV Satb2+ neurons 6 days post electroporation, although replicates were not fully consistent, there was no significant change in the distribution of the neurons (Figure 21b,c,e) but there was still a significant increase of deep- (Figure 21d) but not of upper- (Figure 21f) layer neurons. This indicates that the first hypothesis is probably true. ZBTB16 overexpression results in a delayed but extended neurogenic period which results in bigger neuronal output with no additional migration defect present. Given the high variability of the replicates, these results should be replicated in an independent experiment.

Lastly, up until now all the analysis of ZBTB16 effects, either in hCOs or in mice, was done on the cell-autonomous effects of this TF, this is on effects directly in the cells that overexpress ZBTB16 since only the GFP positive cells were analysed. To account for potential non-cell autonomous phenotypes, I analysed the non-cell autonomous effects

of ZBTB16 overexpression at E13.5-E16.5. Thus, I focused on all cells of the mouse cortex, but excluded the GFP+ ones. Indeed, even though ZBTB16 is a TF it seems to affect the whole cellular niche around the area of electroporation with the same effects on both progenitors (more Pax6+Eomes+ and less Pax6-Eomes+ cells) and neurons (more Bcl11b+ neurons that are still migrating to their final place) (Supplementary figure 6).

The phenotype of ZBTB16 in mice is similar to what was seen with dexamethasone and ZBTB16 itself in hCOs, strengthening the role of ZBTB16 as a regulator of gyrencephalic species-enriched neurogenic processes when its levels are altered due to environmental stimuli.

4.10 ZBTB16 activates a forebrain active promoter of PAX6

In rodents, *Pax6* and *Eomes* create a positive feedforward cascade that self-regulates with direct negative feedback effects [170]–[172], thus restricting the expression of the two proteins in different cells. Considering that dexamethasone via *ZBTB16* seems to sustain *PAX6* expression in EOMES+ cells, even in a lissencephalic species where physiologically they are mutually exclusive, and that *ZBTB16* is a TF, I analysed the capacity of *ZBTB16* to activate the *PAX6* human promoters. *PAX6* has three promoter regions that induce tissue-specific expression, and that are highly conserved between humans and rodents: the P0, P1 and Pa promoters [173], [174] (Figure 22a). To study the effects of *ZBTB16* on them, I designed luciferase reporter assays for all three promoters and tested their activity under overexpression of *ZBTB16* or not in HeLa cells, where *ZBTB16* is not expressed under basal conditions (Figure 22b).

Using the luciferase assays, I found that *ZBTB16* activates the P1 promoter of *PAX6*, but not the P0 and Pa promoters (Figure 22c). The P1 promoter is active during neocortical development whereas the P0 and Pa promoters are minimally active [173] during the same period, indicating that *ZBTB16* possibly regulates *PAX6* expression via an important for the cortex regulatory region. Given the consistent effects on more cells expressing *PAX6* after *ZBTB16* overexpression in hCOs and in mice and the fact that *ZBTB16* seems to activate a neocortex-active *PAX6* promoter, it's plausible that *ZBTB16* as a TF sustains the expression of *PAX6* thus resulting in the increased numbers of PAX6+EOMES+ BPs.

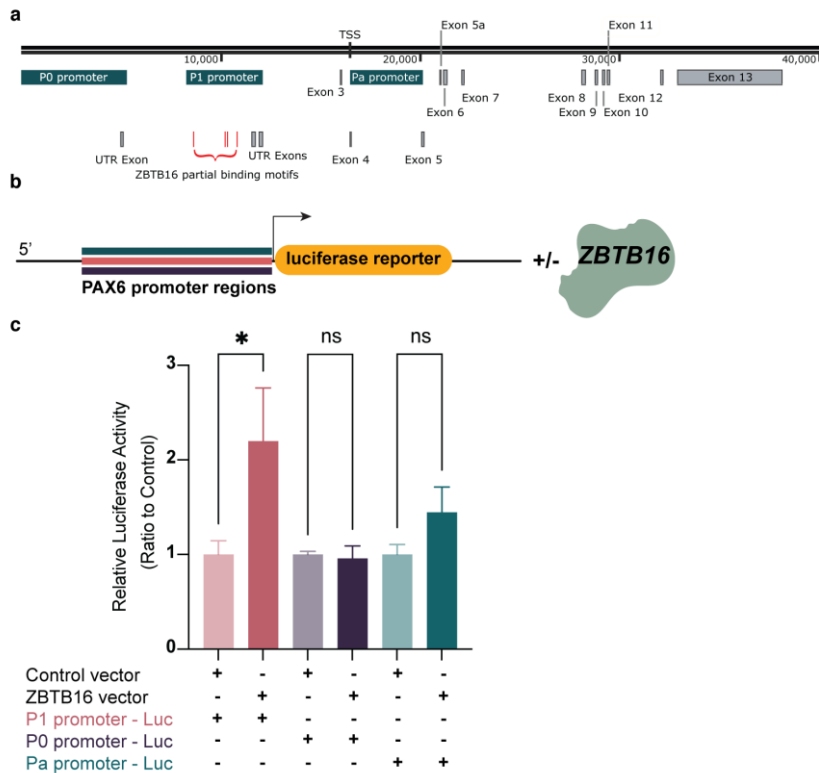


Figure 22| Luciferase reporter assays for *PAX6* promoters. **a**, Schematic of the luciferase plasmids, with the sequences of three *PAX6* promoters driving the expression of firefly luciferase. **b**, Schematic of the *PAX6* locus. **c**, Quantification of the luciferase activity for each promoter with or without *ZBTB16* overexpression. Bar plots with error bars showing standard error of the mean (SEM). P-values, as indicated by asterisks, were calculated using 2-way ANOVA with Benjamini, Krieger and Yekutieli multiple testing correction.

4.11 Gene by environment interactions and postnatal phenotypes

As discussed in the introduction, environmental effects often interact with the genetic landscape to shape responses both at the molecular and the phenotypic levels. Indeed, genetic variants have been shown to modulate glucocorticoid responses in human blood resulting in increased risk for depression [175]. Given the importance of the effects of glucocorticoids via *ZBTB16* on the developing cytoarchitecture of the cortex and the fact that dexamethasone affects *ZBTB16* expression by altering the methylation landscape of regulatory regions in the *ZBTB16* locus that surround GR binding sites (Figure 15), I decided to catalogue genetic variants in the *ZBTB16* locus in proximity to these regulatory regions and with associations to neurobehavioral and brain structural phenotypes (GWAS Catalogue, *ZBTB16* <https://www.ebi.ac.uk/gwas/genes/ZBTB16>).

One SNP, rs648044, fulfilled all three criteria: first, it is associated with educational attainment in two GWAS (genome-wide association study) for this trait (Study 1 [176]: N= 1,131,881 individuals recruited in this study from various cohorts including the UK Biobank and 23andMe, FDR = 9×10^{-9} & Study 2 [177]: N= 3,037,499 individuals recruited from various cohorts including the UK Biobank and 23andMe, FDR = 2×10^{-8}), second it

is associated with a neuroimaging phenotype, cortical thickness [178] (N= 35,657 individuals, FDR = 6×10^{-9}) at a GWAS significant level and third, it is located exactly within the glucocorticoids-responsive regulatory element of the *ZBTB16* locus identified with the methylation analysis (Figure 23, Supplementary Table 9).

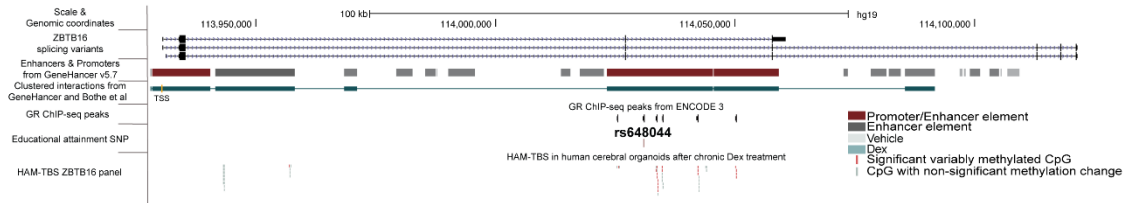


Figure 23| Genomic locus of *ZBTB16*. Rs648044 is located in the regulatory region that bears GR binding sites and is responsive to glucocorticoids at the methylation level. GR, glucocorticoid receptor; ChIP, chromatin immunoprecipitation; seq, sequencing; SNP, single nucleotide polymorphism; HAM-TBS, highly accurate method for targeted bisulfite sequencing.

In the latter GWAS on cortical morphology, gene-level analysis with MAGMA also identified *ZBTB16* itself as significantly associated with cortical area (FDR = 7.2×10^{-14}) and thickness (FDR = 1.9×10^{-8}) when combining associated effects of all SNPs in the locus. This indicates that *ZBTB16* is important for cortical morphology, even when assayed postnatally. The association of educational attainment and cortical morphology is of interest as genetic risk for low or high educational attainment has also been associated with respectively decreased or increased cortical volume and thickness [179]–[181], which are structural phenotypes probably determined by altered developmental cortical trajectories. Thus, rs648044 provided an interesting example of how glucocorticoids in interaction with the genetic landscape could mediate the effects of altered *ZBTB16* expression on developing cytoarchitecture and potentially on postnatal phenotypes.

4.11.1 rs648044 interacts with glucocorticoids to alter *ZBTB16* expression

Given that rs648044 is located in a regulatory element that bears GR binding sites, I sought to analyse if it regulates *ZBTB16* activity. To this end I used a technique that is called STARR- qPCR (self-transcribing active regulatory region- qPCR). With this technique the regulatory elements bearing each of the two alleles of the SNP are cloned into a plasmid to drive the expression of GFP. By transfecting these plasmids in cells that are treated or not with glucocorticoids one can analyse two things: first if this regulatory element indeed regulates expression and second if and in which direction the genotypes of the SNP regulate its activity (Figure 24a).

The genotype of rs648044 is G/A with allele frequencies of 0.65 for the G allele and 0.35 for the A allele in Caucasians. The STARR-qPCR assay revealed that indeed, this region possesses enhancer activity but only after glucocorticoids treatment and not at baseline, showing that this is a glucocorticoids-responsive regulatory region (Figure 24b).

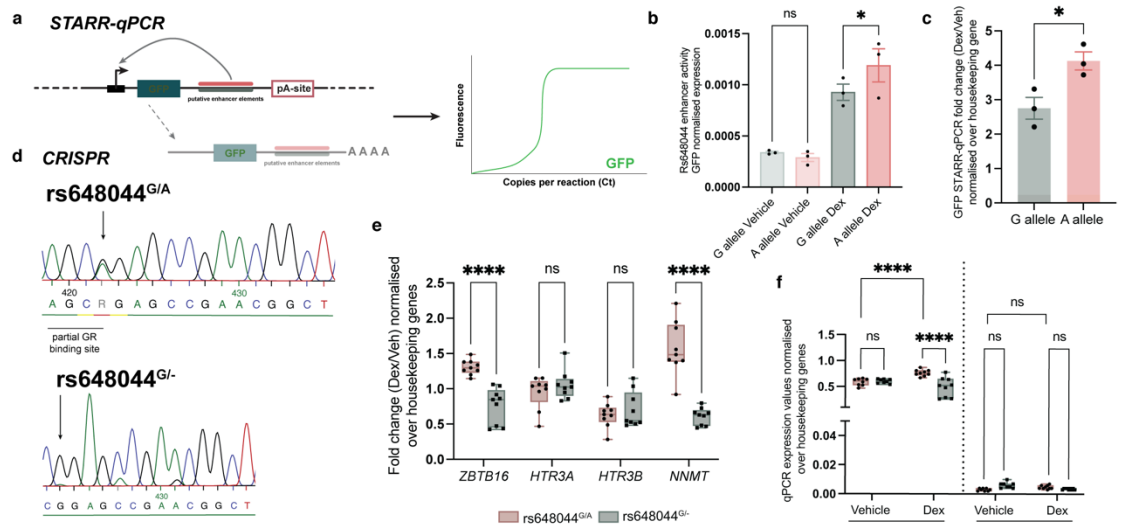


Figure 24| Rs648044 interacts with glucocorticoids to modulate enhancer activity. **a**, Schematic of the STARR technique. **b**, Quantification of the enhancer activity according to the genotype of rs648044. **c**, Fold change of GFP expression according to rs648044 genotype in response to dexamethasone. **d**, Sanger sequencing traces of CRISPR-edited iPSCs to remove the dexamethasone-responsive allele of rs648044. **e**, Rs648044 regulates *ZBTB16* and *NNMT* expression in human cerebral organoids. **f**, *NNMT* is not expressed in the organoids thus the effects of rs648044 on brain phenotypes are most probably associated with its impact on *ZBTB16* expression. Bar plots with error bars showing standard error of the mean (SEM). Box and whisker plots represent 25th to 75th percentile of the data with the center line representing the median and whiskers representing minima and maxima. P values, as indicated by asterisks, for **b** were calculated using 2-way ANOVA with Benjamini, Krieger and Yekutieli multiple testing correction and for **c** and **e** were calculated using Mann–Whitney (two-tailed) comparison of the two conditions.

In addition, the rs648044 genotype modulates the glucocorticoids-induced activity of the enhancer (Figure 24b), indicating that this SNP can modulate the impact of stressful environments, in this case mediated via an increase in glucocorticoids, to affect transcription. The rarer A allele, which is the one associated with higher educational attainment and cortical thickness, confers a stronger increase following dexamethasone (Figure 24c), possibly because it creates a partial GR binding site (AGCA, Figure 24d).

Knowing that indeed rs648044 is responsible for the allele-dependent dexamethasone-induced function of this enhancer, I sought to verify that the enhancer regulates the expression of *ZBTB16*. To this end, I used CRISPR-Cas9 to excise 200bp (base pairs) surrounding rs648044 in Line 2- iPSCs. Line 2- iPSCs are heterozygous for rs648044 (G/A- Figure 24d). I knocked-out this region with the A allele and ended up with a cell line that has the G allele but not the A (rs648044^{G/-} - Figure 24d & Supplementary figure 7). I used this edited line and the control cell line carrying both alleles (rs648044^{G/A} – CRISPR control, see Methods) to create hCOs.

Indeed, rs648044 regulates the dexamethasone-dependent increase of *ZBTB16* (Figure 24e- 15% less induced). In order to identify if this is a specific effect to *ZBTB16* I analysed the expression of all genes that are around rs648044 in the locus. There are three more genes there: *HTR3A*, *HTR3B* and *NNMT* along with *ZBTB16*. In fact, rs648044 regulated glucocorticoids effects on the expression of one more gene located in its genetic locus,

NNMT (nicotinamide-N-methyltransferase, Figure 24e). Interestingly *NNMT* is very lowly expressed in the adult and fetal brain [182] and in the hCOs (Figure 24f), while it's very abundant in the liver. This suggests that horizontal pleiotropy for rs648044 effects can be excluded and that *ZBTB16* is the most probable mediator of the associations of rs648044 with postnatal brain phenotypes.

Here it's important to note two things: first, rs648044^{G/-} cells and in consequence hCOs, still have the enhancer element with the G allele which, as shown with the STARR-qPCR (Figure 24b), possesses enhancer activity and second, the CRISPR targeted only 200bp surrounding the partial binding site created by the A allele and no other GR binding sites that are found in this enhancer element (Figure 23). These facts can explain why the effect size of the A allele KO on *ZBTB16* glucocorticoids-induced expression is small. Nevertheless, rs648044 modulates dexamethasone-induced activity of this enhancer element which affects *ZBTB16* transcription. In fact, this locus has been shown to loop to the *ZBTB16* transcriptional start site (Figure 23- 'Clustered interactions from GeneHancer' and Bothe *et al.*, Life Science Alliance, 2021 [168]), thus strengthening the fact that rs648044 and dexamethasone together affect *ZBTB16* transcription.

4.11.2 rs648044 regulation of glucocorticoid-responses associates with postnatal phenotypes

Having seen that rs648044 modulates the effect of glucocorticoids on *ZBTB16* expression and knowing that this SNP is associated with educational attainment and cortical thickness in adulthood I wanted to understand if the rs648044- and glucocorticoids-induced *ZBTB16* expression could be the molecular mediator of these associations. For this I used Mendelian Randomization (MRa) analysis. MRa is a statistical framework that examines the causal effects of an exposure, for example rs648044- and -glucocorticoids-induced *ZBTB16* transcription, on disease phenotypes [144]. More specifically, MRa uses the effect sizes of the SNP of interest on different phenotypes from GWAS studies ("instrument") and its effect size on an exposure, for example on transcription ("exposure"), to define potential causal relationships of the exposure on the phenotypes (Figure 25).

Rs648044 associations with 7,503 phenotypes from the UK Biobank and the NHGRI-EBI GWAS Catalog (Supplementary Table 5), including neurobehavioral traits and adult imaging data, were used as instrument (Figure 25). The extent of the rs648044 allele-specific changes following dexamethasone on *ZBTB16* transcription from the STARR-qPCR were used as exposure (Figure 25). Thus, MRa was used to identify the causal effects of the rs648044-defined-glucocorticoids-induced *ZBTB16* amounts on these phenotypes in a PheWAS (Phenome Wide Association Study) approach.

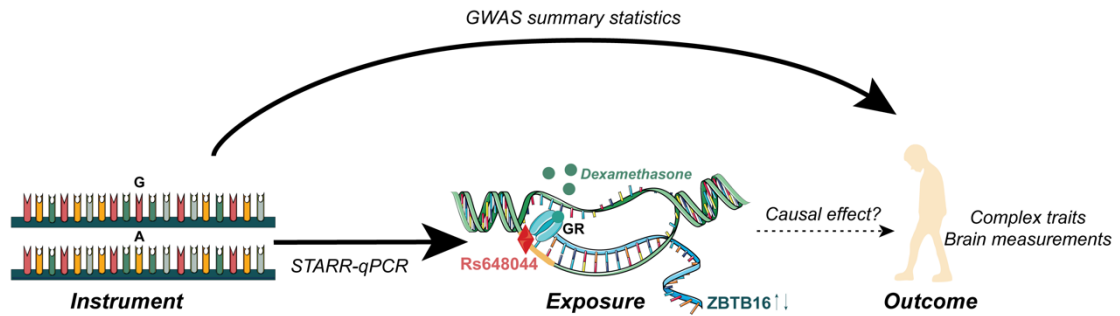


Figure 25| Explanation of Mendelian Randomization analysis. Parts of the figure have been modified based on images from SMART (Servier Medical Art, <http://smart.servier.com/>).

Indeed, MRa-PheWAS analysis provided strong evidence for potential associations of the rs648044-predicted *ZBTB16* transcription with multiple outcomes (Figure 26a). Focusing on the analysis on neurobehavioral outcomes (N= 4,360) there were 22 that were significantly associated with the exposure, so the genetically-predicted *ZBTB16* transcription, after multiple testing correction (Figure 26b, Supplementary Figure 8 & Supplementary Table 10). In these, “years of schooling” and “College or University degree” were included, which are both direct measures of educational attainment. This supports the idea that the effect of rs648044 on *ZBTB16* transcription is, potentially, the biological mediator for the associations of this SNP with educational attainment that are reported in the GWASs. In turn, it can be speculated that the effects of *ZBTB16* on neurogenic processes described throughout this thesis could be the cellular substrate of rs648044 associations with educational attainment.

Given the association of rs648044 with cortical thickness at a GWAS significant level [178] and the effects of glucocorticoids and *ZBTB16* on the cytoarchitecture of the developing cortex analysed throughout this thesis, MRa-PheWAS was also performed on neuroimaging phenotypes. From the 3,143 structural phenotypes analysed 21 survived multiple testing correction (Figure 26c & Supplementary Table 11). Most evidence indicated associations of higher genetically-predicted-*ZBTB16* transcription with reduced brain connectivity measures, as assayed with diffusion magnetic resonance imaging, and with higher insular cortical thickness (Figure 26c,d). The association of higher cortical thickness with reduced white matter connectivity measures has been reported before [183], as has the connection of educational attainment with cortical thickness [179]–[181]. In addition, glucocorticoids have also been associated with higher cortical thickness and lower brain connectivity [184].

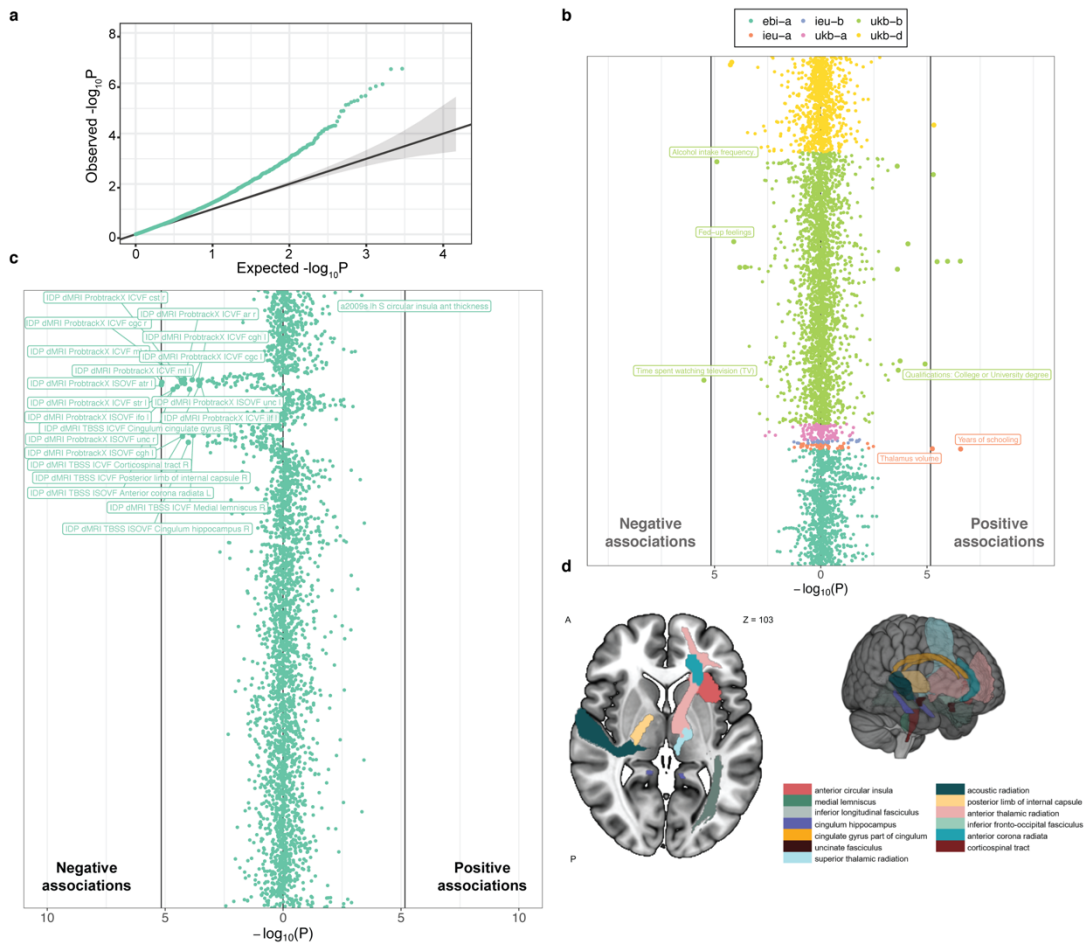


Figure 26| MRa-PheWAS study results of ZBTB16 on neurobehavioral and structural phenotypes. **a**, Quantile-quantile plot of expected versus observed mendelian randomization p-values for the effects of the rs648044 x glucocorticoids predicted ZBTB16 transcription on UK Biobank phenotypes. **b**, Plot describes associations of ZBTB16 transcription on selected neurobehavioral phenotypes of the UK Biobank and NHGRI-EBI GWAS Catalog as individual points. Phenotypes are presented based on negative associations (negative MR estimate) and positive associations (positive MR estimate) effects. Selected traits that remain significant following Benjamini-Hochberg correction are labelled. All significant traits can be found in Supplemental Table 10. To improve interpretation of the strength of evidence, additional vertical lines are shown, which represent the Bonferroni multiple comparison threshold across all outcome traits. **c**, Plot describes associations of ZBTB16 transcription on neuroimaging traits from Elliot *et al.*, Nature, 2018 based on the UK Biobank. Phenotypes are presented based on negative associations (negative MR estimate) and positive associations (positive MR estimate) effects. Colour-coding reflects MRC IEU phenotype batches. Traits that remain significant following Benjamini-Hochberg correction are labelled. To improve interpretation of the strength of evidence, additional vertical lines are shown, which represent the Bonferroni multiple comparison threshold across all outcome traits. MR, mendelian randomization. **d**, Illustration of significant MR associations between brain region phenotypes and genetically-predicted ZBTB16 transcription. Colors are chosen arbitrarily. MR; mendelian randomization; Phe-WAS, phenome wide association study.

Thus, this analysis indicates that the altered cortical cellular architecture during development, as a result of glucocorticoids and rs648044 altered ZBTB16 amounts analysed throughout this thesis, could be the biological substrate that explains the associations of higher educational attainment and of altered brain structural measures in individuals that are carriers of the rs648044 rare A allele. This in turn highlights the importance of altered developmental brain trajectories not only for structural phenotypes but also for behavior

after birth and points to *ZBTB16* as an important node for the developing as well as the adult brain's structure and function in response to the environment.

5 | Discussion

Epidemiological and clinical studies have associated prenatal excess of glucocorticoids with neurobehavioral and structural outcomes for the offspring after birth (*pages 12 and 15, Krontira et al., Trends in Neurosciences, 2020 [26]*). With this work I sought to understand what are the cellular and molecular underpinnings of these associations. I focused on analysing the effects of glucocorticoids during the neurogenic period, a part of development that has been the least studied in association with environmental disturbances. I found that administration of glucocorticoids during neurogenesis increases the numbers of a specific type of neural progenitor cells that is enriched in gyrified species, while it is very rare in lissencephalic species. These cells co-express PAX6 (a major regulator of neurogenesis) and EOMES (basal progenitors' marker) and are one of the features that drive the increased neurogenic potential found in species with gyrified brains. At the molecular level this effect is mediated by the GR, a TF, which in turn activates *ZBTB16*. *ZBTB16*, being a TF itself, activates a promoter of *PAX6* and thus sustains its expression, resulting in increased numbers of PAX6 and EOMES positive progenitors in the SVZ of both hCOs and mice. The increased numbers of these highly proliferative and neurogenic progenitors lead to an extended neurogenic period and ultimately to increased production of neurons. Finally, the altered cytoarchitecture due to prenatal excess of glucocorticoids and *ZBTB16* potentially causally mediates beneficial postnatal outcomes, including increased cortical thickness and higher educational attainment (Figure 27).

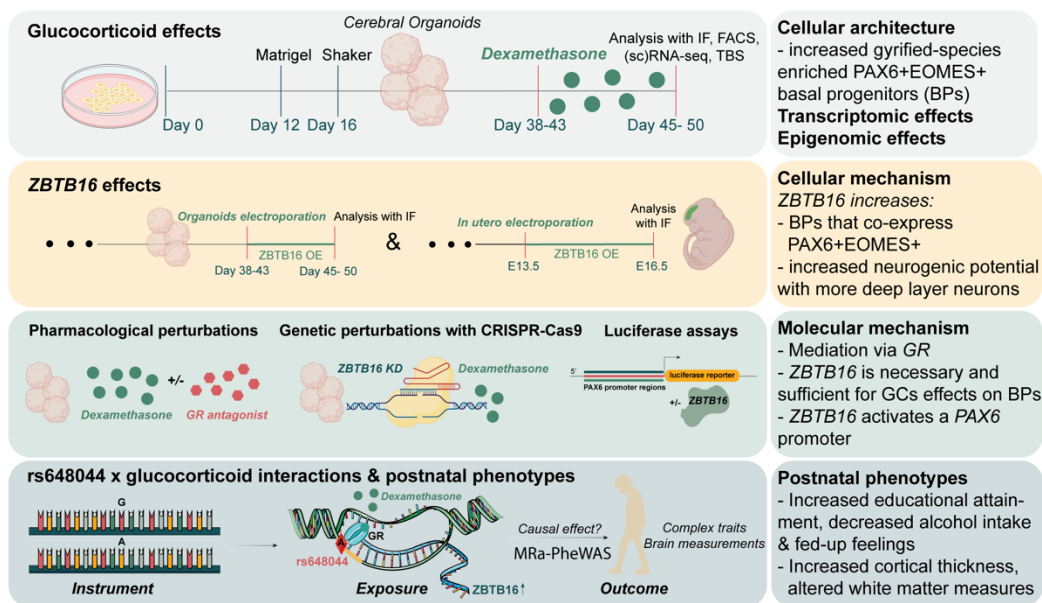


Figure 27| Summary of the main findings of this Ph.D thesis. Glucocorticoids outside of the normal range during neurogenesis alter the cytoarchitecture of the developing neocortex, via *ZBTB16*, by increasing the numbers of a type of basal progenitors found enriched in gyrified brains. These alterations potentially mediate beneficial

postnatal outcomes including increased cortical thickness and more years of schooling. Parts of the figure have been modified based on images from SMART (Servier Medical Art, <http://smart.servier.com/>).

5.1 GR is responsible for the glucocorticoid excess effects

Physiological glucocorticoids, cortisol in humans and corticosterone in mice, are released from the adrenal cortex as a result of the activation of the HPA axis. In turn, they mediate an ultra-short negative feedback loop to terminate the activation [15]. During pregnancy the placenta releases CRH which alters the function of both the maternal and the fetal HPA axes, mediating a positive feedback loop that results in increased production of glucocorticoids (*“Physiological rise of glucocorticoids during pregnancy”*, page 3), a hallmark step for the physiological development of the fetus.

There are two steroid hormone receptors mediating glucocorticoid effects, the MR and the GR. Cortisol and corticosterone are known to have high-affinity for the MR and low affinity for the GR [185]. Due to the different binding efficiencies of glucocorticoids, the MR is relatively fully bound by physiological levels of glucocorticoids, whereas the excess is considered to act via GR [157]. In fact, during the stress response the first receptor to get activated is the MR, but the rising concentration of glucocorticoids causes a switch to GR occupancy [185]. In addition, synthetic glucocorticoids, like dexamethasone and betamethasone that are used in antenatal corticosteroid treatments, bind with much higher affinity the GR than the MR [158], [186]. These observations highlight the significance of GR for potentially mediating the effects of glucocorticoid excess caused either due to stress or to synthetic treatments.

Here by using a combinatorial treatment paradigm of dexamethasone and RU486, a GR inhibitor, in hCOs it was shown that the effects of glucocorticoids on prenatal neurogenesis are dependent on GR (**Figure 17**). In hCOs, GR is expressed in a fraction of cells in the ventricle, including progenitor cells in the VZ and neurons in the CP, and in stromal cells surrounding the ventricle, thus it is neither selectively nor ubiquitously expressed (**Figure 7**). The distribution of GR expression found in this thesis in the hCOs resembles the one described in the literature.

In the developing rat brain GR is first found at E13 in the ventricular zone, the neuroepithelium and the choroid plexus. At E15 the expression in the neuroepithelium is enriched whereas at E17 GR shows a widespread expression in the amygdala, subiculum, olfactory bulb and cortex [187]. During postnatal hippocampal neurogenesis GR is enriched in dividing cells (in 27% of the cells) and in radial glia cells (50% of the cells) of the murine subgranular zone, but not in DCX+ neuroblasts [188]. Interestingly, even though GR is enriched in proliferative cell types of the murine hippocampus MR is not, whereas both are expressed by post-mitotic cells [188], [189]. Recent single cell studies of human fetal samples and hCOs provide an additional level of information of steroid

hormones receptor expression patterns now relevant for the human cortex. One study of 43,498 cells derived from pluripotency to 4-month old hCOs revealed an enrichment of GR in stem cells, RG cells and mesenchymal cells [190], a distribution that is similar to the one of fetal cortex. In the fetal cortex there is additional expression in the excitatory neurons cluster [191]. In contrast, MR is very lowly expressed both in hCOs and in human post-mortem brain single cell datasets [111], [156], [190]–[192].

Thus, the enrichment of GR over MR in the human cortex and models of the cortex, its enrichment in progenitor cells as well as neurons and its known role in mediating some of the effects of glucocorticoid excess, make GR an interesting molecular mediator to study. In fact, GR target genes comprise up to 10-20% of the human genome [193], highlighting the potentially widespread effects of its activation and the importance of studying it. The effects of GR in neurogenic processes have been studied mainly for postnatal hippocampal neurogenesis [94]. In this thesis it was shown that GR is additionally responsible for the effects of glucocorticoids on prenatal cortical neurogenic processes and specifically ones that are enriched in gyrified over lissencephalic species, introducing one more field where GR is important.

5.2 Treatment paradigm and clinical relevance

In this thesis glucocorticoid excess was modeled with dexamethasone, a synthetic GR agonist. The goal of this work was to model amounts of glucocorticoids induced either by prenatal stressful experiences or by antenatal corticosteroid treatments. The exact increase in glucocorticoids due to the environment are very difficult to determine, given the metabolism of glucocorticoids in the maternal circulation, by the placental barrier and in the fetal circulation. In contrast, the guidelines for antenatal corticosteroid treatments, dexamethasone being one of the drugs used, are very specific in the amounts used and, thus, the final levels of synthetic glucocorticoids reaching the fetus can be approximated. Moreover, as discussed, increased glucocorticoids during stress mediate their effects mainly via the GR and dexamethasone has a high affinity for GR over MR. Thus, dexamethasone was chosen as a model of GR activation and of the antenatal corticosteroid treatments administered during pregnancy.

The concentration used throughout this work was 100nM. The guidelines for synthetic glucocorticoid use are 6mg of dexamethasone every 12 hours for 2 days given intramuscularly [41], [45], when used in the 3rd trimester, and 1.5mg per day throughout the pregnancy starting before GW 7 [42], when given for CAH. A single dose of 6mg reaches a C_{max} of 65-95ng/ μ l at T_{max} 3 hours [45] which equals to a concentration of ~162nM-245nM, whereas 1.5mg would equal to ~40.4nM-61.25nM. The maternal to fetal ratio of

glucocorticoids has been reported anywhere from 0.4 and higher, days after the treatment [45]. So, from a single 6mg dose we would expect at the very least ~64.8nM-98nM reaching the fetus after 3 hours from the treatment. Similarly, from 1.5mg given each day we would expect at least ~16.16nM-39.2nM reaching the fetus after 3 hours from the treatment. A previously published study that used 100nM of androgens, which are also steroid hormones, in hCOs measured an actual concentration of 16nM in the hCOs [194]. They attributed this phenomenon to the fact that steroid hormones have high affinity to plastic due to their lipophilic nature [195], so they could be retained in large amounts by the cell culture plate, and to the short hormonal half-life. Dexamethasone has a half-life of ~5.5 hours [45]. Thus, the use of 100nM of dexamethasone every 48 hours models the amounts reaching the embryo by the clinically used concentrations which are re-administered every 12 hours for the 6mg or every 24 hours for the 1.5mg.

5.3 Glucocorticoids impact gyrified species-enriched neurogenic processes

Research on glucocorticoid effects on neurogenic processes has largely focused on postnatal hippocampal neurogenesis [94], [95], with very few studies on prenatal cortical neurogenesis in 2D iPSC-derived neuronal models [98], [196] and one in mice [197]. In the context of adult neurogenesis, glucocorticoids and stress have largely been associated with negative regulation of the process resulting in decreased differentiation of the progenitor cells [198]. The effects on prenatal cortical neurogenesis converge into higher proliferation of progenitor cells, though the molecular and cellular mechanisms are not known. With this work it was shown, for the first time, that glucocorticoids during mammalian cortical neurogenesis result in increased numbers of progenitor cells and neurons by boosting gyrified-species enriched neurogenic processes.

Dexamethasone increased a progenitor subtype that is enriched in gyrencephalic species, the cells that co-express PAX6 and EOMES (**Figure 8**) [87]. During physiological cortical neurodevelopment of lissencephalic species, like rodents, *Pax6*, as a TF, directly represses its own transcription [170] and simultaneously activates the expression of a group of basal progenitor cells determinants, including *Eomes*, thus driving basal cells production and cortical neurogenesis [171]. In turn *Eomes* directly binds and represses *Pax6* and activates *Tbr1* (a neuronal marker) to promote neurogenesis [172]. So, in physiological lissencephalic cortical development *Pax6*, *Eomes* and *Tbr1* create a positive feedforward cascade that self-regulates with direct negative feedback effects. This results in mutually exclusive expression of these proteins, with the only time that they are found co-expressed is in newborn BPs, a transient cell state which does not persist. In

contrast, in ferrets and primate species PAX6 and EOMES are non-mutually exclusively and are co-expressed in BPs that populate the inner- and outer- SVZ of ferrets [199] and primates [87].

The Pax6-Eomes+ IPs, which are the most abundant BP of lissencephalic species, regularly perform one symmetric division producing two neurons [83]. On the contrary, PAX6+EOMES+ BPs can perform proliferative and neurogenic divisions [87]. The S phase (cell cycle phase when the DNA is duplicated) of PAX6+EOMES+ iSVZ cells is similar to the one of PAX6+EOMES- cells (aRGs or bRGs) and is much longer than the one of PAX6-EOMES+ cells (IPs). In the oSVZ, the length of the S phase is between the one of bRGs and of IPs, a phenotype that follows the expression profile being halfway between the two cell types. Given their expression profile and their cell cycle characteristics [199], these cells are considered both proliferative and neurogenic BPs thus, they extensively increase the neurogenic potential by self-renewing in addition to producing neurons. The existence of proliferative BPs is hypothesized to lead to the bigger cortical surface, thickness and folding of the gyrencephalic species [86], [89], [101], [200] in comparison to lissencephalic mammals, like rodents.

In fact, when comparing the two models used in this thesis, the hCOs and the mice, the percentage of progenitors' subtypes in the different expression profiles reveals these basic differences of lissencephalic and gyrencephalic neurogenic processes. Organoids are not gyrified but they are models of the human neurogenesis thus recapitulate certain aspects of it. In the *in utero* electroporations of the mice, the percentage of the total GFP cells that were Pax6+Eomes+ was 3.07% whereas for the Pax6-Eomes+ it was 12.92%, which means that the IPs (Pax6-Eomes+) were approximately 4 times more than the Pax6+Eomes+ cells. In addition, the vast majority of Pax6+Eomes+ cells resided in the VZ so most probably represented newborn BPs, a transient cell state and not a persistent cell type (**Figure 19**). In contrast, in the hCOs the percentage of total GFP cells that were PAX6+EOMES+ was 8.7% whereas for the PAX6-EOMES+ it was 2.02%. This means that the double positive cells were approximately 4.3 times more than the PAX6-EOMES+ cells, with the vast majority of them residing in the basal parts of the ventricle (**Figure 15**). Even though these numbers account only for the electroporated cells and that organoids are a model and not the actual fetal tissue, they still show the expansion of these proliferative and neurogenic double positive progenitors in a model of gyrencephalic neurogenesis as compared to a model of lissencephalic neurogenic processes. Glucocorticoids mediate their effects on PAX6+EOMES+ BPs via *ZBTB16*, both in hCOs (**Figure 16** and **Figure 17**, 25.7% increase) and in mice (**Figure 19**, 8.9% increase). In turn, in both cases this led to a significant increase of the production of deep layer neurons (biggest effect on layer V, BCL11B+ cells, 16% increase in hCOs and 33% in mice).

The specificity of the effects on deep layer neurons could be explained by the developmental timing of the perturbations. The mice were electroporated at E13.5 when layer VI neurons (*Tbr1*⁺) are at peak neurogenesis and layer V neurons (*Bcl11b*⁺) have started to be produced whereas layer IV neurons (*Satb2*⁺) are not produced yet [67] and analysed 3 days later at E16.5. It could be speculated that the specificity of the effect on layer VI and V neurons indicates that the effects of ZBTB16 overexpression on the neuronal populations are defined by the progenitor populations present and thus affected at E13.5 when the cells were firstly electroporated. Indeed, when Tsiarli *et al.* treated with dexamethasone at E14.5, when layer VI neurons are not produced anymore, layer V neurons are at peak neurogenesis and layer IV have started to be produced, they found effects on layer V and IV neurons [67], thus strengthening the idea that the dexamethasone via *ZBTB16* effects in specific deep layer neuronal types observed with this work could be explained by the progenitors and niche stimuli present and affected at the time of the manipulation.

5.4 ZBTB16 mediates the effects of glucocorticoids on neurogenesis

Dexamethasone altered the developing cytoarchitecture of the cortex via altering the expression profile of *ZBTB16*. *ZBTB16* is a zinc-finger transcription factor that can both activate and repress its targets [201], known to balance stem cell self-renewal and differentiation of spermatogonial, osteogenic, myeloid, lymphoid and neuronal progenitors [160], [161]. It was first discovered fused with the retinoic acid receptor (*RA*) and involved in the pathogenesis of acute promyelocytic leukemia, thus taking the additional name *PLZF* (promyelocytic leukemia zinc finger protein) [202], [203]. It has been shown to repress *Cyclin-A2*, which is a protein important for the G1/S and G2/M transitions of the cell cycle, thus resulting in accumulation of cells in the S phase [161]. It is involved in chromatin remodeling by being in a complex with histone deacetylases (*HDACs*) thus mediating its repressive effects [161] and it also regulates ubiquitination by being a member of the Cullin3-Roc1- E3 ubiquitin ligase complex [204]. In the CNS it is important for the regionalization of the vertebrate hindbrain by being enriched in the rhombomere boundaries [205] and restricting the expression of *Hox* genes [206]. Biallelic loss of function of this TF caused by a single nucleotide variation in the zinc finger domain (pMet617Val) is causative for mental retardation, skeletal defects and genital hypoplasia [207] whereas other duplications, SNPs and variations have been associated with autism spectrum disorders, schizophrenia and educational attainment [208].

As already discussed, *ZBTB16* has a very dynamic expression pattern in the developing brain (“*ZBTB16* is dynamically expressed during development”, page 49). In the mouse it appears at E7.5 in the neuroectoderm and increasingly accumulates in the CNS until E10.5 when it gets downregulated and is then only expressed in specific areas of the hindbrain and the septum but not the forebrain [166]. Thus, in the mouse, and possibly in lissencephalic species in general, *Zbtb16* is not expressed during the neurogenic period [167]. The expression pattern of *ZBTB16* is very dynamic in gyrified species too, with the important difference that in them it is expressed in the first steps of neurogenesis until approximately GW 13 (**Supplementary Figure 2 & Figure 13**). This points to a potential role of this TF in gyrified species-enriched processes, at least at the start of neurogenesis of physiological neurodevelopment and indicates that non-physiological levels of this TF, for example in response to glucocorticoids, could alter the balance of renewal and differentiation and impact gyrified-enriched neurogenic processes.

In fact, with this work it is shown that the environmentally-induced increased expression of this TF in a developmental window when this protein is physiologically not expressed, has important effects on neurogenic processes of both hCOs, used as a model of human neurodevelopment, and of a lissencephalic species, the mouse. The importance of *Zbtb16* in early neurodevelopment has been discussed in the literature with studies in chicken, zebra fish and mice. In zebra fish, *zbtb16* suppresses neurogenesis by inhibiting the expression of *neurog1* [209], whereas in the chicken central spinal cord it suppresses neurogenesis and biases progenitors towards a glial fate by inhibiting the expression of *neurog2* via an *fgfr3*- and *stat3*- dependent manner [210]. The importance of this TF for early mammalian development was shown recently with two studies in KO, for this protein, mice. It was shown that the absence of *Zbtb16* before E10, when it should be expressed, led to decreased numbers of mitotic cells in the VZ (Ph3+), decreased production of deep layer neurons (Tbr1+) and microcephaly [167], with these mice exhibiting social and cognitive impairments [208]. Thus, it is clear that *ZBTB16* is important for early neurodevelopment by balancing proliferation and differentiation processes while its loss leads to altered behaviors for the offspring early in postnatal life. While these are important pieces of literature they focus on the effects of this TF in non-mammalian species or during very early neurodevelopment in mammalian species and do not consider environmental effects. With this work, the importance of *ZBTB16* for the balance of self-renewal and differentiation has been verified and a novel role of environmentally-induced non-physiological levels of this TF for specific neurogenic processes enriched in gyrified species identified.

5.4.1 *ZBTB16* sustains *PAX6* expression

Here it was found that upregulation of *ZBTB16* due to glucocorticoids outside of the normal range sustains *PAX6* expression in BPs. This was true even in mice where, being a lissencephalic species, *Pax6* and *Eomes* are rarely co-expressed [170]–[172]. Nevertheless, increased expression of *ZBTB16* during mouse neurogenesis sustained the expression of *Pax6* in *Eomes* positive cells. This was probably achieved due to the direct activation of the P1 promoter of *PAX6* by *ZBTB16* (Figure 22). *PAX6* has three promoters which confer cell-type-, tissue- and temporal- specificity in the expression of the protein. The P1 promoter is the most active of the three during neurogenesis in the neocortex of rodents [173], while the regulatory regions of *PAX6* are highly conserved between humans and mouse [174]. It could be hypothesised that a regulator of one of these regions in one species probably has the ability to regulate *PAX6* also in the other. This seems true for *ZBTB16* since its overexpression leads to a similar phenotype in both hCOs, which are of human origin, and mice (Figure 15 & 19).

PAX6 is one of the most important modulators of neurogenic processes for the developing cortex and it's the major marker of RG cells [171], [211], [212]. Expression of *PAX6* defines bRG cells (cells found enriched in gyrencephalic species). bRG cells are partly driving the extended neurogenic period and neuronal production found in ferrets and primates [213]. In addition, sustained *Pax6* expression, result of a genetic manipulation, in mice induced the presence of cells with the characteristics of bRGs, which physiologically are very rare in mice [214], thus highlighting the importance of *PAX6* for regulating progenitor subtypes among species and developmental windows. Here it was shown that glucocorticoids via *ZBTB16* modulate the activity of a regulatory region of *PAX6*, thus sustaining its expression which results in increased numbers of a subtype of progenitors which is highly proliferative and neurogenic and is enriched in gyrified species. In fact, glucocorticoids, via GR activation, have been shown before to increase the promoter activity of *pax6* in the chicken cerebellum [215], underlying their role as potential regulators of *PAX6*.

5.5 Glucocorticoids and beneficial postnatal outcomes

As discussed in detail in the introduction (“Prenatal environment and neurobehavioral outcomes”, page 12) the adverse outcomes result of exposures to prenatal stressors and prenatal excess of glucocorticoids [55] are very well characterised and are associated with a wide variety of phenotypes including cardio-metabolic, cognitive and temperament alterations [55], neurodevelopmental disorders [61] and increased risk for mental disorders [62] for the offspring. When focusing though on the timing of the exposures the

majority of studies concern third trimester environments. This is especially true for synthetic glucocorticoids the guidelines for which recommend their use after the 25th GW [41], [216], when treating premature births. This is an important point since neurogenesis in humans lasts approximately until the 25th GW (“Cortical development length in humans and rodents”, *page 16*). This suggests that for the majority of studies associating glucocorticoid excess with adverse outcomes without defining the timing of the exposure, one could theorize that the exposure concerns mainly a time-window when neurogenesis is completed. Of course, this is not always true and there are prenatal exposures happening during the neurogenic period so starting much earlier, in the middle of first trimester. While one could assume this is the reality for psychological prenatal exposures, we do know is true for antenatal corticosteroid treatment of CAH, which is administered throughout pregnancy starting before the 7th GW [42]. This is not trivial, since even if we exclude any other potential sources of glucocorticoid excess in the first and second trimesters, CAH alone accounts for a large number of embryos affected since it is the most common autosomal recessive disorder affecting 1 to 10,000- 15,000 births [42]. In fact, as already discussed (“Prenatal environment and neurobehavioral outcomes”, *page 12*), glucocorticoids early on in pregnancy during the neurogenic period have been associated with reduced risk for neurodevelopmental impairments [65], anxiolytic and anti-depressive effects [197], highlighting the importance of considering the developmental time-window of exposure and suggesting that there could be beneficial outcomes of glucocorticoid excess too, if this happens during the neurogenic period.

In fact, with this work it was shown that glucocorticoids interact with the genetic landscape of *ZBTB16* to define its amount. In turn the genetically-predicted levels of the TF were causally associated with altered brain structural outcomes, including increased cortical thickness and decreased white matter connectivity, and more years of schooling (**Figure 25 & 26**), which is indeed a beneficial outcome. Glucocorticoid associations with cortical thickness have been shown before with higher maternal cortisol being associated with greater child cortical thickness in the frontal regions [76]. In addition, genetic risk for high educational attainment has been correlated with increased cortical volume and thickness [179]–[181] and decreased white matter connectivity measures [183], while cognitive performance and cerebral cortical morphology seem to share genetic contributions [179]. Interestingly, educational attainment is protective even at the level of psychiatric disorders as individuals with increased levels of education show significantly less risk of suffering from major depressive disorder [217].

This Ph.D. work suggests that the effects of glucocorticoid excess and *ZBTB16* early on in gestation, during the neurogenic period, on increased gyrified species-enriched pro-

cesses that result in higher proliferative and neurogenic potential and thus larger production of neurons, could be causally explaining the increased cortical thickness associated with glucocorticoids and, in turn, with higher educational attainment. Overall this suggests that the altered developmental cellular architecture caused by glucocorticoids and *ZBTB16* during neurogenesis could lead to beneficial outcomes for the offspring after birth.

5.6 Limitations

This study has a number of limitations. First, while it is important that the effects were studied in two models of mammalian neurogenesis, the one modeling human neurogenesis was organoids. As discussed in the introduction (“Modelling the human developing cerebral cortex”, *page 21*) organoids are an important and useful tool to study human neurogenesis but they do have a lot of caveats, including the lack of vascularization, lack of glial cells and higher variability between organoids of the same batch and among batches. The ideal resource would be post-mortem fetal cortex. Of course, this is very rare to find and its use is confined by many ethical regulations. In addition, genetic manipulations would be very difficult thus significantly limiting the type and amount of molecular experiments able to be done. In addition, the effects of glucocorticoid excess on postnatal cytoarchitecture were not studied. Especially in the mouse, where glucocorticoids via *ZBTB16* increased the production of a cell type that is rare in this species, it would be very interesting to study its effects on postnatal cortical morphology and wiring. Moreover, *ZBTB16* was shown to activate a *PAX6* promoter thus providing one of explanation of how sustained expression of *PAX6* could be achieved. *ZBTB16* is a TF thus affects a multitude of targets. It would be interesting to know which are affected in the context of glucocorticoids in these models. This was in fact tried during this Ph.D. work with extensive efforts to achieve a successful ChIP-sequencing or Cut & Run experiment for *ZBTB16* but it was never achieved. None of the *ZBTB16* antibodies produced now was successful for neither of the two techniques. In fact, this seems to be a common problem for people working with this TF, with the vast majority of the ChIP-sequencing experiments out there for *ZBTB16* having been done with one antibody which is not produced anymore. Last, it was shown that glucocorticoids via *ZBTB16* increase the numbers of *PAX6*+*EOMES*+ BPs in hCOs and mice. The expression profile of these cells was not assayed; thus, it is not known if these cells after glucocorticoids and between the two models are the same or not.

5.7 Future directions

Going forward there is a variety of questions interesting to answer arising from this work. Starting with the ones that were already mentioned in the previous paragraph, the expression profile of the double positive progenitors among species and after glucocorticoids can be analysed. This could be achieved either with sorting these cells and running an RNA sequencing experiment or even better with proteomics. In fact, this will be tried with proteomics after laser-capture microdissection of the area of interest.

Additionally, the shape of these cells should be determined. As discussed, BPs of gyrified species can be found as non-polar, with one apical process, one basal process or both processes. Double positive cells have been shown to exhibit all shapes but mainly being non-polar in macaques [87]. This is indeed an important point to be addressed since, in neurodevelopment, shape together with expression profile define the type of progenitors and their function.

Moreover, there are interesting questions that need to be addressed on the functional genomics part of this thesis. Here I focused on the effects of one SNP of the *ZBTB16* locus, because it was indeed one of the most interesting ones in relation to its position, inside a glucocorticoids-responsive enhancer, and its associations with both structural, cortical thickness, and neurobehavioral, educational attainment, outcomes. When though looking through the GWAS Catalogue there are more interesting SNPs that could affect *ZBTB16* transcription and thus explain more or even different postnatal phenotypes.

Finally, in the results it was shown that there is evidence of non-cell autonomous effects of *ZBTB16* overexpression in the mice. This is intriguing since *ZBTB16* is a TF so, normally, it would not be directly associated with extracellular signals. Thus, how these non-cell autonomous effects arise should be determined. This is of great importance because it suggests an extension of the effects of glucocorticoids in cells that have not, potentially, been directly affected by them.

6 | Conclusions

This work highlights the importance of prenatal development for postnatal health in relation to developmental time-windows. Prenatal environmental exposures have lasting impacts on health throughout life which are defined by the type as well as the timing of the exposure. While the majority of studies highlight adverse outcomes of prenatal environmental factors, such as stress and glucocorticoids, on neurobehavioral phenotypes after birth [6] they mostly focus on exposures during the end of gestation, after neurogenesis is concluded.

Here I focused on glucocorticoids. Endogenous glucocorticoids are important for the physiological development of the brain, with nature specifically rising their concentrations towards the end of gestation to boost organ maturation and function [11]. Levels of glucocorticoids outside the normal range during the last weeks of gestation, either as a result of prenatal stress or of antenatal corticosteroid treatments, have been shown to impact brain structure and function in an adverse way [26]. Recent studies highlight divergent effects of glucocorticoids on neurodevelopmental trajectories according to the timing of the exposure [218]. In fact, when the administration of glucocorticoids is early in gestation, during neurogenesis, it seems to mediate beneficial outcomes including reduced risk for neurodevelopmental disorders [65], anxiolytic and anti-depressive effects [197]. This dual role of glucocorticoids on beneficial and adverse outcomes could be associated with the timing of the exposure. Interestingly, while the adverse effects of glucocorticoid excess during late gestation are very well characterized [26], the cellular and molecular phenotypes when increased in early development during the neurogenic period have rarely been studied.

With this work I show how glucocorticoids during neurogenesis can also mediate beneficial postnatal effects via impacting the levels of an important TF, *ZBTB16*. *ZBTB16* affects neurogenic processes that are enriched in gyrified species which ultimately result in increased numbers of proliferative and neurogenic basal progenitors, extended neurogenic period and ultimately higher numbers of neurons produced. These potentially are the cellular underpinnings of the higher postnatal cortical thickness associated with glucocorticoids and *ZBTB16* that in turn correlates with higher educational attainment, a protective phenotype even against stress-related disorders [217].

Thus, this work provides a molecular and cellular mechanism of how exposure to glucocorticoids during neurogenesis in early gestation could be potentially associated with the beneficial outcomes found in the large clinical studies and highlights the importance of considering the developmental time-window when analysing environmental effects on postnatal health.

7 | Bibliography

- [1] D. J. P. Barker and C. Osmond, "Death rates from stroke in England and Wales predicted from past maternal mortality," *British Medical Journal (Clinical research ed.)*, vol. 295, no. 6590, pp. 83–86, 1987.
- [2] D. J. P. Barker, C. Osmond, J. Golding, D. Kuh, and M. Wadsworth, "Growth in utero, blood pressure in childhood and adult life, and mortality from cardiovascular disease," *BMJ*, vol. 298, no. March, pp. 564–567, 1989.
- [3] D. J. P. Barker, "The fetal and infant origins of adult disease The womb may be more important than the home," *BMJ*, no. 156, p. 1990, 1990.
- [4] D. J. P. Barker, "The developmental origins of chronic adult disease," *Acta Paediatr Suppl*, no. 8, pp. 26–33, 2004.
- [5] J. R. Seckl and M. C. Holmes, "Mechanisms of disease: Glucocorticoids, their placental metabolism and fetal 'programming' of adult pathophysiology," *Nature Clinical Practice Endocrinology and Metabolism*, vol. 3, no. 6, pp. 479–488, 2007.
- [6] K. J. O'Donnell and M. J. Meaney, "Fetal origins of mental health: The developmental origins of health and disease hypothesis," *American Journal of Psychiatry*, vol. 174, no. 4, pp. 319–328, 2017.
- [7] C. Monk, C. Lugo-Candelas, and C. Trimpff, "Prenatal Developmental Origins of Future Psychopathology: Mechanisms and Pathways," *Annual Review of Clinical Psychology*, vol. 15, no. 1, 2019.
- [8] B. R. H. Van den Bergh *et al.*, "Prenatal developmental origins of behavior and mental health: The influence of maternal stress in pregnancy," *Neuroscience and Biobehavioral Reviews*, no. November 2016, 2017.
- [9] D. Mongan *et al.*, "Prevalence of self-reported mental disorders in pregnancy and associations with adverse neonatal outcomes: a population-based cross-sectional study," *BMC Pregnancy and Childbirth*, vol. 19, no. 1, pp. 1–10, 2019.
- [10] O. Vesga-Lopez, C. Blanco, K. Keyes, M. Olfson, B. F. Grant, and D. S. Hasin, "Psychiatric Disorders in Pregnant and Postpartum Women in the United States," *Archives of General Psychiatry*, vol. 65, no. 7, pp. 805–815, 2008.
- [11] E. P. Davis and A. J. Narayan, "Pregnancy as a period of risk, adaptation, and resilience for mothers and infants," *Development and Psychopathology*, vol. 32, no. 5, pp. 1625–1639, 2020.
- [12] H. Yan, Y. Ding, and W. Guo, "Mental Health of Pregnant and Postpartum Women During the Coronavirus Disease 2019 Pandemic: A Systematic Review and," *Frontiers in Psychology*, vol. 11, no. November, pp. 1–12, 2020.
- [13] R. M. Meredith, "Sensitive and critical periods during neurotypical and aberrant

- neurodevelopment: A framework for neurodevelopmental disorders,” *Neuroscience and Biobehavioral Reviews*, vol. 50, pp. 180–188, 2015.
- [14] D. Rice and S. Barone, “Critical periods of vulnerability for the developing nervous system: Evidence from humans and animal models,” *Environmental Health Perspectives*, vol. 108, no. SUPPL. 3, pp. 511–533, 2000.
- [15] T. Klengel and E. B. Binder, “Epigenetics of Stress-Related Psychiatric Disorders and Gene × Environment Interactions,” *Neuron*, vol. 86, no. 6, pp. 1343–1357, 2015.
- [16] V. G. Moisiadis and S. G. Matthews, “Glucocorticoids and fetal programming part 2: mechanisms,” *Nature Reviews Endocrinology*, vol. 10, no. 7, pp. 403–411, 2014.
- [17] K. O’Donnell, T. G. O’Connor, and V. Glover, “Prenatal stress and neurodevelopment of the child: Focus on the HPA axis and role of the placenta,” *Developmental Neuroscience*, vol. 31, no. 4, pp. 285–292, 2009.
- [18] P. D. Edwards and R. Boonstra, “Glucocorticoids and CBG during pregnancy in mammals: diversity, pattern, and function,” *General and Comparative Endocrinology*, vol. 259, pp. 122–130, 2018.
- [19] M. McLean and R. Smith, “Corticotrophin-releasing hormone and human parturition,” *Reproduction*, vol. 121, no. 4, pp. 493–501, 2001.
- [20] A. Munck, P. M. Guyre, and N. J. Holbrook, “Physiological Functions of Glucocorticoids in Stress and Their Relation to Pharmacological Actions*,” *Endocrine Reviews*, vol. 5, no. 1, pp. 25–44, Jan. 1984.
- [21] R. J. Bolt, M. M. van Weissenbruch, H. N. Lafeber, and H. A. Delemarre-van de Waal, “Glucocorticoids and lung development in the fetus and preterm infant,” *Pediatric Pulmonology*, vol. 32, no. 1, pp. 76–91, 2001.
- [22] S. G. Matthews, “Antenatal Glucocorticoids and Programming of the Developing CNS,” *Pediatric Research*, vol. 47, no. 3, pp. 291–300, 2000.
- [23] S. J. Lupien and B. S. McEwen, “The acute effects of corticosteroids on cognition: Integration of animal and human model studies,” *Brain Research Reviews*, vol. 24, no. 1, pp. 1–27, 1997.
- [24] M. Weinstock, “The potential influence of maternal stress hormones on development and mental health of the offspring,” *Brain, Behavior, and Immunity*, vol. 19, no. 4, pp. 296–308, 2005.
- [25] A. Harris and J. Seckl, “Hormones and Behavior Glucocorticoids , prenatal stress and the programming of disease,” *Hormones and Behavior*, vol. 59, no. 3, pp. 279–289, 2011.
- [26] A. C. Krontira, C. Cruceanu, and E. B. Binder, “Glucocorticoids as Mediators of

- Adverse Outcomes of Prenatal Stress,” *Trends in Neurosciences*, vol. 43, no. 6, pp. 394–405, Apr. 2020.
- [27] A. Barbazanges, P. V. Piazza, M. Le Moal, and S. Maccari, “Maternal glucocorticoid secretion mediates long-term effects of prenatal stress,” *Journal of Neuroscience*, vol. 16, no. 12, pp. 3943–3949, 1996.
- [28] Z. M. Thayer, M. A. Wilson, A. W. Kim, and A. V. Jaeggi, “Impact of prenatal stress on offspring glucocorticoid levels: A phylogenetic meta-analysis across 14 vertebrate species,” *Scientific Reports*, vol. 8, no. 1, pp. 1–9, 2018.
- [29] V. Glover, T. G. O’Connor, and K. O’Donnell, “Prenatal stress and the programming of the HPA axis,” *Neuroscience and Biobehavioral Reviews*, vol. 35, no. 1, pp. 17–22, 2010.
- [30] A. Charil, D. P. Laplante, C. Vaillancourt, and S. King, “Prenatal stress and brain development,” *Brain Research Reviews*, vol. 65, no. 1, pp. 56–79, 2010.
- [31] V. G. Moisiadis and S. G. Matthews, “Glucocorticoids and fetal programming part 1 : outcomes,” *Nature Reviews Endocrinology*, vol. 10, pp. 391–402, 2014.
- [32] J. R. Seckl and M. J. Meaney, “Glucocorticoid Programming,” *Annals of the New York Academy of Sciences*, vol. 84, no. 44, pp. 63–84, 2004.
- [33] R. Schiffner *et al.*, “Effects of late gestational fetal exposure to dexamethasone administration on the postnatal hypothalamus-pituitary-adrenal axis response to hypoglycemia in pigs,” *International Journal of Molecular Sciences*, vol. 18, no. 11, pp. 1–11, 2017.
- [34] N. S. Levitt, R. S. Lindsay, M. C. Holmes, and J. R. Seckl, “Dexamethasone in the Last Week of Pregnancy Attenuates Hippocampal Glucocorticoid Receptor Gene Expression and Elevates Blood Pressure in the Adult Offspring in the Rat,” *Neuroendocrinology*, vol. 64, no. 6, pp. 412–418, 1996.
- [35] E. P. Davis, F. Waffarn, and C. A. Sandman, “Prenatal treatment with glucocorticoids sensitizes the hpa axis response to stress among full-term infants,” *Developmental Psychobiology*, vol. 53, no. 2, pp. 175–183, 2011.
- [36] F. J. G. Shearer, S. Wyrwoll, and M. C. Holmes, “The Role of 11 β -Hydroxy Steroid Dehydrogenase Type 2 in Glucocorticoid Programming of Affective and Cognitive Behaviours,” *Neuroendocrinology*, vol. 109, no. 3, pp. 257–265, 2019.
- [37] L. I. Stirrat *et al.*, “Transfer and metabolism of cortisol by the isolated perfused human placenta,” *Journal of Clinical Endocrinology and Metabolism*, vol. 103, no. 2, pp. 640–648, 2018.
- [38] K. J. O. Donnell, A. Bugge, L. Freeman, N. Khalife, T. G. O. Connor, and V. Glover, “Maternal prenatal anxiety and downregulation of placental 11 b -HSD2,”

- Psychoneuroendocrinology*, vol. 37, no. 6, pp. 818–826, 2012.
- [39] J. F. Briffa, S. S. Hosseini, M. Tran, K. M. Moritz, J. S. M. Cuffe, and M. E. Wlodek, “Maternal growth restriction and stress exposure in rats differentially alters expression of components of the placental glucocorticoid barrier and nutrient transporters,” *Placenta*, vol. 59, pp. 30–38, 2017.
- [40] A. Ozmen, G. Unek, and E. T. Korgun, “Effect of glucocorticoids on mechanisms of placental angiogenesis,” *Placenta*, vol. 52, pp. 41–48, 2017.
- [41] Committee on Obstetric Practice, “Antenatal Corticosteroid Therapy for Fetal Maturation,” *Obstetrics and Gynecology*, vol. 130, no. 2, pp. 102–109, 2017.
- [42] S. Lajic, L. Karlsson, and A. Nordenström, “Prenatal Treatment of Congenital Adrenal Hyperplasia: Long-Term Effects of Excess Glucocorticoid Exposure,” *Hormone Research in Pediatrics*, 2018.
- [43] D. El-Maouche, W. Arlt, and D. P. Merke, “Congenital adrenal hyperplasia,” *The Lancet*, vol. 390, no. 10108, pp. 2194–2210, 2017.
- [44] M. David, M. G. Forest, and P. D. L. Cedex, “Prenatal treatment of congenital adrenal hyperplasia resulting from 21-hydroxylase deficiency,” *The journal of Pediatrics*, vol. 1, 1984.
- [45] A. H. Jobe, M. Kemp, A. Schmidt, T. Takahashi, J. Newnham, and M. Milad, “Antenatal corticosteroids: a reappraisal of the drug formulation and dose,” *Pediatric Research*, no. September 2020, 2021.
- [46] J. C. Chan, B. M. Nugent, and T. L. Bale, “Parental Advisory: Maternal and Paternal Stress Can Impact Offspring Neurodevelopment,” *Biological Psychiatry*, vol. 83, no. 10, pp. 886–894, 2018.
- [47] C. Buss *et al.*, “Intergenerational Transmission of Maternal Childhood Maltreatment Exposure: Implications for Fetal Brain Development,” *Journal of the American Academy of Child and Adolescent Psychiatry*, vol. 56, no. 5, pp. 373–382, 2017.
- [48] H. Thomassin, M. Flavin, M. L. Espinás, and T. Grange, “Glucocorticoid-induced DNA demethylation and gene memory during development,” *EMBO Journal*, vol. 20, no. 8, pp. 1974–1983, 2001.
- [49] N. Provençal, J. Arloth, A. Cattaneo, C. Anacker, and N. Cattane, “Glucocorticoid exposure during hippocampal neurogenesis primes future stress response by inducing changes in DNA methylation,” *Proceedings of the National Academy of Sciences*, 2019.
- [50] E. B. Binder, “Dissecting the molecular mechanisms of gene x environment interactions: implications for diagnosis and treatment of stress-related psychiatric disorders,” *European Journal of Psychotraumatology*, vol. 8, no. 00, 2017.

- [51] C. Cruceanu, N. Matosin, and E. B. Binder, "Interactions of early-life stress with the genome and epigenome: from prenatal stress to psychiatric disorders," *Current Opinion in Behavioral Sciences*, vol. 14, pp. 167–171, 2017.
- [52] T. Wiechmann *et al.*, "Identification of dynamic glucocorticoid-induced methylation changes at the FKBP5 locus," *Clinical Epigenetics*, vol. 11, no. 1, p. 83, 2019.
- [53] T. Klengel *et al.*, "Allele-specific FKBP5 DNA demethylation mediates gene–childhood trauma interactions," *Nature Neuroscience*, vol. 16, no. 1, pp. 33–41, 2012.
- [54] D. Czamara *et al.*, "Integrated analysis of environmental and genetic influences on cord blood DNA methylation in new-borns," *Nature Communications*, vol. 10, no. 1, p. 2548, 2019.
- [55] B. R. H. Van den Bergh *et al.*, "Prenatal developmental origins of behavior and mental health: The influence of maternal stress in pregnancy," *Neuroscience & Biobehavioral Reviews*, no. July, 2017.
- [56] K. J. O'Donnell, V. Glover, E. D. Barker, and T. G. O'Connor, "The persisting effect of maternal mood in pregnancy on childhood psychopathology," *Development and Psychopathology*, vol. 26, no. 2, pp. 393–403, 2014.
- [57] A. S. Brown, J. Van Os, C. Driessens, H. W. Hoek, and E. S. Susser, "Further evidence of relation between prenatal famine and major affective disorder," *American Journal of Psychiatry*, vol. 157, no. 2, pp. 190–195, 2000.
- [58] M. T. Kinsella and C. Monk, "Impact of Maternal Stress, Depression & Anxiety on Fetal Neurobehavioral Development," *Clinical obstetrics and gynecology*, vol. 52, no. 3, pp. 425–440, 2009.
- [59] J. R. Seckl, "Prenatal glucocorticoids and long-term programming," *European Journal of Endocrinology, Supplement*, vol. 151, no. 3, pp. 49–62, 2004.
- [60] L. A. M. Welberg, J. R. Seckl, and M. C. Holmes, "Prenatal glucocorticoid programming of brain corticosteroid receptors and corticotrophin-releasing hormone: Possible implications for behaviour," *Neuroscience*, vol. 104, no. 1, pp. 71–79, 2001.
- [61] N. Melamed *et al.*, "Neurodevelopmental disorders among term infants exposed to antenatal corticosteroids during pregnancy : a population-based study," pp. 3–10, 2019.
- [62] K. Räikkönen, M. Gissler, and E. Kajantie, "Associations Between Maternal Antenatal Corticosteroid Treatment and Mental and Behavioral Disorders in Children Supplemental content," *Jama*, vol. 323, no. 19, pp. 1924–1933, 2020.
- [63] J. Bock, T. Wainstock, K. Braun, and M. Segal, "Stress In Utero: Prenatal Programming of Brain Plasticity and Cognition," *Biological Psychiatry*, vol. 78, no.

- 5, pp. 315–326, 2015.
- [64] A. E. Michael and A. T. Papageorgiou, “Potential significance of physiological and pharmacological glucocorticoids in early pregnancy,” *Human Reproduction Update*, vol. 14, no. 5, pp. 497–517, 2008.
- [65] K. Ninan, S. K. Liyanage, K. E. Murphy, E. V Asztalos, and S. D. McDonald, “Evaluation of Long-term Outcomes Associated With Preterm Exposure to Antenatal Corticosteroids: A Systematic Review and Meta-analysis.,” *JAMA pediatrics*, p. e220483, 2022.
- [66] S. Chawla *et al.*, “Association of Neurodevelopmental Outcomes and Neonatal Morbidities of Extremely Premature Infants With Differential Exposure to Antenatal Steroids,” *JAMA Pediatrics*, vol. 170, no. 12, pp. 1164–1172, Dec. 2016.
- [67] M. A. Tsiarli *et al.*, “Antenatal dexamethasone exposure differentially affects distinct cortical neural progenitor cells and triggers long-term changes in murine cerebral architecture and behavior,” *Translational psychiatry*, no. February, 2017.
- [68] B. S. McEwen and C. Liston, *Mediators of Glucocorticoid-Regulated Adaptive Plasticity*, no. May. 2017.
- [69] N. K. Moog *et al.*, “Intergenerational Effect of Maternal Exposure to Childhood Maltreatment on Newborn Brain Anatomy,” *Biological Psychiatry*, vol. 83, no. 2, pp. 120–127, 2018.
- [70] E. P. Davis, B. L. Hankin, L. M. Glynn, K. Head, D. J. Kim, and C. A. Sandman, “Prenatal Maternal Stress, Child Cortical Thickness, and Adolescent Depressive Symptoms,” *Child Development*, vol. 00, no. 0, pp. 1–19, 2019.
- [71] C. Buss, E. P. Davis, B. Shahbaba, J. C. Pruessner, K. Head, and C. A. Sandman, “Maternal cortisol over the course of pregnancy and subsequent child amygdala and hippocampus volumes and affective problems,” *Proceedings of the National Academy of Sciences*, vol. 109, no. 20, pp. E1312–E1319, 2012.
- [72] A. M. Graham *et al.*, “Maternal Cortisol Concentrations During Pregnancy and Sex-Specific Associations With Neonatal Amygdala Connectivity and Emerging Internalizing Behaviors,” *Biological Psychiatry*, vol. 85, no. 2, pp. 172–181, 2019.
- [73] N. Modi, H. Lewis, N. Al-Naqeeb, M. Ajayi-Obe, C. J. Dore, and M. Rutherford, “The effects of repeated antenatal glucocorticoid therapy on the developing brain,” *Pediatric Research*, vol. 50, no. 5, pp. 581–585, 2001.
- [74] N. Parker *et al.*, “Corticosteroids and Regional Variations in Thickness of the Human Cerebral Cortex across the Lifespan,” *Cerebral Cortex*, no. June 2019, pp. 575–586, 2020.
- [75] R. A. Morey *et al.*, “Widespread Cortical Thickness Is Associated With Neuroactive Steroid Levels,” *Frontiers in Neuroscience*, vol. 13, no. November,

- pp. 1–17, 2019.
- [76] E. P. Davis, K. Head, C. Buss, and C. A. Sandman, “Prenatal maternal cortisol concentrations predict neurodevelopment in middle childhood,” *Psychoneuroendocrinology*, vol. 75, pp. 56–63, 2017.
- [77] Q. Li *et al.*, “Meta-analysis of cortical thickness abnormalities in medication-free patients with major depressive disorder,” *Neuropsychopharmacology*, no. September, 2019.
- [78] R. N. Lippert and J. C. Brüning, “Review Maternal Metabolic Programming of the Developing Central Nervous System: Unified Pathways to Metabolic and Psychiatric Disorders,” *Biological Psychiatry*, vol. 91, no. 10, pp. 898–906, 2022.
- [79] B. K. Stepien, S. Vaid, and W. B. Huttner, “Length of the Neurogenic Period—A Key Determinant for the Generation of Upper-Layer Neurons During Neocortex Development and Evolution,” *Frontiers in Cell and Developmental Biology*, vol. 9, no. May, pp. 1–20, 2021.
- [80] R. Pressler and S. Auvin, “Comparison of brain maturation among species: an example in translational research suggesting the possible use of bumetanide in newborn,” *Frontiers in Neurology*, vol. 4, no. April, pp. 1–4, 2013.
- [81] R. Carson, A. P. Monaghan-nichols, D. B. Defranco, and A. C. Rudine, “Effects of Antenatal Glucocorticoids On The Developing Brain,” *Steroids*, pp. 25–32, 2017.
- [82] M. Götz and W. B. Huttner, “THE CELL BIOLOGY OF NEUROGENESIS,” vol. 6, pp. 777–788, 2005.
- [83] E. Taverna, M. Götz, and W. B. Huttner, *The Cell Biology of Neurogenesis: Toward an Understanding of the Development and Evolution of the Neocortex*, vol. 30, no. 1. 2014.
- [84] S. A. Fietz *et al.*, “OSVZ progenitors of human and ferret neocortex are epithelial-like and expand by integrin signaling,” *Nature Neuroscience*, vol. 13, no. 6, pp. 690–699, 2010.
- [85] C. Dehay, H. Kennedy, and K. S. Kosik, “The Outer Subventricular Zone and Primate-Specific Cortical Complexification,” *Neuron*, vol. 85, no. 4, pp. 683–694, 2015.
- [86] V. Borrell and M. Götz, “Role of radial glial cells in cerebral cortex folding,” *Current Opinion in Neurobiology*, vol. 27, pp. 39–46, 2014.
- [87] M. Betizeau *et al.*, “Precursor Diversity and Complexity of Lineage Relationships in the Outer Subventricular Zone of the Primate,” *Neuron*, vol. 80, no. 2, pp. 442–457, 2013.
- [88] D. V. Hansen, J. H. Lui, P. R. L. Parker, and A. R. Kriegstein, “Neurogenic radial glia in the outer subventricular zone of human neocortex,” *Nature*, vol. 464, no.

- 7288, pp. 554–561, 2010.
- [89] M. Florio and W. B. Huttner, “Neural progenitors, neurogenesis and the evolution of the neocortex,” *Development (Cambridge)*, vol. 141, no. 11, pp. 2182–2194, 2014.
- [90] I. Reillo, C. De Juan Romero, M. Á. García-Cabezas, and V. Borrell, “A Role for intermediate radial glia in the tangential expansion of the mammalian cerebral cortex,” *Cerebral Cortex*, vol. 21, no. 7, pp. 1674–1694, 2011.
- [91] Y. Shinmyo, T. Hamabe-Horiike, K. Saito, and H. Kawasaki, “Investigation of the Mechanisms Underlying the Development and Evolution of the Cerebral Cortex Using Gyrencephalic Ferrets,” *Frontiers in Cell and Developmental Biology*, vol. 10, no. March, pp. 1–12, 2022.
- [92] I. H. M. Smart, C. Dehay, P. Giroud, M. Berland, and H. Kennedy, “Unique morphological features of the proliferative zones and postmitotic compartments of the neural epithelium giving rise to striate and extrastriate cortex in the monkey,” *Cerebral Cortex*, vol. 12, no. 1, pp. 37–53, 2002.
- [93] I. Y. Buchsbaum and S. Cappello, “Neuronal migration in the CNS during development and disease: Insights from in vivo and in vitro models,” *Development (Cambridge)*, vol. 146, no. 1, 2019.
- [94] P. J. Lucassen *et al.*, “Regulation of Adult Neurogenesis and Inflammation,” *Cold Spring Harbor Perspective in Biology*, pp. 1–16, 2017.
- [95] C. Anacker *et al.*, “Glucocorticoid-related molecular signaling pathways regulating hippocampal neurogenesis,” *Neuropsychopharmacology*, vol. 38, no. 5, pp. 872–883, 2013.
- [96] C. Anacker *et al.*, “Role for the kinase SGK1 in stress, depression, and glucocorticoid effects on hippocampal neurogenesis,” *Proceedings of the National Academy of Sciences*, vol. 110, no. 21, pp. 8708–8713, 2013.
- [97] C. Anacker *et al.*, “Hippocampal neurogenesis confers stress resilience by inhibiting the ventral dentate gyrus,” *Nature*, vol. 559, no. 7712, pp. 98–102, 2018.
- [98] E. Ninomiya, T. Hattori, M. Toyoda, A. Umezawa, T. Hamazaki, and H. Shintaku, “Glucocorticoids promote neural progenitor cell proliferation derived from human induced pluripotent stem cells,” *SpringerPlus*, vol. 3, no. 1, pp. 1–8, 2014.
- [99] C. Kyrousi and S. Cappello, “Using brain organoids to study human neurodevelopment, evolution and disease,” *Wiley Interdisciplinary Reviews: Developmental Biology*, vol. 9, no. 1, pp. 1–19, 2020.
- [100] I. Reillo and V. Borrell, “Germinal zones in the developing cerebral cortex of ferret: Ontogeny, cell cycle kinetics, and diversity of progenitors,” *Cerebral Cortex*, vol. 22, no. 9, pp. 2039–2054, 2012.

- [101] C. D. J. Romero, C. Bruder, U. Tomasello, J. M. Sanz-anquela, and V. Borrell, “Discrete domains of gene expression in germinal layers distinguish the development of gyrencephaly,” *The EMBO Journal*, vol. 34, no. 14, pp. 1859–1874, 2015.
- [102] S. Uebbing *et al.*, “Massively parallel discovery of human-specific substitutions that alter enhancer activity,” *Proceedings of the National Academy of Sciences of the United States of America*, vol. 118, no. 2, pp. 1–11, 2021.
- [103] J. A. Bagley, D. Reumann, S. Bian, J. Lévi-Strauss, and J. A. Knoblich, “Fused cerebral organoids model interactions between brain regions,” *Nature Methods*, vol. 14, no. 7, pp. 743–751, 2017.
- [104] F. Birey *et al.*, “Assembly of functionally integrated human forebrain spheroids,” *Nature*, vol. 545, no. 7652, pp. 54–59, 2017.
- [105] T. Kadoshima *et al.*, “Self-organization of axial polarity, inside-out layer pattern, and species-specific progenitor dynamics in human ES cell-derived neocortex,” *Proceedings of the National Academy of Sciences of the United States of America*, vol. 110, no. 50, pp. 20284–20289, 2013.
- [106] P. R. Ormel *et al.*, “Microglia innately develop within cerebral organoids,” *Nature Communications*, vol. 9, no. 1, 2018.
- [107] A. A. Pollen *et al.*, “Establishing Cerebral Organoids as Models of Human-Specific Brain Evolution,” *Cell*, 2019.
- [108] X. Qian *et al.*, “Brain-Region-Specific Organoids Using Mini-bioreactors for Modeling ZIKV Exposure,” *Cell*, vol. 165, no. 5, pp. 1238–1254, 2016.
- [109] S. A. Sloan, J. Andersen, A. M. Paşca, F. Birey, and S. P. Paşca, “Generation and assembly of human brain region-specific three-dimensional cultures,” *Nature Protocols*, vol. 13, no. 9, pp. 2062–2085, 2018.
- [110] S. P. Paşca, “Building three-dimensional human brain organoids,” *Nature Neuroscience*, p. 41593, 2018.
- [111] S. Velasco *et al.*, “Individual brain organoids reproducibly form cell diversity of the human cerebral cortex,” *Nature*, vol. 570, no. 7762, pp. 523–527, 2019.
- [112] T. Usui, M. Sakurai, H. Kawasaki, T. Ohama, H. Yamawaki, and K. Sato, “Establishment of a novel three-dimensional primary culture model for hippocampal neurogenesis,” *Physiological Reports*, vol. 5, no. 12, 2017.
- [113] M. A. Lancaster and J. A. Knoblich, “Generation of cerebral organoids from human pluripotent stem cells,” *Nature Protocols*, vol. 9, no. 10, pp. 2329–2340, 2014.
- [114] M. Renner *et al.*, “Self-organized developmental patterning and differentiation in cerebral organoids,” vol. 36, no. 10, pp. 1316–1329, 2017.
- [115] J. G. Camp *et al.*, “Human cerebral organoids recapitulate gene expression

- programs of fetal neocortex development,” *Proceedings of the National Academy of Sciences of the United States of America*, vol. 112, no. 51, pp. 15672–15677, 2015.
- [116] A. Uzquiano *et al.*, “Single-cell multiomics atlas of organoid development uncovers longitudinal molecular programs of cellular diversification of the human cerebral cortex,” *bioRxiv*, p. 2022.03.17.484798, 2022.
- [117] A. J. Kedaigle *et al.*, “Individual brain organoids reproducibly form cell diversity of the human cerebral cortex,” *Nature*, vol. 570, pp. 523–527, 2019.
- [118] P. Arlotta and S. P. Paşca, “Cell diversity in the human cerebral cortex: from the embryo to brain organoids,” *Current Opinion in Neurobiology*, vol. 56, pp. 194–198, 2019.
- [119] A. Gordon *et al.*, “Long-term maturation of human cortical organoids matches key early postnatal transitions,” *Nature Neuroscience*, vol. 24, no. 3, pp. 331–342, 2021.
- [120] M. Koyanagi-Aoi *et al.*, “Differentiation-defective phenotypes revealed by large-scale analyses of human pluripotent stem cells,” *Proceedings of the National Academy of Sciences of the United States of America*, vol. 110, no. 51, pp. 20569–20574, 2013.
- [121] K. Okita *et al.*, “A more efficient method to generate integration-free human iPS cells,” *Nature Methods*, vol. 8, no. 5, pp. 409–412, 2011.
- [122] A. Cárdenas *et al.*, “Evolution of Cortical Neurogenesis in Amniotes Controlled by Robo Signaling Levels,” *Cell*, vol. 174, no. 3, pp. 590-606.e21, 2018.
- [123] T. Saito, “In vivo electroporation in the embryonic mouse central nervous system,” *Nature Protocols*, vol. 1, no. 3, pp. 1552–1558, 2006.
- [124] J. Schindelin *et al.*, “Fiji: an open-source platform for biological-image analysis,” *Nature Methods* 2012 9:7, vol. 9, no. 7, pp. 676–682, Jun. 2012.
- [125] Y. Kashiwagi *et al.*, “Cotylenin a inhibits cell proliferation and induces apoptosis and PAX6 mRNA transcripts in retinoblastoma cell lines,” *Molecular Vision*, vol. 16, no. June 2010, pp. 970–982, 2010.
- [126] S. Roeh, T. Wiechmann, S. Sauer, M. Ködel, E. B. Binder, and N. Provençal, “HAM-TBS: High-accuracy methylation measurements via targeted bisulfite sequencing,” *Epigenetics and Chromatin*, vol. 11, no. 1, pp. 1–10, 2018.
- [127] M. J. Andrews Simon, Krueger Felix, Segonds-Pichon Anne, Biggins Laura, Krueger Christel, “fastQC,” 2019. [Online]. Available: <https://www.bioinformatics.babraham.ac.uk/projects/fastqc/>.
- [128] M. Martin, “Cutadapt removes adapter sequences from high-throughput sequencing reads.”

- [129] F. Krueger and S. R. Andrews, "Bismark: A flexible aligner and methylation caller for Bisulfite-Seq applications," *Bioinformatics*, vol. 27, no. 11, pp. 1571–1572, 2011.
- [130] A. Akalin *et al.*, "MethylKit: a comprehensive R package for the analysis of genome-wide DNA methylation profiles," *Genome Biology*, vol. 13, no. 10, 2012.
- [131] M. Martin, "Cutadapt removes adapter sequences from high-throughput sequencing reads," *EMBnet.journal*, vol. 17, pp. 10–12, 2011.
- [132] R. Patro, G. Duggal, M. I. Love, R. A. Irizarry, and C. Kingsford, "Salmon provides fast and bias-aware quantification of transcript expression," *Nature Methods*, vol. 14, no. 4, pp. 417–419, 2017.
- [133] M. I. Love, W. Huber, and S. Anders, "Moderated estimation of fold change and dispersion for RNA-seq data with DESeq2," *Genome Biology*, vol. 15, no. 12, pp. 1–21, 2014.
- [134] E. Becht *et al.*, "Dimensionality reduction for visualizing single-cell data using UMAP," *Nature Biotechnology*, vol. 37, no. 1, pp. 38–47, 2019.
- [135] C. Cruceanu *et al.*, "Cell-Type-Specific Impact of Glucocorticoid Receptor Activation on the Developing Brain: A Cerebral Organoid Study," *American Journal of Psychiatry*, 2021.
- [136] F. A. Wolf, P. Angerer, and F. J. Theis, "Open Access SCANPY: large-scale single-cell gene expression data analysis," *Genome Biology*, pp. 1–5, 2018.
- [137] I. Rogatsky, J. M. Trowbridge, and M. J. Garabedian, "Glucocorticoid receptor-mediated cell cycle arrest is achieved through distinct cell-specific transcriptional regulatory mechanisms," *Molecular and Cellular Biology*, vol. 17, no. 6, pp. 3181–3193, 1997.
- [138] R. C. Team, "R: A language and environment for statistical computing," 2017. [Online]. Available: <https://www.r-project.org/>.
- [139] B. Elsworth *et al.*, "The MRC IEU OpenGWAS data infrastructure," *bioRxiv*, p. 2020.08.10.244293, 2020.
- [140] C. Bycroft *et al.*, "The UK Biobank resource with deep phenotyping and genomic data," *Nature*, vol. 562, no. 7726, pp. 203–209, 2018.
- [141] A. Buniello *et al.*, "The NHGRI-EBI GWAS Catalog of published genome-wide association studies, targeted arrays and summary statistics 2019," *Nucleic Acids Research*, vol. 47, no. D1, pp. D1005–D1012, 2019.
- [142] L. T. Elliott *et al.*, "Genome-wide association studies of brain imaging phenotypes in UK Biobank," *Nature*, vol. 562, no. 7726, pp. 210–216, 2018.
- [143] M. P. J. van der Loo, "The stringdist package for approximate string matching," *R Journal*, vol. 6, no. 1, pp. 111–122, 2014.

- [144] G. Hemani *et al.*, “The MR-base platform supports systematic causal inference across the human phenome,” *eLife*, vol. 7, pp. 1–29, 2018.
- [145] T. M. Palmer *et al.*, “Instrumental variable estimation of causal risk ratios and causal odds ratios in mendelian randomization analyses,” *American Journal of Epidemiology*, vol. 173, no. 12, pp. 1392–1403, 2011.
- [146] Y. Benjamini and Y. Hochberg, “Controlling the False Discovery Rate: A Practical and Powerful Approach to Multiple Testing,” *Journal of the Royal Statistical Society: Series B (Methodological)*, vol. 57, no. 1, pp. 289–300, 1995.
- [147] J. M. Bland and D. G. Altman, “Multiple significance tests: The Bonferroni method,” *Bmj*, vol. 310, no. 6973, p. 170, 1995.
- [148] I. Faillenot, R. A. Heckemann, M. Frot, and A. Hammers, “Macroanatomy and 3D probabilistic atlas of the human insula,” *NeuroImage*, vol. 150, no. December 2016, pp. 88–98, 2017.
- [149] S. Mori *et al.*, “Stereotaxic white matter atlas based on diffusion tensor imaging in an ICBM template,” *NeuroImage*, vol. 40, no. 2, pp. 570–582, 2008.
- [150] K. Hua *et al.*, “Tract Probability Maps in Stereotaxic Spaces: Analyses of White Matter Anatomy and Tract-Specific Quantification,” *Neuroimage*, vol. 32, no. 7, pp. 736–740, 2008.
- [151] S. Warrington *et al.*, “XTRACT - Standardised protocols for automated tractography in the human and macaque brain,” *NeuroImage*, vol. 217, no. October 2019, pp. 1–15, 2020.
- [152] K. Watanabe, E. Taskesen, A. Van Bochoven, and D. Posthuma, “Functional mapping and annotation of genetic associations with FUMA,” *Nature Communications*, vol. 8, no. 1, Dec. 2017.
- [153] S. Carbon *et al.*, “The Gene Ontology resource: Enriching a GOld mine,” *Nucleic Acids Research*, vol. 49, no. D1, pp. D325–D334, 2021.
- [154] M. Ashburner *et al.*, “Gene ontology: Tool for the unification of biology,” *Nature Genetics*, vol. 25, no. 1, pp. 25–29, 2000.
- [155] Y. Benjamini and Y. Hochberg, “Controlling the False Discovery Rate: A Practical and Powerful Approach to Multiple Testing,” 1995.
- [156] C. Cruceanu *et al.*, “Cell-Type-Specific Impact of Glucocorticoid Receptor Activation on the Developing Brain: A Cerebral Organoid Study,” *American Journal of Psychiatry*, no. 11, pp. 1–13, 2021.
- [157] J. M. H. M. Reul and E. R. De Kloet, “Two receptor systems for corticosterone in rat brain: Microdistribution and differential occupation,” *Endocrinology*, vol. 117, no. 6, pp. 2505–2511, 1985.
- [158] J. Flowerroderick and G. William, “Dexamethasone,” in *Small Animal Clinical*

- Pharmacology (Second Edition)*, 2008, pp. 1–6.
- [159] C. Grossmann *et al.*, “Transactivation via the human glucocorticoid and mineralocorticoid receptor by therapeutically used steroids in CV-1 cells: A comparison of their glucocorticoid and mineralocorticoid properties,” *European Journal of Endocrinology*, vol. 151, no. 3, pp. 397–406, 2004.
- [160] T. M. Liu, E. H. Lee, B. Lim, and N. Shyh-Chang, “Balancing Stem Cell Self-renewal and Differentiation with PLZF.,” *Stem cells (Dayton, Ohio)*, pp. 277–287, 2015.
- [161] B. A. Suliman, D. Xu, and B. R. G. Williams, “The Promyelocytic Leukemia Zinc Finger Protein: Two Decades of Molecular Oncology,” *Frontiers in Oncology*, vol. 2, no. July, pp. 1–12, 2012.
- [162] A. J. Lesiak, K. Coffey, J. H. Cohen, K. J. Liang, C. Chavkin, and J. F. Neumaier, “Sequencing the serotonergic neuron transcriptome reveals a new role for Fkbp5 in stress,” *Molecular Psychiatry*, 2020.
- [163] A. Menke *et al.*, “Dexamethasone stimulated gene expression in peripheral blood is a sensitive marker for glucocorticoid receptor resistance in depressed patients,” *Neuropsychopharmacology*, vol. 37, no. 6, pp. 1455–1464, 2012.
- [164] N. Gerstner *et al.*, “Differential analyses add new insights into the response to glucocorticoids at the level of genes , networks and brain regions,” *Neurobiology of Stress*, vol. 21, no. July, p. 100496, 2022.
- [165] A. C. Gerstner, Nathalie & Krontira *et al.*, “DiffBrainNet: differential analyses add new insights into the response to glucocorticoids at the level of genes, networks and brain regions,” *bioRxiv*, pp. 1–36, 2022.
- [166] V. Avantaggiato *et al.*, “Developmental analysis of murine Promyelocyte Leukemia Zinc Finger (PLZF) gene expression: implications for the neuromeric model of the forebrain organization.,” *The Journal of Neuroscience*, vol. 15, no. 7 Pt 1, pp. 4927–42, 1995.
- [167] H. Lin *et al.*, “Promyelocytic leukemia zinc finger is involved in the formation of deep layer cortical neurons,” pp. 1–13, 2019.
- [168] M. Bothe, R. Buschow, and S. H. Meijnsing, “Glucocorticoid signaling induces transcriptional memory and universally reversible chromatin changes,” *Life Science Alliance*, vol. 4, no. 10, pp. 1–17, 2021.
- [169] L. Hai, M. M. Szwarc, D. G. Lanza, J. D. Heaney, and J. P. Lydon, “Using CRISPR / Cas9 engineering to generate a mouse with a conditional knockout allele for the promyelocytic leukemia zinc finger transcription factor,” no. December 2018, pp. 1–8, 2019.
- [170] M. Manuel *et al.*, “Controlled overexpression of Pax6 in vivo negatively auto-

- regulates the Pax6 locus , causing cell-autonomous defects of late cortical progenitor proliferation with little effect on cortical arealization,” *Development*, vol. 555, pp. 545–555, 2007.
- [171] S. N. Sansom *et al.*, “The Level of the Transcription Factor Pax6 Is Essential for Controlling the Balance between Neural Stem Cell Self- Renewal and Neurogenesis,” *PLoS Genetics*, vol. 5, no. 6, pp. 20–23, 2009.
- [172] G. E. Elsen, F. Bedogni, R. D. Hodge, and T. K. Bammler, “The Epigenetic Factor Landscape of Developing Neocortex Is Regulated by Transcription Factors,” *Frontiers in Neuroscience*, vol. 12, no. August, 2018.
- [173] T. R. Anderson, E. Hedlund, and E. M. Carpenter, “Differential Pax6 promoter activity and transcript expression during forebrain development,” *Mechanisms of Development*, vol. 114, pp. 171–175, 2002.
- [174] D. A. Tyas *et al.*, “Functional conservation of Pax6 regulatory elements in humans and mice demonstrated with a novel transgenic reporter mouse,” *BMC Developmental Biology*, vol. 6, pp. 1–11, 2006.
- [175] J. Arloth *et al.*, “Genetic Differences in the Immediate Transcriptome Response to Stress Predict Risk-Related Brain Function and Psychiatric Disorders,” *Neuron*, vol. 86, no. 5, pp. 1189–1202, 2015.
- [176] J. J. Lee *et al.*, “Gene discovery and polygenic prediction from a genome-wide association study of educational attainment in 1.1 million individuals,” *Nature genetics*, vol. 50, no. August, 2018.
- [177] A. Okbay *et al.*, “Polygenic prediction of educational attainment within and between families from genome-wide association analyses in 3 million individuals,” *Nature genetics*, vol. 54, no. April, 2022.
- [178] C. Makowski *et al.*, “Vertex-wise multivariate genome-wide association study identifies 780 unique genetic loci associated with cortical morphology,” *Neuroimage*, pp. 1–19, 2022.
- [179] T. Ge *et al.*, “The Shared Genetic Basis of Educational Attainment and Cerebral Cortical Morphology,” *Cerebral Cortex*, vol. 29, no. 8, pp. 3471–3481, 2019.
- [180] J. P. Kim *et al.*, “Effects of education on aging-related cortical thinning among cognitively normal individuals,” *Neurology*, vol. 85, no. 9, pp. 806–812, 2015.
- [181] D. Bartrés-Faz *et al.*, “Characterizing the molecular architecture of cortical regions associated with high educational attainment in older individuals,” *Journal of Neuroscience*, vol. 39, no. 23, pp. 4566–4575, 2019.
- [182] M. Uhlén *et al.*, “Tissue-based map of the human proteome,” *Science*, vol. 347, no. 6220, 2015.
- [183] L. Vaqué-alcázar, R. Sala-Illonch, and C. Valls-pedret, “Differential age-related

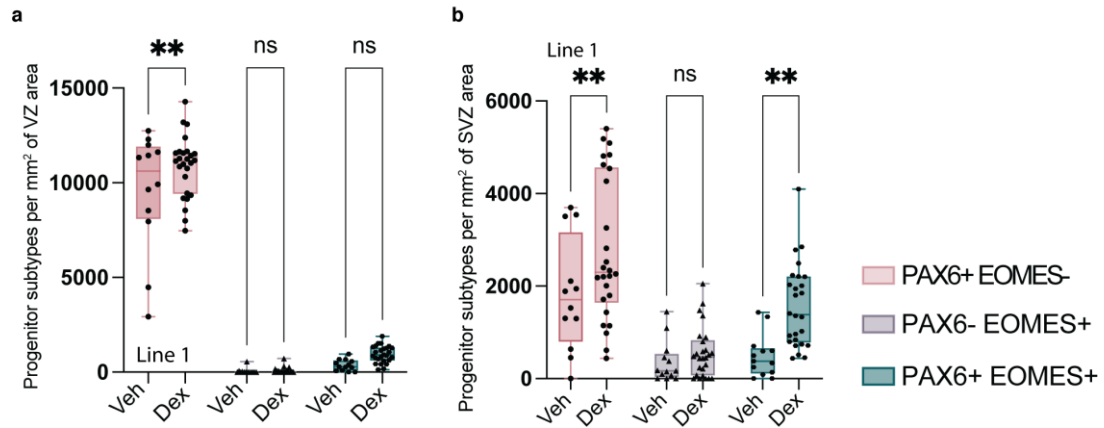
- gray and white matter impact mediates educational influence on elders' cognition," *Brain Imaging and Behavior*, vol. 11, pp. 318–332, 2017.
- [184] B. S. Hall, R. N. Moda, and C. Liston, "Glucocorticoid mechanisms of functional connectivity changes in stress-related neuropsychiatric disorders," *Neurobiology of stress*, vol. 1, pp. 174–183, 2015.
- [185] E. R. De Kloet, "From receptor balance to rational glucocorticoid therapy," *Endocrinology*, vol. 155, no. 8, pp. 2754–2769, 2014.
- [186] J. M. H. M. Reul, F. R. Van Den Bosch, and E. R. De Kloet, "Relative occupation of type-I and type-II corticosteroid receptors in rat brain following stress and dexamethasone treatment: Functional implications," *Journal of Endocrinology*, vol. 115, no. 3, pp. 459–467, 1987.
- [187] E. Kitraki, M. N. Alexis, M. Papalopoulou, and F. Stylianopoulou, "Glucocorticoid receptor gene expression in the embryonic rat brain," *Neuroendocrinology*, vol. 63, no. 4, pp. 305–317, 1996.
- [188] A. Garcia, B. Steiner, G. Kronenberg, A. Bick-Sander, and G. Kempermann, "Age-dependent expression of glucocorticoid- and mineralocorticoid receptors on neural precursor cell populations in the adult murine hippocampus," *Aging Cell*, vol. 3, no. 6, pp. 363–371, 2004.
- [189] M. Egeland, P. A. Zunszain, and C. M. Pariante, "Molecular mechanisms in the regulation of adult neurogenesis during stress," *Nature Reviews Neuroscience*, vol. 16, no. 4, pp. 189–200, 2015.
- [190] S. Kanton *et al.*, *Organoid single-cell genomic atlas uncovers human-specific features of brain development*, vol. 574. 2019.
- [191] D. Polioudakis *et al.*, "A Single-Cell Transcriptomic Atlas of Human Neocortical Development during Mid-gestation," *Neuron*, vol. 103, no. 5, pp. 785-801.e8, 2019.
- [192] A. Bhaduri *et al.*, "Cell stress in cortical organoids impairs molecular subtype specification," *Nature*, vol. 578, no. February, 2020.
- [193] J. C. R. Oakley, "The Biology of the Glucocorticoid Receptor: New Signaling Mechanism in Health and Disease," *J allergy clin immunol*, vol. 132, no. 5, pp. 1033–1044, 2013.
- [194] I. Kelava, I. Chiaradia, L. Pellegrini, A. T. Kalinka, and M. A. Lancaster, "Androgens increase excitatory neurogenic potential in human brain organoids," no. October 2020, 2021.
- [195] J. M. McManus and N. Sharifi, "Structure-dependent retention of steroid hormones by common laboratory materials," *Journal of Steroid Biochemistry and Molecular Biology*, vol. 198, pp. 1–19, 2020.

- [196] E. Nürnberg, S. Horschitz, P. Schloss, and A. Meyer-Lindenberg, "Basal glucocorticoid receptor activation induces proliferation and inhibits neuronal differentiation of human induced pluripotent stem cell-derived neuronal precursor cells," *Journal of Steroid Biochemistry and Molecular Biology*, vol. 182, no. April, pp. 119–126, 2018.
- [197] M. A. Tsiarli *et al.*, "Antenatal dexamethasone exposure differentially affects distinct cortical neural progenitor cells and triggers long-term changes in murine cerebral architecture and behavior," *Translational Psychiatry*, no. February, 2017.
- [198] P. J. Lucassen *et al.*, "Prenatal stress reduces postnatal neurogenesis in rats selectively bred for high, but not low, anxiety: possible key role of placental 11 β -hydroxysteroid dehydrogenase type 2," *European Journal of Neuroscience*, vol. 29, no. 1, pp. 97–103, 2009.
- [199] M. T. Garcia, Y. Chang, Y. Arai, and W. B. Huttner, "S-Phase Duration Is the Main Target of Cell Cycle Regulation in Neural Progenitors of Developing Ferret Neocortex," *The Journal of comparative neurology*, vol. 470, pp. 456–470, 2016.
- [200] N. Matsumoto, S. Tanaka, T. Horiike, and Y. Shinmyo, "A discrete subtype of neural progenitor crucial for cortical folding in the gyrencephalic mammalian brain," *Elife*, pp. 1–26, 2020.
- [201] J. Y. Li, M. A. English, H. J. Ball, P. L. Yeyati, S. Waxman, and J. D. Licht, "Sequence-specific DNA binding and transcriptional regulation by the promyelocytic leukemia zinc finger protein," *Journal of Biological Chemistry*, vol. 272, no. 36, pp. 22447–22455, 1997.
- [202] R. J. Lin, L. Nagy, S. Inoue, W. Shao, J. Miller, and R. M. Evans, "Role of the histone deacetylase complex in acute promyelocytic leukaemia," *Nature*, vol. 391, no. 6669, pp. 811–814, 1998.
- [203] H. Boukarabila *et al.*, "The PRC1 polycomb group complex interacts with PLZF/RARA to mediate leukemic transformation," *Genes and Development*, vol. 23, no. 10, pp. 1195–1206, 2009.
- [204] T. Zhang *et al.*, "G-protein Coupled Receptors Regulate Autophagy by ZBTB16-mediated Ubiquitination and Proteasomal Degradation of Adaptor Protein Atg14L," *eLife*, vol. 2015, no. 4, pp. 1–19, 2015.
- [205] M. Cook *et al.*, "Expression of the zinc-finger gene PLZF at rhombomere boundaries in the vertebrate hindbrain," *Proceedings of the National Academy of Sciences of the United States of America*, vol. 92, no. 6, pp. 2249–2253, 1995.
- [206] L. Zhou *et al.*, "PLZF regulates germline progenitor self-renewal by opposing mTORC1," *Proceedings of the National Academy of Sciences*, vol. 3, no. 1, pp. 1–12, 2019.

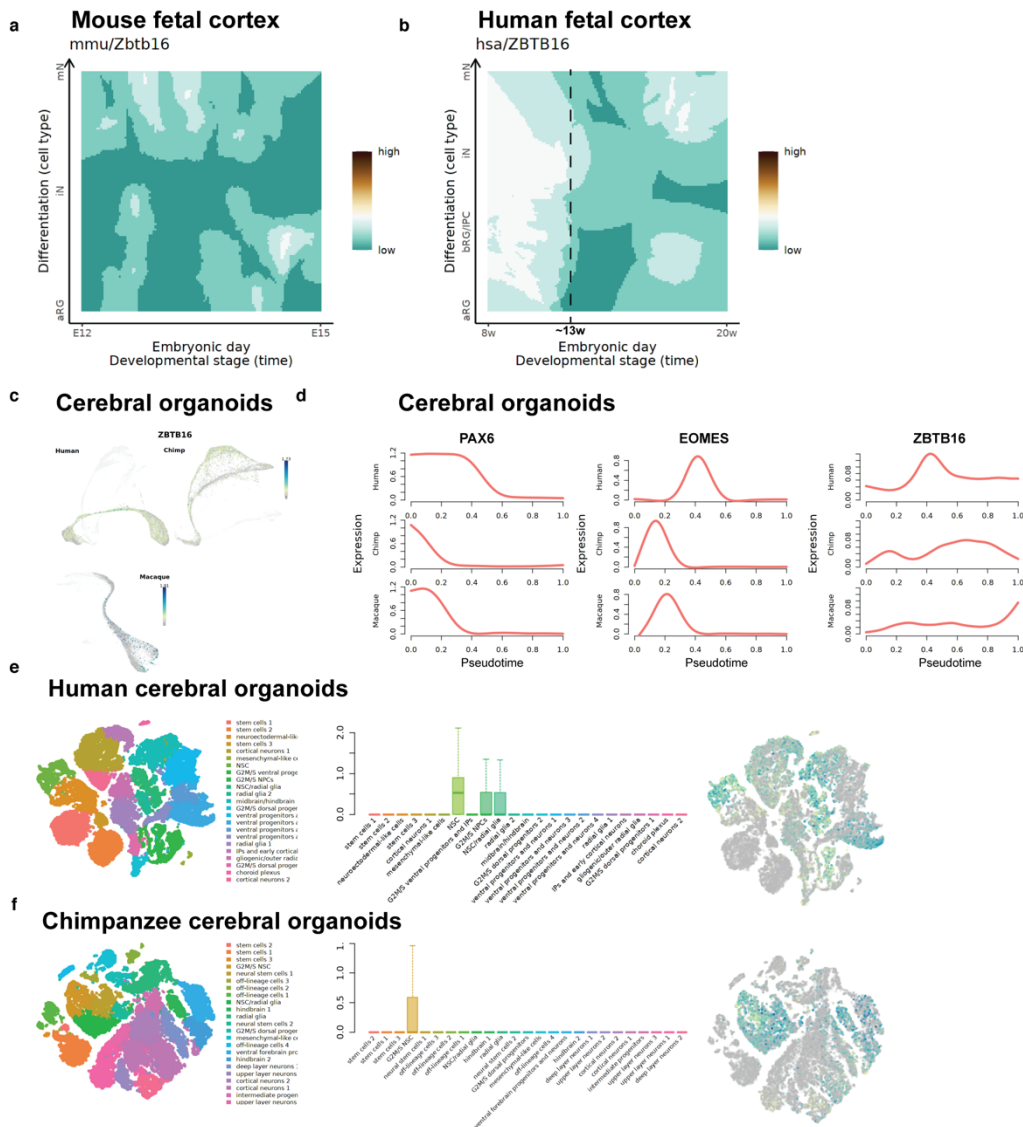
- [207] S. Fischer *et al.*, “Biallelic loss of function of the promyelocytic leukaemia zinc finger (PLZF) gene causes severe skeletal defects and genital hypoplasia,” *Journal of Medical Genetics*, vol. 45, no. 11, pp. 731–737, 2008.
- [208] N. Usui *et al.*, “Zbtb16 regulates social cognitive behaviors and neocortical development,” *Translational psychiatry*, vol. 11, 2021.
- [209] D. F. Sobieszczuk, A. Poliakov, Q. Xu, and D. G. Wilkinson, “A feedback loop mediated by degradation of an inhibitor is required to initiate neuronal differentiation,” *Genes and Development*, vol. 24, no. 2, pp. 206–218, 2010.
- [210] Z. B. Gaber, S. J. Butler, and B. G. Novitch, “PLZF Regulates Fibroblast Growth Factor Responsiveness and Maintenance of Neural Progenitors,” *PLoS Biology*, vol. 11, no. 10, 2013.
- [211] M. Götz, A. Stoykova, and P. Gruss, “Pax6 controls radial glia differentiation in the cerebral cortex,” *Neuron*, vol. 21, no. 5, pp. 1031–1044, 1998.
- [212] N. Warren *et al.*, “The transcription factor, Pax6, is required for cell proliferation and differentiation in the developing cerebral cortex,” *Cerebral Cortex*, vol. 9, no. 6, pp. 627–635, 1999.
- [213] M. N. Manuel, D. Mi, J. O. Masonand, and D. J. Price, “Regulation of cerebral cortical neurogenesis by the Pax6 transcription factor,” *Frontiers in Cellular Neuroscience*, vol. 9, no. March, pp. 1–21, 2015.
- [214] F. K. Wong *et al.*, “Sustained pax6 expression generates primate-like basal radial glia in developing mouse neocortex,” *PLoS Biology*, vol. 13, no. 8, 2015.
- [215] L. P. E. Austdal *et al.*, “Glucocorticoid Effects on Cerebellar Development in a Chicken Embryo Model: Exploring Changes in PAX6 and Metalloproteinase-9 After Exposure to Dexamethasone Neuroendocrinology,” *Journal of Neuroendocrinology*, vol. 15, no. 7, pp. 8–15, 2016.
- [216] X. Miracle, G. Carlo, D. Renzo, A. Fanaroff, X. Carbonell-, and W. Prematurity, “Guideline for the use of antenatal corticosteroids for fetal maturation *,” vol. 36, pp. 191–196, 2008.
- [217] A. K. Cohen, J. Nussbaum, M. L. R. Weintraub, C. R. Nichols, and I. H. Yen, “Attainment , Aspirations , and Expectations,” *Prev. Chronic Dis*, pp. 1–10, 2020.
- [218] M. L. Lehmann, R. A. Brachman, K. Martinowich, R. J. Schloesser, and M. Herkenham, “Glucocorticoids orchestrate divergent effects on mood through adult neurogenesis,” *Journal of Neuroscience*, vol. 33, no. 7, pp. 2961–2972, 2013.
- [219] E. Klingler, F. Francis, D. Jabaudon, and S. Cappello, “Mapping the molecular and cellular complexity of cortical malformations,” *Science*, vol. 371, no. 6527, 2021.

8 | Appendix

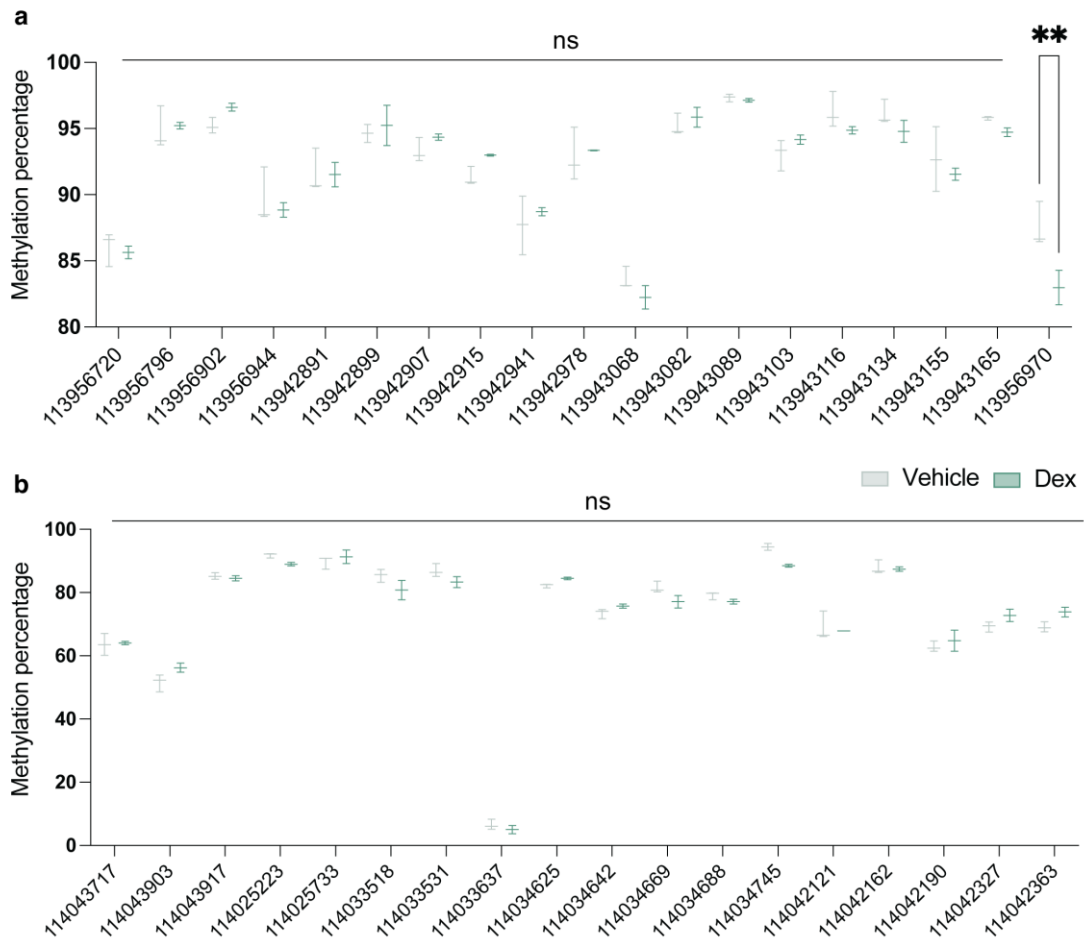
8.1 Supplementary Figures



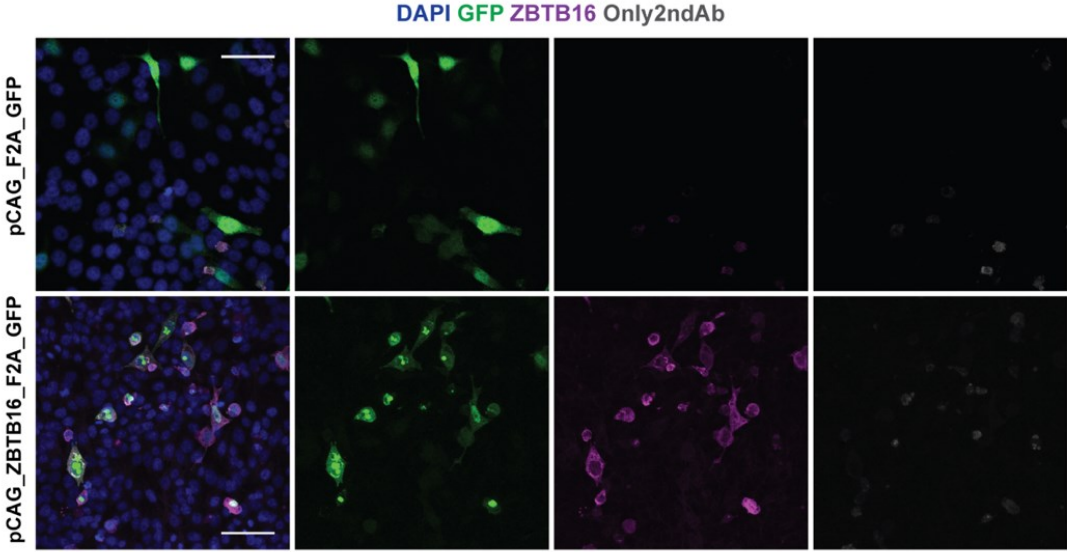
Supplementary Figure 1 | Dexamethasone effects on basal progenitors' subtypes in human cerebral organoids. **a**, Quantification of the progenitors' subtypes in the VZ of Line 1-derived hCOs. **b**, Quantification of the progenitors' subtypes in the SVZ of Line 1-derived hCOs. Veh, vehicle; Dex, dexamethasone; hCOs, human cerebral organoids; VZ, ventricular zone; SVZ, subventricular zone. Box and whisker plots represent 25th to 75th percentile of the data with the centre line representing the median and whiskers representing minima and maxima. P-values, as indicated by asterisks, were calculated using 2-way ANOVA with Benjamini, Krieger and Yekutieli multiple testing correction.



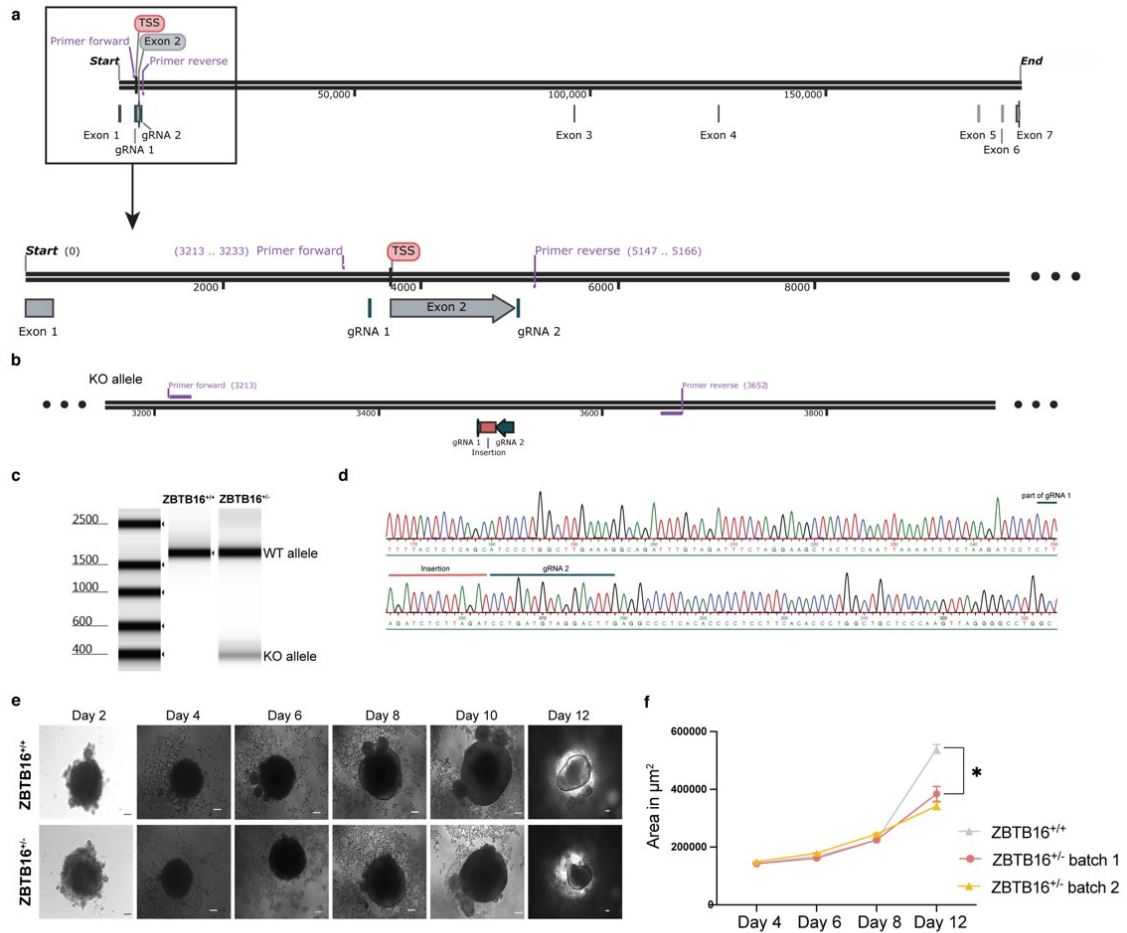
Supplementary Figure 2| ZBTB16 expression in different lissencephalic and gyrencephalic species. a, ZBTB16 expression in the mouse developing cortex from Klingler et al., Science, 2021. **b,** ZBTB16 expression in the human developing cortex from Klingler et al., Science, 202 [219]. **c,** Trajectory of ZBTB16 expression in human, chimpanzee and macaque cerebral organoids from Scapex (<https://bioinf.eva.mpg.de/shiny/sample-apps/scApeX/>). Chimp, chimpanzee. **d,** Pseudotime pattern of ZBTB16 expression in human, chimpanzee and macaque cerebral organoids from Scapex. **e,** ZBTB16 expression in each cell cluster of human cerebral organoids from Scapex. **f,** ZBTB16 expression in each cell cluster of chimpanzee cerebral organoids from Scapex.



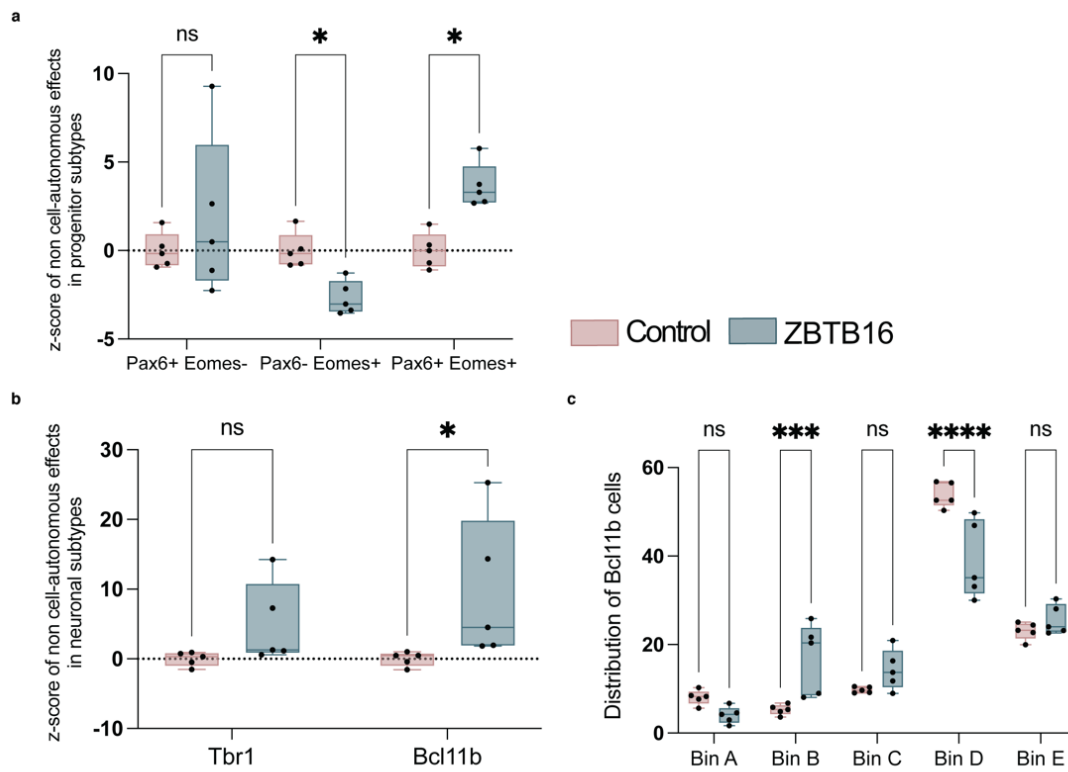
Supplementary Figure 3| Methylation levels of CpGs in the *ZBTB16* locus. a, Methylation levels changes of CpGs located in enhancer elements without GR binding sites after treatment of day 30 hCOs with dexamethasone for 7 days. **b**, Methylation levels changes of CpGs located in enhancer elements with GR binding sites after treatment of day 30 hCOs with dexamethasone for 7 days. hCOs, human cerebral organoids. P-values, as indicated by asterisks, were calculated using 2-way ANOVA with Benjamini, Krieger and Yekutieli multiple testing correction.



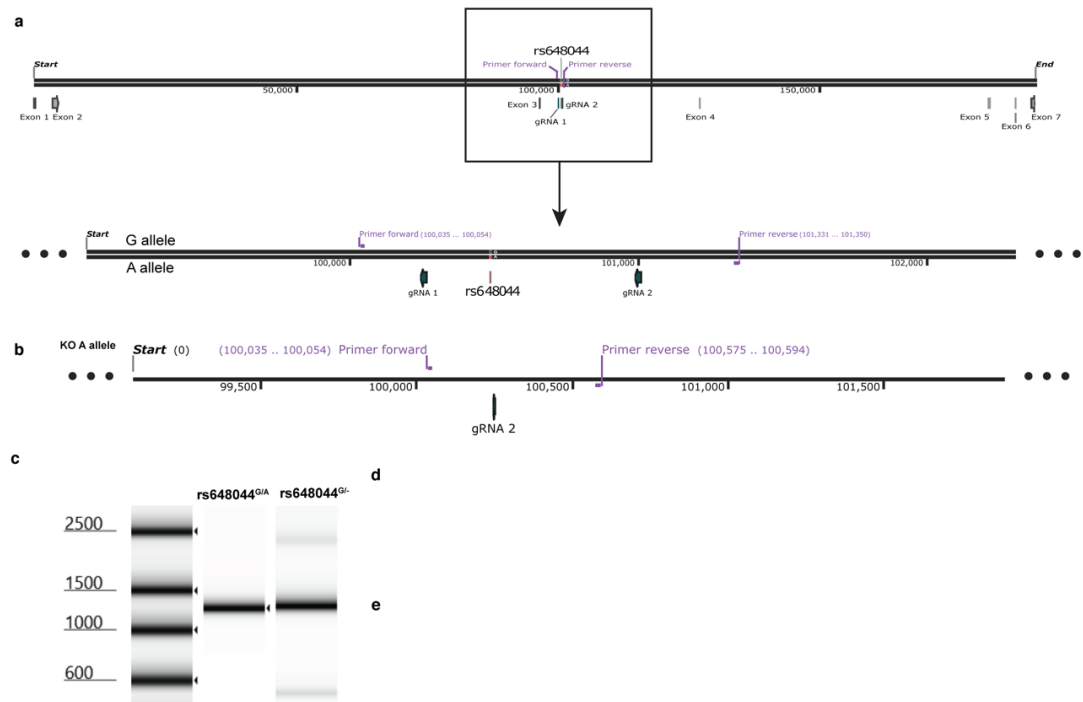
Supplementary Figure 4| ZBTB16 overexpressing plasmids validation in HELA cells. Scale bars, 50µm.



Supplementary Figure 5 | CRISPR-Cas9 editing of iPSCs to remove exon 2 of the *ZBTB16* locus. a, Schematic of the locus showing the location of gRNAs used to remove exon 2. **b**, Schematic of the allele after the removal of exon 2. **c**, DNA gel validating the existence of the KO band in the edited cells. **d**, Sanger trace of the KO allele. **e**, Representative images of EBs from the control and edited cells during development. **f**, Quantification of the area of EBs from the control and the edited iPSC lines. gRNA, guide RNA; TSS, transcription start site; WT, wild-type; KO, knock-out. P values, as indicated by asterisks, were calculated using 2-way ANOVA with Benjamini, Krieger and Yekutieli multiple testing correction.



Supplementary Figure 6 | Non-cell autonomous effects of ZBTB16 overexpression in the mouse cortex from E13.5-E16.5. **a**, Quantification of the number of cells belonging to each progenitor subtype and normalized over the physiological variance of the control samples. **b**, Quantification of the number of cells belonging to each neuronal subtype and normalized over the physiological variance of the control samples. **c**, Quantification of the distribution of the Bcl11b neurons. P values, as indicated by asterisks, were calculated using 2-way ANOVA with Benjamini, Krieger and Yekutieli multiple testing correction.



Supplementary Figure 7 | CRISPR-Cas9 editing of rs648044. **a**, Schematic of the *ZBTB16* locus showing the position of the gRNAs used for the KO. **b**, Schematic of the allele after the KO of the 200bp region surrounding rs648044. **c**, PCR showing the KO band. KO, knock-out; PCR, polymerase chain reaction; gRNAs, guide RNAs.



Supplementary Figure 8 | MR-PheWAS results of *ZBTB16* expression on neurobehavioral traits. Plot describes associations of *ZBTB16* transcription on each neurobehavioral phenotype of the UK Biobank and NHGRI-EBI GWAS Catalog as individual points. Phenotypes are presented based on negative associations (negative MR estimate) and positive associations (positive MR estimate) effects. Traits that remain significant following Benjamini-Hochberg correction are labelled. To improve interpretation of the strength of evidence, additional vertical lines are shown, which represent the Bonferroni multiple comparison threshold across all outcome traits.

8.2 Supplementary Tables

Supplementary Table 1| Primary and secondary antibodies. IF, immunofluorescence

Antigen	Species	Dilution	Type	Use	Vendor	Catalogue number
GFP	Chicken	1:1000	Primary	IF	Aves Laboratory	GFP-1020
PAX6	Rabbit	1:500	Primary	IF, Flow Cytometry	Biozol	BLD-901301
PAX6	Mouse IgG1	1:500	Primary	IF	Abcam	ab78545
NEUN	Mouse IgG1	1:500	Primary	IF	Millipore	MAB377
Ki-67	Rabbit	1:500	Primary	IF	Abcam	ab15580
BCL11B	Rat IgG2a	1:1000	Primary	IF	Abcam	ab18465
HOPX	Rabbit	1:1000	Primary	IF	Sigma	HPA030-180
EOMES	Sheep	1:300, 1:200	Primary	IF, Flow Cytometry	R&D Systems	AF6166
EOMES	Rabbit	1:300	Primary	IF	Abcam	ab23345
MAP2	Chicken	1:1000	Primary	IF	Abcam	ab5392
ZBTB16	Mouse IgG2a	1:100	Primary	IF	Active Motif	39988
ZBTB16	Mouse IgG1	1:250	Primary	Western blot	Santa Cruz	sc-28319
ACTIN	Rabbit	1:10000	Primary	Western blot	Cell Signaling	4967
Chicken-Alexa Fluor 488	Donkey	1:1000, 1:800	Secondary	IF, Flow Cytometry	Dianova	703-545-155
Rabbit-Alexa Fluor 647	Donkey	1:1000	Secondary	IF	Dianova	711-606-152
Mouse-Alexa Fluor 594	Donkey	1:1000	Secondary	IF	Dianova	715-585-150
Rat-Alexa Fluor 647	Goat	1:1000	Secondary	IF	Abcam	ab150167
Sheep-Alexa Fluor 594	Donkey	1:1000, 1:800	Secondary	IF, Flow Cytometry	Dianova	713-585-147
Rabbit-HRP linked	Goat	1:10000	Secondary	Western blot	Cell Signaling	7074
Mouse-HRP linked	Horse	1:3000	Secondary	Western blot	Cell Signaling	7076

Supplementary Table 2| PrimeTime assays, rtPCR primers, qPCR primers, genomic primers. qPCR, quantitative polymerase chain reaction; rtPCR, reverse transcription polymerase chain reaction; gRNA guide RNA; HetKO, heterozygous knock-out; STARR, self-transcribing active regulatory region sequencing; for, forward; rev, reverse

Gene ID	Prime-Time Assay	Primer sequence (5'-3')		Use	Vendor
		Forward	Reverse		
ZBTB16	Hs.PT.5 8.60574 3	-	-	qPCR	Integrated DNA Technologies
MAP2	Hs.PT.5 8.20103 440	-	-	qPCR	Integrated DNA Technologies
POLR2A	Hs.PT.3 9a.1963 9531	-	-	qPCR	Integrated DNA Technologies
YWHAZ	Hs.PT.3 9a.2221 4858	-	-	qPCR	Integrated DNA Technologies
ZBTB16	Mm.PT. 58.1623 4865	-	-	qPCR	Integrated DNA Technologies
POLR2A	Mm.PT. 39a.222 14849	-	-	qPCR	Integrated DNA Technologies
GFP	-	CCAGCTGTT- GGGGTGTCCA	GACAGAGAACTT- GTGGCCGT	STARR-qPCR	Integrated DNA Technologies
RPL19	-	TCGCCTCTAGTGCCT CCG	GCGGGCCAAGGT GTTTTTC	STARR-qPCR	Integrated DNA Technologies
mRNA GFP	-	CAAACATCAATG- TATCTTATCATG	-	STARR-rtPCR	Integrated DNA Technologies
mRNA RPL19	-	GAGGCCAGTATG- TACAGACAAAGTGG	-	STARR-rtPCR	Integrated DNA Technologies
STARR-sanger		GCGAT- GGCCCTGTCCTTTTA	GCATTCTAGTT- GTGGTTTGTCCA	STARR-sanger sequencing	Integrated DNA Technologies
ZBTB16 Exon 2	-	GGAAGGGGCTAAAGT CTTGCT	TAGGCCCCCTCA- CTACACTT	Genomic primers, CRISPR for ZBTB16 allele KO	Integrated DNA Technologies
Rs648044	-	GACCTGGACTTGTT- GGGGAG	TTCACCCTCCAT- CAGGGCTA	Genomic primers, CRISPR for rs648044 A allele KO	Integrated DNA Technologies

ZBTB16 cloning	-	ggtaccg ^{cg} gggccc ^{cg} - gatccaccatggatct- gacaaaaatgggcat	aaattcaaagtctgttca- ctccgcttccagatctca- catagcacaggtag- aggtagctct	Takara In-Fusion cloning of ZBTB16 fragment into the the pCAG-ZBTB16-F2A-GFP plasmid, overlap with CAG vector , BamHI site, overlap with ZBTB16 fragment, overlap with F2A fragment, GSG sequence for better cleavage of F2A, BglI site	Integrated DNA Technologies
F2A-GFP cloning	-	acctctac ^{ct} gtgctatgtga- gatctggaagcggag ^t - gaaacagacttgaatttgacct	actatag- aatagggccg ^{ttt} - gctagcttacttg- tacagctcgtccatgc	Takara In-Fusion cloning of F2A-GFP fragment into the the pCAG-ZBTB16-F2A-GFP plasmid, overlap with ZBTB16 , BglI site, GSG sequence for better cleavage of F2A, overlap with the F2A-GFP fragment, overlap with CAG vector, NheI site	Integrated DNA Technologies
pCAG-ZBTB16-F2A-GFP sanger	-	GGCAACGTGCTGGT- TATTGT	TGCAG- GAGAGACTGTCC TATG	Plasmid-sanger sequencing	Integrated DNA Technologies
	-	CCTTTGAGTG- TAAGCTCTGCC	TAG- AAGGCACAGTCG AGGCT		
pCAG-F2A-GFP sanger	-	GGAACAGTGCCTGAA- GATGC	CTGTGGGCAT- GAAGTCAGAG		

Supplementary Table 3| STARR-qPCR inserts for rs648044.

Name	Sequence (5'-3')	Information	Vendor
Rs648044_G allele	5'TAGAGCATGCACCGGtGTGGA- GAAGTGAGTCCAGGATCTGGG- TAGGGGTTGTGGTT- GCCCCCTAAATGTTGCTGCCCTTGCA CTGG- CACATTCCTGCTGTTTTCTTCTGCTCAG CGGAGCCGAACGGCTCTCAC- TTCCTGGCTAGCTCTGTGTGCTGCCCC ACCCCCTCTGGCGAGCATT- GCCTGTGTTTGTATTGTAG- TCCTGGCTCCAGGCCgTCGAC- GAATTCGGCC 3'	Sequence homologous to the STARR reporter construct in red; addition of two bases to reconstruct the AgeI and Sall restriction enzyme sites in small letters; rs648044 alleles in bold; 100bp spanning rs648044 in capital letters	gBlocks, gene fragments IDT DNA Technologies
Rs648044_A allele	5'TAGAGCATGCACCGGtGTGGA- GAAGTGAGTCCAGGATCTGGG- TAGGGGTTGTGGTT- GCCCCCTAAATGTTGCTGCCCTTGCA CTGG- CACATTCCTGCTGTTTTCTTCTGCTCAG- CAGAGCCGAACGGCTCTCAC- TTCCTGGCTAGCTCTGTGTGCTGCCCC ACCCCCTCTGGCGAGCATT- GCCTGTGTTTGTATTGTAG- TCCTGGCTCCAGGCCgTCGAC- GAATTCGGCC 3'	Sequence homologous to the STARR reporter construct in red; addition of two bases to reconstruct the AgeI and Sall restriction enzyme sites in small letters; rs648044 alleles in bold; 100bp spanning rs648044 in capital letter	gBlocks, gene fragments IDT DNA Technologies

Supplementary Table 4| Primers used for HAM-TBS on the *ZBTB16* locus.

	Primer Sequence	final range on hg19	final spanning length	CpGs covered
1	YGGGTAAGTGATAGGAATATTTT	chr11:114,025,195-114,025,501	307	2
	CCAAAAACAAATAATTTCTC			
2	TTTTGTTGAGAGAATTTTGTG	chr11:114,025,553-114,025,769	217	2
	CACTCAAACAAACAATATCT			
3	TTTTTTTTTGTTTAGTAGAGT	chr11:114,030,783-114,031,200	418	13
	ATCTCCTACAAACTAATTC			
4	GGTTAGGTTGTTTTTTTTYGGT	chr11:114,033,494-114,033,828	335	12
	CAATTTTTATTTTCCTTTTCCTCTC			
5	GGTTTTGTGTTTTTAATTTG	chr11:114,034,591-114,034,972	382	7
	ATAATTTCCACTTTCTCCCT			
6	TTTTTGTTAATAATTTGAG	chr11:114,037,638-114,038,009	372	3
	AAAACCTTCCTAACTACTAA			
7	AGAATTTTTATTAGGAGTTAGG	chr11:114,042,096-114,042,441	346	8
	TAACTCTATAAACTCTATAT			
8	GGTTGTTGAATTTTGAGTTTGTA	chr11:114,043,683-114,043,992	310	3
	ATTTTAAACCCTTCTCACCT			
9	TTGATAAAGGAGAAAGAGTAAGA	chr11:114,049,971-114,050,377	407	4
	AAAACCACTAAAAAACACC			

Supplementary Table 5| Phenotype batches selected for Mendelian Randomisation analysis. Batch descriptions were obtained from the MRC IEU OpenGWAS platform (<https://gwas.mrcieu.ac.uk/datasets/>) on November 11th 2021.

Batch		No. of Phenotypes	
ID	Description	Initial	Selected
ebi-a	Datasets that satisfy minimum requirements imported from the EBI database of complete GWAS summary data	1302	1061
ieu-a	GWAS summary datasets generated by many different consortia that have been manually collected and curated, initially developed for MR-Base	440	116
ieu-b	GWAS summary datasets generated by many different consortia that have been manually collected and curated, initially developed for MR-Base (round 2)	80	38
ubm-a	Complete GWAS summary data on brain region volumes as described by Elliott et al 2018	3143	3143
ukb-a	Neale lab analysis of UK Biobank phenotypes, round 1	596	132
ukb-b	IEU analysis of UK Biobank phenotypes	2514	2227
ukb-d	Neale lab analysis of UK Biobank phenotypes, round 2	904	786

Supplementary Table 6| Differentially expressed genes from bulk RNA seq at an FDR 10% cut-off in hCOs after 7 days of 100nM dexamethasone. lfcSE, standard error of log2FoldChange estimate; FDR, false discovery rate; baseMean, mean of normalized counts of all samples, normalizing for sequencing depth.

Gene	Ensemblid	baseMean	Log2Fold-Change	lfcSE	P-value	FDR
SAA1	ENSG00000173432.10	29.3500184	4.947688953	0.73586524	1.77E-11	3.16E-07
PNMT	ENSG00000141744.3	13.1370575	4.289361404	0.68357945	3.50E-10	3.11E-06
SLCO4A1	ENSG00000101187.15	19.8677695	3.103171444	0.51280647	1.44E-09	6.39E-06
FKBP5	ENSG00000096060.14	117.805784	3.009072809	0.49440827	1.16E-09	6.39E-06
TUBA3D	ENSG00000075886.10	12.0223523	4.321857844	0.73957131	5.10E-09	1.36E-05
SFTPD	ENSG00000133661.15	33.5689101	4.217616573	0.72269019	5.35E-09	1.36E-05
SLPI	ENSG00000124107.5	120.457048	3.984343893	0.682655	5.33E-09	1.36E-05
NEGR1	ENSG00000172260.14	58.5069535	3.624219316	0.6356102	1.18E-08	2.64E-05
IL1RL1	ENSG00000115602.16	5.17871601	4.034956672	0.71095939	1.38E-08	2.74E-05
PLXDC2	ENSG00000120594.16	105.52377	2.208496838	0.39266632	1.86E-08	3.31E-05
SERPINA3	ENSG00000196136.17	21.6890117	3.843707413	0.71162921	6.62E-08	0.00010708
PLA2G5	ENSG00000127472.10	6.19489643	3.510293034	0.68806146	3.37E-07	0.0004993
TSC22D3	ENSG00000157514.16	881.724677	2.389586265	0.47335083	4.46E-07	0.00061059
GSTM3	ENSG00000134202.10	143.221197	1.895954051	0.38837766	1.05E-06	0.00133711
PLA2G2A	ENSG00000188257.10	50.9204506	2.717654811	0.58142032	2.95E-06	0.00350266
TTC23	ENSG00000103852.12	41.7587074	1.712974773	0.37872843	6.10E-06	0.00678439
BCRP2	ENSG00000169668.11	12.915064	2.588300408	0.57554076	6.89E-06	0.00681049
LOX	ENSG00000113083.13	109.634446	2.487259136	0.55245049	6.72E-06	0.00681049
BCL2A1	ENSG00000140379.7	6.66883138	3.228709896	0.72120925	7.58E-06	0.00709885
CYP4X1	ENSG00000186377.7	9.50953803	- 2.778738823	0.63284985	1.13E-05	0.01005014
SYNM	ENSG00000182253.14	23.9231738	2.287298298	0.53010437	1.60E-05	0.0135408
LIMS2	ENSG00000072163.19	7.06422371	2.631973089	0.63342525	3.25E-05	0.02411167
PPP1R1B	ENSG00000131771.13	16.9550293	2.487883224	0.59824235	3.20E-05	0.02411167
AKR1B1	ENSG00000085662.13	176.054072	1.115446112	0.26834828	3.23E-05	0.02411167
QSOX1	ENSG00000116260.16	177.32482	1.704342812	0.41566051	4.13E-05	0.02937677
IGFBP5	ENSG00000115461.4	543.035317	1.803775594	0.4440353	4.86E-05	0.03327773
IGKC	ENSG00000211592.8	1.71425276	2.73549547	0.68607133	6.69E-05	0.03719352
KLF9	ENSG00000119138.4	13.5129468	2.218741494	0.5543457	6.27E-05	0.03719352
ST3GAL3	ENSG00000126091.19	12.4025268	2.066379385	0.51388677	5.79E-05	0.03719352
ASAP2	ENSG00000151693.9	57.5795553	1.416602012	0.35464678	6.49E-05	0.03719352
IDUA	ENSG00000127415.12	4.76647354	- 2.752785544	0.68735012	6.20E-05	0.03719352
CNTNAP5	ENSG00000155052.14	5.7131363	- 3.000241827	0.75013191	6.34E-05	0.03719352
TUBA3E	ENSG00000152086.8	4.89125694	2.940634614	0.7409005	7.22E-05	0.0374683
IL1R2	ENSG00000115590.13	2.97190086	2.837185923	0.71553133	7.34E-05	0.0374683
SMIM1	ENSG00000235169.7	81.8680761	2.254652009	0.56876589	7.37E-05	0.0374683

<i>ANGPTL7</i>	ENSG00000171819.4	2.84525734	2.878794751	0.73740813	9.46E-05	0.0467971
<i>SLC7A4</i>	ENSG00000099960.12	49.9450098	2.678645389	0.68785775	9.85E-05	0.0469089
<i>AC116050.1</i>	ENSG00000143429.10	64.745191	1.721897603	0.44261764	0.00010014	0.0469089
<i>AKR1B1</i>	ENSG00000166033.11	84.8587583	1.500610325	0.39096727	0.00012394	0.05515633
<i>MTCH1</i>	ENSG00000137409.19	441.782621	0.738459715	0.19229117	0.00012287	0.05515633
<i>CDK14</i>	ENSG00000058091.16	67.9885643	1.768798134	0.47292298	0.00018392	0.07985173
<i>ZBTB16</i>	ENSG00000109906.13	45.0225312	1.761917876	0.47185628	0.00018845	0.07987229
<i>SCGN</i>	ENSG00000079689.13	13.0636541	2.348163425	0.632363	0.00020456	0.08275906
<i>HEYL</i>	ENSG00000163909.7	33.5664728	2.085369646	0.56142236	0.00020365	0.08275906
<i>SPRR2F</i>	ENSG00000244094.1	9.98924266	2.626686903	0.71026555	0.00021715	0.08403405
<i>PDPN</i>	ENSG00000162493.16	283.172278	1.998048343	0.53958744	0.00021313	0.08403405
<i>DBIL5P2</i>	ENSG00000242412.1	1.73423248	- 2.675393643	0.72826832	0.00023912	0.09056623
<i>PTGDS</i>	ENSG00000107317.12	10.8439673	2.40264135	0.65551035	0.00024705	0.09161948
<i>KCNMA1</i>	ENSG00000156113.22	79.2069533	1.914091202	0.52383507	0.00025819	0.09192095
<i>SAPCD2</i>	ENSG00000186193.8	42.9636593	1.352605115	0.37007724	0.00025726	0.09192095

Supplementary Table 7 | Cross-reference of gene lists to identify progenitor-specific genes with large effect sizes. The 50 DE genes found with bulk sequencing from the day 45 organoids treated with 100nM of dexamethasone for 7 days and the DE genes in neural progenitors and non-neural progenitors from day 30 organoids treated with 12 hours of dexamethasone from Cruceanu, Dony, Krontira *et al.*, AJP, 2021. DE, differentially expressed.

Day 45 chronic treatment + Day 30 acute in neural progenitors + Day 30 acute in non-neural progenitors	Day 45 chronic treatment + Day 30 acute in neural progenitors	Day 45 chronic treatment + Day 30 acute in non-neural progenitors	Day 45 chronic treatment
SMIM1	PLA2G2A	KCNMA1	CDK14
LOX	PNMT	SLC7A4	LIMS2
SLPI	ZBTB16	IGFBP5	akr1b1
PLA2G5	TUBA3D	GSTM3	SAPCD2
TUBA3D	QSOX1		TUBA3E
SFTPD			ASAP2
SLPI			PPP1R1B
NEGR1			SPRR2F
IL1RL1			BCRP2
PLXDC2			SFTPD
SERPINA3			NEGR1
PLA2G5			FKBP5
TSC22D3			KLF9
GSTM3			BCL2A1
PLA2G2A			IGKC
TTC23			AKR1B1
BCRP2			SAA1
LOX			CNTNAP5
BCL2A1			SERPINA3
CYP4X1			SYNM
SYNM			ANGPTL7
LIMS2			TSC22D3
PPP1R1B			IL1RL1
AKR1B1			SCGN
QSOX1			MTCH1
IGFBP5			AC116050.1
IGKC			SLCO4A1
KLF9			PDPN
ST3GAL3			CYP4X1
ASAP2			PTGDS
IDUA			PLXDC2
CNTNAP5			IL1R2
TUBA3E			DBIL5P2
IL1R2			ST3GAL3

<i>SMIM1</i>			<i>IDUA</i>
<i>ANGPTL7</i>			<i>TTC23</i>
<i>SLC7A4</i>			<i>HEYL</i>

Supplementary Table 8| Enrichment analysis of the *Zbtb16* differential network in the PFC of the adult mouse brain from Gerstner & Krontira et al., BioRxiv, 2022. FDR, false discovery rate.

Gene Ontology Biological Processes	Gene ratio %	Odds Ratio	FDR	Genes
go_negative_regulation_of_transcription_by_rna_polymerase_ii	2.12 7659 57	2.35 3305 76	0.00 0248 81	<i>PRDM16:ZBTB16:ZBTB4:DNMT1:SIN3B:CUL3:THRB:ZBTB20:SOX2:DLG1:EGR1:BACH2</i>
go_embryo_development	1.78 8375 56	2.07 8808 84	0.00 0750 6	<i>ZBTB16:RNF112:DNMT1:KEAP1:DLL3:EPAS1:ERBB4:CUL3:SOX2:DLG1:SEMA3A:STK3</i>
go_negative_regulation_of_developmental_process	1.76 5650 08	2.02 7885 93	0.00 1422 43	<i>ZBTB16:STAT5B:DNMT1:DLL3:LIMS2:ERBB4:THRB:SOX2:ENPP1:SEMA3A:STK3</i>
go_regulation_of_cell_differentiation	1.19 5219 12	1.51 0349 44	0.00 1528 48	<i>PRDM16:ZBTB16:RNF112:STAT5B:DNMT1:KEAP1:DLL3:CHN1:ERBB4:THRB:SOX2:ENPP1:SEMA3A:STK3:CSMD3</i>
go_apoptotic_process	1.15 5624 04	1.45 2912 88	0.00 1528 48	<i>PRKAA2:ZBTB16:STAT5B:DNMT1:PRKCE:LIMS2:ERBB4:CUL3:CSNK2A1:THRB:SOX2:EGR1:SEMA3A:STK3:HNRNPK</i>
go_positive_regulation_of_protein_metabolic_process	1.28 0878 32	1.59 7749 61	0.00 1528 48	<i>PRKAA2:TOLLIP:STAT5B:DNMT1:KEAP1:PRKCE:ERBB4:CUL3:GNL3:SOX2:DLG1:EGR1:SEMA3A:STK3</i>
go_regulation_of_cell_population_proliferation	1.30 5220 88	1.60 0262 58	0.00 1528 48	<i>HP1BP3:ZBTB16:STAT5B:DNMT1:LIMS2:ERBB4:CUL3:CSNK2A1:GNL3:SOX2:DLG1:EGR1:STK3</i>
go_positive_regulation_of_protein_modification_process	1.524 77764	1.82 4132 44	0.00 1528 48	<i>PRKAA2:TOLLIP:DNMT1:PRKCE:ERBB4:CUL3:GNL3:SOX2:DLG1:EGR1:SEMA3A:STK3</i>
go_negative_regulation_of_rna_biosynthetic_process	1.466 99267	1.76 1950 41	0.00 1528 48	<i>PRDM16:ZBTB16:ZBTB4:DNMT1:SIN3B:CUL3:THRB:ZBTB20:SOX2:DLG1:EGR1:BACH2</i>
go_negative_regulation_of_cell_differentiation	1.898 73418	2.08 2758 1	0.00 1528 48	<i>ZBTB16:STAT5B:DNMT1:DLL3:ERBB4:THRB:SOX2:ENPP1:SEMA3A</i>
go_heart_process	3.076 92308	2.73 4617 84	0.00 1528 48	<i>EPAS1:CACNB4:THRB:DLG1:SGCD:SEMA3A</i>
go_regulation_of_generation_of_precursor_metabolites_and_energy	4.347 82609	3.23 1065 3	0.00 1528 48	<i>PRDM16:PRKAA2:ZBTB20:NUP153:ENPP1</i>
go_gland_development	2.380 95238	2.37 3257 75	0.00 1846 06	<i>STAT5B:LIMS2:ERBB4:CUL3:THRB:SOX2:SEMA3A</i>
go_negative_regulation_of_biosynthetic_process	1.248 79923	1.52 7332 92	0.00 1852 59	<i>PRDM16:ZBTB16:ZBTB4:DNMT1:SIN3B:CUL3:THRB:ZBTB20:SOX2:DLG1:EGR1:BACH2:ENPP1</i>

go_peptidyl_lysine_modification	2.317 88079	2.33 2234 58	0.00 1887 71	<i>PRDM16:PRKAA2:TOL- LIP:DNMT1:GNL3:EGR1:NUP153</i>
go_regulation_of_carbohydrate_metabolic_process	3.448 27586	2.87 8144 78	0.00 2584 29	<i>PRKAA2:PRKCE:ZBTB20:NUP153:ENPP1</i>
go_circulatory_system_process	2.071 00592	2.15 9987 15	0.00 3306 95	<i>FLI1:EPAS1:CACNB4:THRB:DLG1:SGCD:SEMA3A</i>
go_protein_modification_by_small_protein_conjugation	1.418 43972	1.65 2816 05	0.00 3487 93	<i>TOL- LIP:ZBTB16:RNF112:KEAP1:PRKCE:EPAS1:CUL3 :GNL3:EGR1:NUP153</i>
go_negative_regulation_of_multicellular_organismal_process	1.322 75132	1.54 1525 22	0.00 5393 11	<i>ZBTB16:STAT5B:DNMT1:DLL3:LIMS2:ERBB4:THR B:SOX2:SEMA3A:STK3</i>
go_positive_regulation_of_transcription_by_rna_polymerase_ii	1.315 78947	1.53 3091 87	0.00 5393 11	<i>ZBTB16:FLI1:STAT5B:E- PAS1:THRB:GNL3:SOX2:SUB1:EGR1:HNRNPK</i>
go_regulation_of_protein_modification_by_small_protein_conjugation_or_removal	2.793 29609	2.55 8799 78	0.00 5393 11	<i>TOLLIP:PRKCE:CUL3:GNL3:EGR1</i>
go_regulation_of_wnt_signaling_pathway	2.135 23132	2.17 9066 1	0.00 5736 98	<i>TCF7L1:CUL3:CSNK2A1:SOX2:EGR1:STK3</i>
go_regulation_of_blood_circulation	2.673 79679	2.49 2607 84	0.00 5736 98	<i>EPAS1:CACNB4:THRB:DLG1:SEMA3A</i>
go_regulation_of_protein_modification_process	1.049 23325	1.23 5876 66	0.00 5789 53	<i>PRKAA2:TOL- LIP:DNMT1:PRKCE:ERBB4:CUL3:GNL3:SOX2:DL G1:EGR1:ENPP1:SEMA3A:STK3</i>
go_positive_regulation_of_rna_biosynthetic_process	1.108 03324	1.30 3077 58	0.00 5789 53	<i>PRDM16:ZBTB16:FLI1:STAT5B:E- PAS1:ERBB4:THRB:GNL3:SOX2:SUB1:EGR1:HN RNPK</i>
go_cell_cell_signaling_by_wnt	1.728 39506	1.88 2569 32	0.00 6312 13	<i>PRKAA2:TCF7L1:CUL3:CSNK2A1:SOX2:EGR1:ST K3</i>
go_positive_regulation_of_gene_expression	0.987 84195	1.13 3213 37	0.00 9169 28	<i>PRDM16:ZBTB16:FLI1:STAT5B:DNMT1:E- PAS1:ERBB4:THRB:GNL3:SOX2:SUB1:EGR1:HN RNPK</i>
go_positive_regulation_of_biosynthetic_process	0.983 35855	1.12 5426 88	0.00 9217 75	<i>PRDM16:ZBTB16:FLI1:STAT5B:E- PAS1:ERBB4:THRB:GNL3:ZBTB20:SOX2:SUB1:E GR1:HNRNPK</i>
go_protein_modification_by_small_protein_conjugation_or_removal	1.168 2243	1.34 1975 38	0.00 9659 75	<i>TOL- LIP:ZBTB16:RNF112:KEAP1:PRKCE:EPAS1:CUL3 :GNL3:EGR1:NUP153</i>
go_regulation_of_nervous_system_development	1.256 98324	1.43 5677 63	0.00 9844 15	<i>RNF112:DLL3:CHN1:ERBB4:THRB:SOX2:DLG1:S EMA3A:CSMD3</i>

go_lipid_localization	2.212 38938	2.20 5945 64	0.00 9844 15	<i>PRKAA2:STAT5B:PLSCR4:ENPP1:HNRNPK</i>
-----------------------	----------------	--------------------	--------------------	--

Supplementary Table 9 | GWAS Catalogue Associations for Rs648044. (RAF = risk allele frequency, Beta = beta coefficient, OR = odds ratio, CI = confidence intervals)

Variant and risk allele	P-value	RAF	OR	Beta	CI	Mapped gene	Reported trait	Trait(s)	Study accession	Location
rs648044-?	1 x 10 ⁻⁹			0.013834 unit decrease	[0.0094-0.0183]	ZBTB16	Leisure sedentary behaviour (television watching)	lifestyle measurement	GCST010084	11:114160077
rs648044-A	9 x 10 ⁻⁹	0.3892		0.0083 unit increase	[0.0054-0.0112]	ZBTB16	Educational attainment (years of education)	self reported educational attainment	GCST006442	11:114160077
rs648044-A	2 x 10 ⁻⁸	0.3892		0.0076 unit increase	[0.0049-0.0103]	ZBTB16	Educational attainment (MTAG)	self reported educational attainment	GCST006571	11:114160077
rs648044-T	6 x 10 ⁻¹¹	0.38	1.25		[1.17-1.34]	ZBTB16	Non-glioblastoma glioma	central nervous system cancer	GCST003227	11:114160077
rs648044-A	5 x 10 ⁻¹²	0.3919	1.13		1.13-1.25	ZBTB16	Non-glioblastoma glioma	central nervous system cancer, glioma	GCST004348	11:114160077
rs648044-A	6 x 10 ⁻⁹	0.3967				ZBTB16	Cortical thickness	cortical thickness	GCST90091061	11:114160077

Supplementary Table 10| Mendelian randomisation analysis hits of rs648044 x dexamethasone effect on ZBTB16 transcription on neurobehavioral phenotypes. FDR, false discovery rate, is the P-value following Benjamini-Hochberg correction; SE, standard error; β , beta-coefficient

Batch	Phenotype	β (SE)	FDR
ebi-a	Asthma (adult onset)	0.678 (0.006)	<0.001
ebi-a	Asthma (childhood onset)	0.692 (0.008)	<0.001
ieu-a	Years of schooling	0.006 (0.001)	<0.001
ukb-b	Impedance of arm (left)	0.005 (0.001)	<0.001
ukb-b	Impedance of arm (right)	0.005 (0.001)	0.002
ukb-b	Impedance of whole body	0.005 (0.001)	0.003
ukb-b	Time spent watching television (TV)	-0.005 (0.001)	0.003
ukb-b	Cereal intake	0.006 (0.001)	0.003
ukb-d	Monocyte percentage	0.008 (0.002)	0.003
ieu-a	Thalamus volume	21.372 (4.708)	0.003
ukb-b	Qualifications: College or University degree	0.003 (0.001)	0.006
ukb-b	Alcohol intake frequency.	-0.009 (0.002)	0.006
ukb-d	Cereal type: Other (e.g. Cornflakes, Frosties)	-0.003 (0.001)	0.018
ukb-d	Bread type: White	-0.003 (0.001)	0.019
ukb-b	Fed-up feelings	-0.003 (0.001)	0.021
ukb-b	Fortified wine intake	0.004 (0.001)	0.021
ukb-b	Leg fat percentage (right)	-0.003 (0.001)	0.033
ukb-b	Plain cereal intake	0.008 (0.002)	0.039
ukb-b	Sitting height	0.004 (0.001)	0.046
ukb-b	Leisure/social activities: Religious group	0.002 (0.001)	0.048
ukb-b	Average weekly champagne plus white wine intake	0.005 (0.001)	0.048
ukb-b	Leg fat mass (right)	-0.004 (0.001)	0.049

Supplementary Table 11| Mendelian randomisation analysis hits of rs648044 x dexamethasone effect on ZBTB16 transcription on neuroimaging phenotypes. FDR, false discovery rate, is the P-value following Benjamini-Hochberg correction; SE, standard error; β , beta-coefficient; ICVF, intracellular volume fraction; ISOVF, isotropic volume fraction; TBSS, tract based spatial statistics; IDP, image derived phenotypes. The phenotypes that are gray appear twice due to the two analysis streams used by the original paper in the UK Biobank.

Phenotype	Colour	Name	Hemisphere	β (SE)	P _{FDR}	Analysis type	Measure	Name of atlas
a2009s lh S circular insula ant thickness		anterior circular insula	L	0.038 (0.01)	0.048	Freesurfer		Hammers
IDP dMRI TBSS ICVF Medial lemniscus R		medial lemniscus	R	-0.036 (0.009)	0.033	TBSS	ICVF	JHU ICBM DTI 81 white matter labels
IDP dMRI ProbtrackX ICVF ml r		medial lemniscus	R	-0.037 (0.009)	0.018	Probtrack	ICVF	JHU ICBM DTI 81 white matter labels
IDP dMRI ProbtrackX ICVF ilf l		inferior longitudinal fasciculus	L	-0.039 (0.011)	0.049	Probtrack	ICVF	JHU White Matter Tractography
IDP dMRI ProbtrackX ICVF cgc l		cingulate gyrus part of cingulum	L	-0.04 (0.011)	0.032	Probtrack	ICVF	JHU ICBM DTI 81 white matter labels
IDP dMRI ProbtrackX ICVF cgh l		cingulum hippocampus	L	-0.04 (0.011)	0.048	Probtrack	ICVF	JHU ICBM DTI 81 white matter labels
IDP dMRI ProbtrackX ISOVF cgh l		cingulum hippocampus	L	-0.04 (0.011)	0.049	Probtrack	ISOVF	JHU ICBM DTI 81 white matter labels
IDP dMRI TBSS ICVF Cingulum cingulate gyrus R		cingulate gyrus part of cingulum	R	-0.041 (0.011)	0.024	TBSS	ICVF	JHU ICBM DTI 81 white matter labels
IDP dMRI ProbtrackX ISOVF unc l		uncinate fasciculus	L	-0.041 (0.011)	0.026	Probtrack	ISOVF	JHU ICBM DTI 81 white matter labels
IDP dMRI ProbtrackX ICVF str l		superior thalamic radiation	L	-0.042 (0.011)	0.019	Probtrack	ICVF	Xtract HCP Probabilistic tract atlases
IDP dMRI ProbtrackX ICVF ml l		medial lemniscus	L	-0.043 (0.009)	0.004	Probtrack	ICVF	JHU ICBM DTI 81 white matter labels
IDP dMRI ProbtrackX ICVF cgc r		cingulate gyrus part of cingulum	R	-0.043 (0.011)	0.018	Probtrack	ICVF	JHU ICBM DTI 81 white matter labels
IDP dMRI ProbtrackX ICVF ar r		acoustic radiation	R	-0.043 (0.011)	0.019	Probtrack	ICVF	Juelich histological atlas
IDP dMRI TBSS ISOVF Cingulum hippocampus R		cingulum hippocampus	R	-0.043 (0.011)	0.024	TBSS	ISOVF	JHU ICBM DTI 81 white matter labels
IDP dMRI TBSS ICVF Posterior limb of internal capsule R		posterior limb of internal capsule	R	-0.044 (0.011)	0.018	TBSS	ICVF	JHU ICBM DTI 81 white matter labels
IDP dMRI ProbtrackX ICVF cst r		corticospinal tract	R	-0.044 (0.011)	0.018	Probtrack	ICVF	JHU ICBM DTI 81 white matter labels
IDP dMRI ProbtrackX ISOVF atr l		anterior thalamic radiation	L	-0.045 (0.01)	0.004	Probtrack	ISOVF	JHU White Matter Tractography
IDP dMRI ProbtrackX ISOVF ifo l		inferior fronto-occipital fasciculus	L	-0.046 (0.011)	0.013	Probtrack	ISOVF	JHU ICBM DTI 81 white matter labels
IDP dMRI ProbtrackX ISOVF unc r		uncinate fasciculus	R	-0.047 (0.011)	0.009	Probtrack	ISOVF	JHU ICBM DTI 81 white matter labels
IDP dMRI TBSS ISOVF Anterior corona radiata L		anterior corona radiata	L	-0.049 (0.01)	0.002	TBSS	ISOVF	JHU ICBM DTI 81 white matter labels
IDP dMRI TBSS ICVF Corticospinal tract R		corticospinal tract	R	-0.052 (0.011)	0.002	TBSS	ICVF	JHU ICBM DTI 81 white matter labels

Supplementary Table 12| Guide RNAs used for the CRISPR-Cas9 experiments.

Genomic locus targeted	crRNA (5'-3')	PAM (5'-3')	Use	Vendor
ZBTB16 upstream of exon 2	GTTGCCAAGCCCT-TAGCAAG	AGG	KO of exon 2 of ZBTB16	IDT DNA Technologies
ZBTB16 downstream of exon 2	CAAGTCCTACATCA-GGTGCG	GGG	KO of exon 2 of ZBTB16	IDT DNA Technologies
Upstream of rs648044	AT-GGGTCTACTCTACAGACC	TGG	KO of 756bp surrounding rs648044	IDT DNA Technologies
Downstream of rs648044	TCTCA-GAAGGGCCTCCTACA	GGG	KO of 756bp surrounding rs648044	IDT DNA Technologies

Supplementary Table 13| Table of reagents.

Materials	Ab- bre- via- tion	Company	Catalogue or ref- erence Number
100% Methanol		Roth	4627.5
2-Mercaptoethanol		Gibco™	31350-010
2200 TapeStation (Agilent Technologies)			
30 % Acrylamide-Mix		Serva	10688.01
4D-Nucleofector™ Core Unit		LONZA	AAF-1002B
4D-Nucleofector™ X Unit		LONZA	AAF-1002X
96 PCR Plate without skirt	96 PCR Plate	Sarstedt	72.1978.202
Albumin Fraction V (BSA)	BSA	Roth	8076.2
Allegra X-22R Centrifuge (Beckman Coulter)			
Alt-R® Cas9 Electroporation Enhancer, 2 nmol		IDT	1075915
Alt-R® CRISPR-Cas9 crRNA	crRN A	IDT	-
Alt-R® CRISPR-Cas9 tracrRNA	tra- crRN A	IDT	1072532
Alt-R® S.p. HiFi Cas9 Nuclease V3		IDT	1081060
Amaxa Nucleofector II Kit V		Lonza	VACA-1003
Ammonium peroxydisulphate	APS	Roth	9592.3
AMPure XP beads		Beckman Coulter	A63880
Anti-Anti (100X)		Gibco™	15240-062
Aqua-Poly/Mount		Polysciences	18606-20
ArciTect™ Annealing Buffer (5X)		STEMCELL Technologies	76020
B-27 Supplement	B-27 + A	Gibco™	17504-044
B-27 Supplement without Vitamin A	B-27 - A	Gibco™	12587-010
bFGF		Peprtech	100-18B
C-Chip Disposable Hemocytometer	Neub auer Cha mber	NanoEnTek	DHC-N01
Cell Culture Plates		TPP	93100
ChemiDoc XRS+ System		Bio-Rad	#1708265
CloneAmp HiFi PCR Premix		Takara Bio	639298

Costar® 24 well Cell Culture Plate	24 well plate	Corning Incorporated	3526
Costar® 6 Well Cell Culture Plate	6-well plate	Corning Incorporated	REF3516
Costar® 96 Well Cell Culture Cluster	96-well plate	Corning Incorporated	3596
Cover Slips		DURAN GROUP	235503404
Criterion™ Blotter (Bio-Rad, #1704070)			
CryoTube	Cryo Vial	Thermo Scientific™	377267
Cutfix stainless scalpel #22	Sterile scalpel	Braun	5518083
D-luciferine, Beetle Juice luciferase assay		PJK	102511-1
D1000 Ladder		Agilent Technologies	5067-5586
D1000 Reagents		Agilent Technologies	5067-5583
D1000 Screen Tape		Agilent Technologies	5067-5582
D500 Screen Tape		Agilent Technologies	5067-5588
D5000 Ladder		Agilent Technologies	5067-5590
D5000 Reagents		Agilent Technologies	5067-5589
Dimethyl sulfoxide	DMSO	Roth	A994.1
DMEM-F12 medium		Gibco™	11320033
DMEM/F-12 (Dulbecco's Modified Eagle Medium/Nutrient Mixture F-12) with GlutaMAX	DME M/F-12+ GlutaMAX	Gibco™	31331-028
DMEM/F-12 (Dulbecco's Modified Eagle Medium/Nutrient Mixture F-12)	DME M/F-12	Gibco™	31330-038
DNase I		Thermo Fisher Scientific	EN0521
DMEM (Dulbecco's Modified Eagle Medium-high glucose supplemented)		Gibco™	1196508
Dulbecco's phosphate-buffered saline, without Calcium chloride / without Magnesium chloride	D-PBS -/-	Gibco™	14190-094
Electroporation chamber		Harvard Apparatus	ECM830

EndoFree Plasmid Maxi Kit		QUIAGEN	Cat. No. / ID: 12362
EZ DNA Methylation Kit		Zymo Research	D5001
Fast Green		Sigma Aldrich	F7252
Fetal Bovine Serum, ES Cell Qualified One Shot™	FBS ES- qual- ity	Gibco™	16141-061
Fetal Bovine Serum, Qualified	FBS	Gibco™	10270-106
Filteraufsatz 250 "Rapid" Filtermax		TPP	99255
Filteraufsatz 500 "Rapid" Filtermax		TPP	99505
Gel-Casting-System 1.5 mm		Bio-Rad	1658006FC
Gentle Cell Dissociation Reagent	Gen- tle	STEMCELL Technologies	#07174
GlutaMax-I (100X)		Gibco™	35050-038
Glycine		Roth	3187.4
Heparin		Sigma	H3149
Human Stem Cell Nucleofector™ Kit 1 (2b)		LONZA	VPH-5012
Immobilon Western HRP Substrate Luminol Reagent		Millipore	WBKLS0500
Immobilon Western HRP Substrate Peroxide Solution		Millipore	WBKLS0500
Immobilon-P Transfer Membrane		Millipore	IPVH00010
in-Fusion HD Cloning Plus		Takara Bio	636763
Insulin Solution human	Insu- lin	Gibco™	19278-5ML
Isopropanol		Millipore	1.01040.2500
KCl ₂		Roth	6781.1
KH ₂ PO ₄		Merck	K24259773
KnockOut Serum Replacement	KOS R	Gibco™	10828-028
Life Eco Thermal Cycler		BIOER	
Lipofectamine 2000		Thermo Fisher Scientific	11668030
Low Profile Microtome Blades 819		Leica	14035838382
Matrigel		BD Biosciences	356234
Matrigel® hESC-qualified Matrix	Mat- rigel	Corning Incorporated	354277
Maxima H Minus Reverse Transcriptase		Thermo Fisher Scientific	EP0751
MEM-NEAA (100X), Minimum Essential Medium Non-Essential Amino Acids	MEM - NEA A	Gibco™	11140-035
Micro-Fine™	Insu- lin	BD	320801

	sy- ringe		
Milk Powder		Roth	T145.3
Mini-PROTEAN® Tetra Vertical Electrophoresis Cell for Handcast Gels Mini gels, 4-gel		Bio-Rad	1658006FC
MiSeq Reagent Kit v3		Illumina	MS-102-3001
Mr. Frosty™ Freezing Container	Free zing Con- taine r	Thermo Scientific™	5100-0001
mTeSR 1 5X Supplement	mTe SR Supp l.	STEMCELL Technologies	#85852
mTeSR1 Basal Medium	mTe SR	STEMCELL Technologies	#85851
N2 Supplement	N2 Sup- ple- ment	Gibco™	17502-048
Na ₂ HPO ₄ 2H ₂ O		Roth	4984.1
NaCl		Roth	3957.1
NebNext Ultra II library kit		Illumina	E7645
NebNext rRNA Depletion kit		Illumina	E6310
Neurobasal Medium (1x)	Neu- ro- basal	Gibco™	21103-049
Nucleofector™ 2b Device (LONZA, #AAB-1001)			
NucleoSpin Genomic DNA kit		Macherey-Nagel	740952
Nunc™ Delta Surface	Tera- saki plate	Thermo Scientific	163118
OCT Mounting media		VWR BDH Chemicals	361603E
oligo(dT)16 primers		Invitrogen	N8080128
Opti-MEM™ I Reduced Serum Medium		Gibco™	31985062
P3 primary cell 4D_X Kit S		Lonza	V4XP-3032
P3 Primary Cell 4D-Nucleofector™ X Kit		LONZA	V4XP-3032
PageRuler™ Prestained Protein Ladder, 10 to 180 kDa	Pro- tein Lad- der	Thermo Scientific™	26617
Pap Pen Immunostaining Pen	Pap Pen	Kisker Biotech GmbH & Co KG Dutscher Group	MKP-1
Parafilm		Bemis™	HS234526A

Paraformaldehyde	PFA	Millipore	1.04005.1000
passive lysis buffer		Biotium	99821
PCR Pipet 1-10uL w/ 100 Plungers		Drummond Scientific Company	5-000-1001-X10
Peel-A-Way embedding molds	Embedding mold	Sigma Aldrich	E6032-1CS
PhiX Control v3 library		Illumina	FC-110-3001
Phosphatase inhibitors		Sigma Aldrich	4906845001
Ponceau S Solution		Sigma	P7170-1L
Primers		IDT	
PrimeTime® Gene Expression Master Mix		IDT DNA Technologies	1055770
Protease inhibitors		Sigma Aldrich	P8340
Protein Assay Dye Reagent Concentrate		Bio-Rad	5000006
PVDF membrane		Millipore	IPVH00010
Q5 high fidelity master mix		New England Biolabs	M0494S
Q5® Hot Start High-Fidelity 2X Master Mix		New England Biolabs	M0494S
Quantitect Reverse Transcriptase		Qiagen	205311
QuickExtract™ DNA Extraction Solution		Lucigen	QE09050
Random hexamers		IDT DNA Technologies	51-01-18-25
Recombinant Human FGF-basic	b-FGF	Peprtech	100-18B
RevitaCell Supplement (100X)	RC	Gibco™	A2644501
RIPA-Buffer		Sigma-Aldrich	R0278
RNeasy Mini extraction kit		Qiagen	74104
ROCK Inhibitor (Y-27632)	Rock Inhibitor	Millipore	SCM075
Roti-Load 1		Roth	K929.1
Rotilabo-disposable tweezer, unsterile	Plastic forceps	Roth	KL06.1
RU486		Selleck	S2606
SDS Pellets	SDS	Roth	CN30.2
Stellar™ competent cells		Takara Bio	636763
StemPro Accutase Cell Dissociation Reagent	Accutase	Life Technologies	A6964-100ML
SuperFrost™ Plus Microscope Slides		Fisherbrand™	22-037-246

Takara EpiTaq HS Polymerase		Clontech	R110A
TEMED		Roth	2367.3
Tissue Culture Dish 100	10 cm tis- sue cul- ture dish	TPP	93100
Tri-Sodium citrate-Dihydrate		Roth	3580.3
TRIS Pufferan		Roth	4855.2
Tritonx100	Tri- ton	Roth	3051.4
TruSeq DNA PCR-Free HT Library Prep Kit		Illumina	20015963
Trypan Blue Solution		Sigma Aldrich	93595-50ML
Tween-20		Roth	9127.1
Ultra-Low Cluster, 96 Well Round Bottom, Ultra-Low Attachment Plate		Costar, Corning Incorporated	7007
water, molecular biology grade		Fisher bioreagents	bp2819-100
Whatman™ Filter Paper	Filter Pa- per	GE Healthcare	10311647

List of Figures

Figure 1 Hypothalamic- Pituitary- Adrenal axis in physiology and pregnancy. __	3
Figure 2 Glucocorticoid effects on multiple organ systems during development. 8	8
Figure 3 Neurobehavioral outcomes of prenatal environmental exposures. ____	13
Figure 4 Developmental timeline of the fate decisions processes for the human and mouse cerebral cortex. _____	16
Figure 5 Neurogenesis in lissencephalic and gyrencephalic species. _____	18
Figure 6 Human cerebral organoids from induced pluripotent stem cells. _____	21
Figure 7 Glucocorticoid receptor machinery in human cerebral organoids. _____	40
Figure 8 Glucocorticoids increase gyrencephalic species-specific basal progenitors. _____	41
Figure 9 Glucocorticoids lead to delayed neurogenesis. _____	42
Figure 10 The GR and not the MR is responsible for the effects of dexamethasone on basal progenitors. _____	43
Figure 11 Transcriptomic effects of chronic treatment with dexamethasone on cerebral organoids. _____	44
Figure 12 Differential network of <i>Zbtb16</i> in the adult mouse brain. _____	46
Figure 13 ZBTB16 expression pattern in organoids and mouse cortex. _____	48
Figure 14 Glucocorticoids alter the expression pattern of ZBTB16 in organoids and fetal mouse cortex. _____	49
Figure 15 Glucocorticoids affect the methylation landscape of <i>ZBTB16</i> . _____	50
Figure 16 ZBTB16 mimics the effect of dexamethasone on basal progenitors. _	52
Figure 17 <i>ZBTB16</i> is necessary and sufficient for the effects of glucocorticoids on basal progenitors. _____	55
Figure 18 Distribution of GFP cells in the mouse cortex. _____	56
Figure 19 <i>In utero</i> electroporations in mice. _____	57
Figure 20 Effects of ZBTB16 overexpression on the neuronal output in mice. _	58
Figure 21 <i>In utero</i> electroporations of ZBTB16 overexpression from E13.5 to E19.5. _____	59
Figure 22 Luciferase reporter assays for <i>PAX6</i> promoters. _____	61
Figure 23 Genomic locus of <i>ZBTB16</i> . _____	62
Figure 24 Rs648044 interacts with glucocorticoids to modulate enhancer activity. _____	63
Figure 25 Explanation of Mendelian Randomization analysis. _____	65
Figure 26 MRa-PheWAS study results of <i>ZBTB16</i> on neurobehavioral and structural phenotypes. _____	66
Figure 27 Summary of the main findings of this Ph.D thesis. _____	68
Supplementary Figure 1 Dexamethasone effects on basal progenitors' subtypes in human cerebral organoids. _____	99

Supplementary Figure 2 <i>ZBTB16</i> expression in different lissencephalic and gyrencephalic species. _____	100
Supplementary Figure 3 Methylation levels of CpGs in the <i>ZBTB16</i> locus. ____	101
Supplementary Figure 4 <i>ZBTB16</i> overexpressing plasmids validation in HELA cells. _____	102
Supplementary Figure 5 CRISPR-Cas9 editing of iPSCs to remove exon 2 of the <i>ZBTB16</i> locus. _____	103
Supplementary Figure 6 Non-cell autonomous effects of <i>ZBTB16</i> overexpression in the mouse cortex from E13.5-E16.5. _____	104
Supplementary Figure 7 CRISPR-Cas9 editing of rs648044. _____	105
Supplementary Figure 8 MR-PheWAS results of <i>ZBTB16</i> expression on neurobehavioral traits. _____	106

List of Tables

Supplementary Table 1 Primary and secondary antibodies. _____	107
Supplementary Table 2 PrimeTime assays, rtPCR primers, qPCR primers, genomic primers. _____	108
Supplementary Table 3 STARR-qPCR inserts for rs648044. _____	110
Supplementary Table 4 Primers used for HAM-TBS on the <i>ZBTB16</i> locus. ____	111
Supplementary Table 5 Phenotype batches selected for Mendelian Randomisation analysis. _____	112
Supplementary Table 6 Differentially expressed genes from bulk RNA seq at an FDR 10% cut-off in hCOs after 7 days of 100nM dexamethasone. _____	113
Supplementary Table 7 Cross-reference of gene lists to identify progenitor-specific genes with large effect sizes. _____	115
Supplementary Table 8 Enrichment analysis of the <i>Zbtb16</i> differential network in the PFC of the adult mouse brain from Gerstner & Krontira et al., BioRxiv, 2022. _____	117
Supplementary Table 9 GWAS Catalogue Associations for Rs648044. _____	120
Supplementary Table 10 Mendelian randomisation analysis hits of rs648044 x dexamethasone effect on <i>ZBTB16</i> transcription on neurobehavioral phenotypes. _____	121
Supplementary Table 11 Mendelian randomisation analysis hits of rs648044 x dexamethasone effect on <i>ZBTB16</i> transcription on neuroimaging phenotypes. _____	122
Supplementary Table 12 Guide RNAs used for the CRISPR-Cas9 experiments. _____	123
Supplementary Table 13 Table of reagents. _____	124

Acknowledgements

I would like to express my deepest gratitude to my supervisor Prof.Dr.Dr. Elisabeth Binder for giving me the opportunity to work with her and for providing a very well-organized lab that supports scientific work with all the tools needed. Most of all though I want to thank Elisabeth for always supporting all my ideas, for helping me grow them and for never discouraging any project or experiment, even the ones that maybe were outside of the general scope of the lab. I deeply appreciate our scientific discussions and your continuing support and, may I say, patience for the time it took me to grow and continue growing as a scientist.

In addition, I want to thank dr. Silvia Cappello. This work is a combination of stress biology and neurodevelopment and without Silvia's lab but also Silvia herself it would have never reached the point it has today. Silvia thank you for always having open arms for me even not being a member of your lab, for sharing your knowledge and mainly for sharing your love on neurodevelopment that got me addicted!

A big thank you is also owed to the members of my TAC committee, Prof. Dr. Magdalena Götz, PD dr. Mathias Schmidt and dr. Janine Arloth. All our meetings were very helpful for this project and many of the experiments in this thesis were a result of these meetings. Your support, ideas and guidance are most appreciated!

Instrumental to this work have been three incredible scientists, dr. Cristiana Cruceanu, dr. Christina Kyrousi and dr. Marta Labeur. Cristiana thank you for always being there for me both scientifically and as a friend. I deeply appreciate all our discussions, you supporting my growth as a scientist on all levels and for never saying no to reading what I wrote or for chatting on weird ideas. These years would have been very different without you as my partner in crime! Christina you are one of the main reasons that made me fall in love with neurodevelopment. Your passion for experimental biology and your consistency in doing experiments that aim at answering questions with simple but inspired ways was a big lesson for me. Marta your love of science is addicting. I deeply appreciate all your help. Your persistence in truly understanding how the cells are built and function and your efforts on always designing experiments in a simple yet fully supported way will be with me for all my scientific career. I will miss dearly you coming up with an idea for something we had discussed hours earlier!

I want to thank all members of the department of Translational Research in Psychiatry, past and present. To the technicians Cinzia, Bärbel, Susi and Maik that have always been so helpful and consistent in their work and to Monika for arranging all we need to do our experiments, thank you! Signe and Ane thank you for sharing the Ph.D. life, the

successes and the failures. I also want to thank Marie-Helen for being such a great first student and for making it so easy to supervise and collaborate with someone!

Anna, Elena and Alessandro thank you for becoming real friends, for sharing this experience with me, for all our scientific discussions but also all our chats on life, music, baking, traveling, politics. Thank you and Osama for making Munich home, these years would have been very very different without you!

To my friends in Greece, Manina, Katerina, Christina, Mika, Foteini, Marko, Niko and Andrea, who I grew up with and whose influence in my life has been instrumental thank you. I am very lucky to have you as my chosen family and your help in grounding me and reminding how much life there is outside of science has been more helpful than you can imagine.

Last, I want to thank my family. To my sisters, Sofia and Andriani (and Alma), who are my best friends, my support system and my safe haven thank you for all the laughs and all the fights! To my mom and dad who raised us in the best way possible, providing us with all the opportunities and all the tools to survive with respect in this world. Mom, thank you for teaching us how to respect others. Dad your love for science is addicting and the reason I am here today. Σας αγαπώ και σας ευχαριστώ πιο πολύ από ό,τι μπορείτε να φανταστείτε.

Declaration of Contributions

Cerebral organoids

Production	Anthodesmi Krontira
Dexamethasone treatment	Anthodesmi Krontira
Electroporations	Anthodesmi Krontira
Tissue fixation, Preparation, Immunofluorescence	Anthodesmi Krontira, Marie-Helen Link for Ki-67/BCL11B staining
Confocal Imaging	Anthodesmi Krontira, Marie-Helen Link for Ki-67/BCL11B staining
Flow cytometry	Anthodesmi Krontira
Overexpressing plasmids: design & cloning	Anthodesmi Krontira
Quantifications	Anthodesmi Krontira
Protein, RNA isolation	Anthodesmi Krontira
Western blot	Anthodesmi Krontira, Barbara Wölfel, Vincenza Sportelli
RT- qPCR	Anthodesmi Krontira, Maik Ködel
Organoids for bulk sequencing	Anthodesmi Krontira, Cristiana Cruceanu
Bulk sequencing library preparation	Anthodesmi Krontira, Cristiana Cruceanu
Sequencing	Sequencing Core Facility, <i>Berlin</i>
Bulk sequencing analysis	Simone Röh

Mice

<i>In utero</i> electroporations	Anthodesmi Krontira, Christina Kyrousi
Tissue fixation, Preparation, Immunofluorescence	Anthodesmi Krontira
Confocal Imaging	Anthodesmi Krontira
Quantifications	Anthodesmi Krontira

DiffBrainNet

Mice treatment	
----------------	--

		Anthodesmi Krontira, Mathias Schmidt
	Organ extractions, brain region isolation	Anthodesmi Krontira
	Libraries preparation	Anthodesmi Krontira, Susann Sauer
	Data pre-processing	Simone Röh
	Data analysis	Anthodesmi Krontira, Nathalie Gerstner
CRISPR-Cas9	Design and protocol iPSCs editing	Anthodesmi Krontira, Marta Labeur Anthodesmi Krontira
Luciferase assays		
	Plasmids design	Anthodesmi Krontira
	Plasmids cloning	Vector Builder
	Assay	Anthodesmi Krontira
Rs648044		
	Plasmids cloning	Anthodesmi Krontira
	STARR-qPCR	Anthodesmi Krontira
	Mendelian randomization	Nils Kappelmann
	Illustration of brain associations	Dorothee Pölchen
Targeted Bisulfite Sequencing		
	Design	Anthodesmi Krontira
	Primer validation	Susann Sauer
	Libraries preparation	Anthodesmi Krontira, Susann Sauer
	Data pre-processing	Simone Röh
	Data analysis	Anthodesmi Krontira

Affidavit



LUDWIG-
MAXIMILIANS-
UNIVERSITÄT
MÜNCHEN

Promotionsbüro
Medizinische Fakultät



Affidavit

Krontira, Anthodesmi

Surname, first name

Kraepelinstr. 2-10

Street

80804, Munich, Germany

Zip code, town, country

I hereby declare, that the submitted thesis entitled:
Neurodevelopment under the prism of environmental challenges
Prenatal glucocorticoids and neurogenesis

is my own work. I have only used the sources indicated and have not made unauthorised use of services of a third party. Where the work of others has been quoted or reproduced, the source is always given.

I further declare that the submitted thesis or parts thereof have not been presented as part of an examination degree to any other university.

Munich, 29.11.2022

place, date

Krontira, Anthodesmi

Signature doctoral candidate

Confirmation of Congruency



LUDWIG-
MAXIMILIANS-
UNIVERSITÄT
MÜNCHEN

Promotionsbüro
Medizinische Fakultät



**Confirmation of congruency between printed and electronic version of
the doctoral thesis**

Krontira, Anthodesmi

Surname, first name

Kraepelinstr. 2-10

Street

80804, Munich, Germany

Zip code, town, country

I hereby declare, that the submitted thesis entitled:

Neurodevelopment under the prism of environmental challenges
Prenatal glucocorticoids and neurogenesis

is congruent with the printed version both in content and format.

Munich, 29.11.2022

place, date

Krontira, Anthodesmi

Signature doctoral candidate

*«Ποτέ μην αναγνωρίζεις τα σύνορα του ανθρώπου! Να σπας
τα σύνορα! Ν' αρνιέσαι ό,τι θωρούν τα μάτια σου».*

Νίκος Καζαντζάκης

*"Never recognize the limits of the man! Break the limits!
Abjure what your eyes see".*

Nikos Kazantzakis